VIBRATIONAL BAND SHAPE ANALYSIS IN COMPLEX MOLECULAR SYSTEMS

(ABSTRACT)

By

THONGAM GOMTI DEVI

A Thesis

submitted in partial fulfilment of the

requirement of the Degree of

DOCTOR OF PHILOSOPHY IN PHYSICS

DEPARTMENT OF PHYSICS

NORTH-EASTERN HILL UNIVERSITY

SHILLONG

INDIA

ABSTRACT

Vibrational Band Shape Analysis in Complex Molecular Systems

Thongam Gomti Devi

Under the supervision of

Prof. Kamal Kumar

There has been considerable interest in studying the molecular dynamics in liquids and disordered condensed phases. This study is of great importance for a large number of chemical, biological and physical phenomena. Liquids are strongly interacting disordered systems and are the least understood state of matter. The importance of liquid phases in chemical reactions and biology makes liquid science an important and rapidly developing field of research. The dynamics of molecules in disordered condensed phases are complicated by the presence of strong, fluctuating intermolecular interactions and the lack of long-range symmetry. Many attempts have been made in the past to analyze the

Raman band shape in liquids and to investigate which dynamic processes and interactions may contribute to the shape. The knowledge of the structure and dynamics in liquids/solutions is expected to contribute significantly to the understanding of the condensed phases and the reactions that occur in solution. The two interacting situations, in pure solute and when dissolved in solvents, differ markedly. The solvent electric field influences the band shape of a reference mode significantly. Moreover, a considerable amount of information about vibrational relaxation and non-coincidence effect can be obtained by analyzing the experimentally measured shapes of the isotropic and anisotropic components of the Raman band of molecular liquids. In our present work, we use Laser Raman technique to explore liquid structure and dynamics at the molecular level. In this study, the theoretical models are tested and the information on the nature of the solute-solvent interactions in liquid phase has been obtained. The carbonyl containing aliphatic and aromatic molecules have been chosen for laser Raman studies in order to get information about the molecular dynamics and interaction processes.

Chapter 1 contains a brief introduction to the thesis emphasizing the application of Laser Raman scattering technique in the study of vibrational relaxation and dephasing processes in liquids. The importance of analyzing the experimentally measured band shapes of isotropic and anisotropic components

of the Raman band of molecular liquids has been discussed here. The band shape of the reference mode is influenced by the concentration fluctuations of the environment in liquid mixtures. In order to examine the various interactions involved in the solute-solvent interactions we have studied the Raman band shapes of molecules containing C=O bond namely o-Chlorobenzaldehyde (OCBD) and Methyl Isobutyl Ketone (MIBK) in various polar and nonpolar solvents such as benzene, carbon tetrachloride, methylbenzene, chlorobenzene, acetonitrile and chloroform. The choice of these solvents was such that the solvent molecules are of varying size and shape, and different multipolar moments and dielectric constants. The benzene and substituted benzene molecules have significant effects in solute-solvent interactions from the point of view of quadrupole moment and plate like structure. The CH_3CN and CCl_4 molecules have dipole moment and octupole moment respectively. They are also having different shapes. The $CHCl_3$ has a symmetric top structure and provides the possibility of hydrogen bonding through C-H bond as hydrogen is acidic here. These molecules because of their different size, shape and electrical properties are important in the study of the intermolecular forces in solute-solvent systems. The non-coincidence effect (NCE) and the effect of van der Waals' volume of the sphere of influence on the Raman bandwidth were studied for OCBD in order to explain the intermolecular interactions involved.

Vibrational dephasing of the C=O stretching mode of OCBD is very sensitive to the details of the interaction potentials and it can be used to probe the influence of the solvent. The study of isotropic bandwidth of the Raman band provides a direct probe of vibrational relaxation (mainly vibrational dephasing).

Chapter 2 gives a general theoretical background including the different types of mechanism involved in vibrational relaxation, intermolecular interaction in liquids and parameters affecting the band shape of the Raman active vibration of totally symmetric type. The various types of models are also discussed which provide a good semi-quantitative description of dephasing, resonant energy transfer responsible for non-coincidence effect and vibrational relaxation phenomenon. The van der Waals' type of interactions and their role in the band shape broadening have been discussed, taking into account the van der Waals' volume of the interacting fragments of the molecules. The various types of potentials and the intermolecular potential parameters have been discussed in this chapter. The dielectric properties have also been discussed in detail.

Chapter 3 deals with the experimental work related to the recording of Laser Raman spectra of the liquid and solution. The methods adopted for the measurement of the isotropic and anisotropic Raman bandwidth are also

explained in detail. A brief description of the technique for recording Raman spectra at room temperature using Spex Ramalog 1403 double monochromator, a cooled RCA C31034 photomultiplier tube, photon counting arrangement and Ar-ion laser source is given. The brief account of HP-4263B multi-frequency LCR-meter for measuring capacitance is also given in this chapter.

Chapter 4 is devoted to the solvent dependent study of the non-coincidence effect (NCE) and anisotropic component of the Raman band. Raman Spectra of C=O stretching mode of OCBD were measured using CCl_4, CH_3CN, $CH_3C_6H_5$ and C_6H_5Cl solvents at different solvent concentrations ranging from 10% to 90% . The peak frequencies of isotropic and anisotropic components were found out. The anisotropy shift ($\delta\nu = \nu_{aniso} - \nu_{iso}$) was measured for different solvent concentrations ranging from 10% to 90% solvent concentrations using the above four solvents. It has been found that the anisotropy shift decreases as the solvent concentration is increased because the solvent molecules decrease the interaction between the pair of identical molecules. For the molecules having aromatic rings, the coupling mechanism for the NCE may also be associated with quadrupolar resonant coupling besides transition dipole-transition dipole interactions. The Onsager- Fröhlich dielectric model, which treats the dielectric as a continuum has been tested by studying the behaviour of the NCE at various solvent concentration.

The parameter $F= \delta\nu(2\varepsilon +n^2)^2\varepsilon^{-1}$ was plotted as a function of the solute volume fraction ϕ. The data points fit well in exponential curve rather than a straight line for all the solvents except CH_3CN. In case of OCBD- CH_3CN system, the data points are lying in a straight line, which indicates that the dielectric continuum theory probably holds better in this system. The high dielectric constant of CH_3CN solvent may be responsible for such behaviour. The exponential nature of the curves for the three solvents (CCl_4, $CH_3C_6H_5$ and C_6H_5Cl) show that the Onsager- Fröhlich dielectric continuum model does not hold good in these systems. Therefore, in these solvents, the discreteness of the medium exists. Further, the screening effect may not be as effective as envisaged by the Onsager-Fröhlich model in such systems. The role of the repulsive forces in most of the interacting situations is clearly indicated by the exponential fitting of the data points.

In order to get more information about the intermolecular interactions in liquid mixtures, the anisotropic Raman components of OCBD in different solvents were studied and the bandwidths were measured . The plot of Γ_{aniso} as a function of solvent concentration shows that the data points are scattered and cannot be fitted into a single curve. For CCl_4 solvent, the data points show a decrease in the bandwidth while going from lower to higher solvent concentration, whereas for CH_3CN and C_6H_5Cl solvents, the data points show

an initial increase and then a decrease in the bandwidth as the concentration increases. In case of $CH_3C_6H_5$ solvent, the data points show somewhat different pattern as compared to others. However, the bandwidth is found to decrease at high solvent concentration for all the solvents. The bandwidths of isotropic Raman component (Γ_{iso}) were also found out in order to see the changing pattern according to different solvent concentrations and plotted with respect to the solvent concentration. Interestingly, the isotropic bandwidths are also found to decrease at higher solvent concentration. The dramatic change in shape on going from lower to higher solvent concentration region reflects the changes in liquid dynamics brought about by solvent collisions. This complicated nature has been explained in terms of van der Waals' volume of the sphere of influence in a solute dissolved in solvents. The calculation of van der Waals' volume assumes knowledge of bond distance, intermolecular van der Waals' radii and shapes of atoms in various molecular configurations. The main interaction is considered to be between the dipole moment of C=O and the dipole, quadrupole and octupole moments of the solvents.

The van der Waals' volume of the interacting system was calculated by using the equation $V_w = \Phi\, V_w(\text{solute}) + (1 - \Phi)\, V_w(\text{solvent})$

where Φ is the concentration of the solute.

The values of (Γ_{aniso}/ V_w) have been calculated for each solvent and plotted as a function of solvent concentration. This graph is an exponential curve for all the solvents, which indicates that the repulsive potential of the type $e^{-\alpha R}$ is playing a significant role.

Chapter 5 deals with the studies on vibrational dephasing in molecular liquids. The vibrational phase relaxation is important for the band shape of complex molecular systems, and is responsible for the line broadening of the isotropic Raman spectral component. However, the vibrational phase relaxation process for complex molecular systems cannot be explained simply on a macroscopic perception of the interacting systems. There may be a marked difference between the interacting situations in the pure solute and when dissolved in solvents especially at high dilution. A detailed study at the microscopic level is therefore required in order to explain the interacting situations, especially the solvent effects on vibrational relaxation rates.

The Raman spectra of OCBD dissolved in various polar and non-polar solvents ($CH_3C_6H_5$, C_6H_6, C_6H_5Cl, CCl_4 and $CHCl_3$) were recorded and the isotropic components obtained. The band shapes of the isotropic Raman component for OCBD in different solvents were checked for Lorentzian shape by curve fitting and found to be near Lorentzian in nature at high dilutions

(~90%). For Lorentzian line shape the vibrational relaxation rate (τ_v^{-1}) is related to the isotropic bandwidth by the expression,

$$\tau_v^{-1} = \pi c \Gamma_{iso}$$

where Γ_{iso} is the Full Width at Half Maximum (FWHM) of the isotropic component of the Raman band, τ_v is vibrational relaxation time and c is the velocity of light.

The bandwidths (FWHM) of the isotropic component of C=O stretching mode of OCBD were measured at 90% solvent concentration. The data were used to calculate the vibrational relaxation rate (τ_v^{-1}). The various models which have been proposed for the dephasing process take into account of the dynamic viscosity (η) which is a macroscopic property. The parameter f (ρ,η,n) was calculated for OCBD and correlated with the experimental values of the vibrational relaxation rate. The correlation is roughly linear for all the solvents, with the exception of chloroform. The point for $CHCl_3$ is too far away from the correlation line. This indicates that the bandwidth cannot be fully explained by the molecular properties contained in this parameter.

It is probable that the discreteness of the medium due to solvent may be playing a role therefore the microscopic model was used in order to explain the environmental effects around the molecule. In this model, since the solute-solvent systems may not always be homogeneous and some heterogeneity may

exist due to associative nature of the molecules, the concept of microviscosity was taken into account.

The microviscosity (η_m) is calculated using the relation

$\eta_m = \eta[0.16+0.4(a/b)]$ or $\eta_m = \eta\gamma$

where $\gamma = [0.16+0.4(a/b)]$ is the microfriction factor. **a** and **b** are the radius of solute and solvent molecules respectively.

The modified parameter has the form $$f_m = \rho\eta_m\left[\frac{n^2-1}{2n^2+1}\right]^{-1}$$

where ρ is the density and n is the refractive index of the solvent molecule.

The variation of the vibrational relaxation rate (τ_v^{-1}) as a function of f_m has been plotted, which is clearly a linear plot indicating a better fitting of data points. This shows the discreteness of the medium, which has significant influence on the bandwidth in such complex molecular systems. The correlation coefficient (r) for the τ_v^{-1} vs. f (ρ,η,n) and τ_v^{-1} vs. f_m plots have been calculated and their values are found to be 0.824 and 0.993 respectively. It may therefore be concluded that f_m is a better parameter than **f** for explaining the vibrational relaxation rates of OCBD molecule. Thus, the microviscosity rather than dynamic viscosity is playing a major role in determining the Raman band shape in this solute-solvent system.

Chapter 6 deals with the study of Raman anisotropic bandwidth of C=O stretching vibration of Methyl Isobutyl Ketone (MIBK) in several solvents like benzene, carbon tetrachloride, methylbenzene, chlorobenzene, acetonitrile and chloroform in order to see the effect of solvents of different nature. The anisotropic Raman bandwidth gives information about the angular dependent intermolecular forces. The dielectric measurements (capacitance) in liquid mixtures were also carried out to correlate the anisotropic Raman bandwidth with changing environment. The bandwidths of the anisotropic component of Raman band (Γ_{aniso}) of MIBK were measured at different solvent concentrations ranging from 10% to 90% using polar and non-polar solvents (C_6H_6, CCl_4, $CH_3C_6H_5$, C_6H_5Cl, CH_3CN and $CHCl_3$) of varying dielectric constant. Examination of spectral properties reveals that the anisotropic Raman bandwidth strongly depends on solvent concentration and is sensitive to environmental changes. In low solvent concentration region, the plot of Γ_{aniso} as a function of solvent concentration shows marked curvatures for all solvents except for CH_3CN. However, the data points in higher solvent concentration region appear to be linear for most of the solvents. In case of C_6H_5Cl solvent, the data points cannot be fitted in one curve. However, they may be fitted in two curvatures in the two ranges; lower and higher solvent concentration. In the intermediate region, there is no uniformity or continuous pattern of the

plot. For CH_3CN solvent, the data points may be fitted in two straight lines rather than one implying a discontinuity in the uniform linear pattern in the intermediate region. This is a complicated nature, which is due to the fluctuation of the chemical composition in a given site of the liquid and to the structure breaking effects.

In order to interpret the complicated behaviour we have taken into account the van der Waals' volume (V_w) of the sphere of influence in solute dissolved in all solvents. The van der Waals' volume of the interacting system was calculated by using the equation $V_w = \Phi\, V_w(\text{solute}) + (1-\Phi)\, V_w(\text{solvent})$ where Φ is the concentration of the solute.

A quantity (Γ_{aniso}/V_w) was defined and plotted as a function of solvent concentration. The exponential nature of the graph (Γ_{aniso}/V_w vs. solvent concentration) clearly indicates that the repulsive potential of the type $e^{-\alpha R}$ is playing an important role in such complex interacting systems (R being the distance of closest approach and α is a constant). The pair interaction between the solute molecules leads to the local ordering in liquids under consideration. However due to the increasing concentration of the solvent the weakening of the pair correlation may occur. The hydrodynamic forces are dominant over the electrical forces in maintaining the smooth flow of the liquid. In order to study the effect of screening on the bandwidth Γ_{aniso}, the capacitances of the

liquid mixture at different solvent concentrations varying from 10% to 90% were measured for all the solvents. The plot of capacitance vs. solvent concentrations for each solvent shows that there is no uniformity or continuity in the graph around 50% of solvent concentration. This is of somewhat similar nature as seen for the variation of bandwidth Γ_{aniso} with solvent concentration, which supports the findings that the repulsive type of intermolecular forces are responsible in the line broadening mechanism.

Chapter 7 deals with the conclusion drawn from the present work. From the present work the following conclusions can be drawn.

1. The non-coincidence effect was studied taking into account the screening factor in order to interpret the various interaction involved in solute-solvent interactions. The continuum model of Onsager-Fröhlich is not found to be valid for most of the systems. The discreteness of the medium accounts for the complex situation in the molecular system studied by us.
2. The van der Waals' volume of the interacting systems has been found to play a very important role in the study of solute-solvent interactions. The molecular fragments are also playing significant role.

3. The complex processes involved in the interacting systems may not be understood by dynamic viscosity; therefore, there is a definite need to consider the microenvironment incorporating microviscosity.

The interesting feature of the present results is the dependence of vibrational relaxation rate on the dispersion and hydrodynamic forces. The role of microenvironment through microviscosity has been established in the interacting systems. The results also indicate that repulsive potential of the type $e^{-\alpha R}$ plays an important role in the interactions as well as in the vanishing of the anisotropy shift (non-coincidence effect) in complex molecules.

VIBRATIONAL BAND SHAPE ANALYSIS IN COMPLEX MOLECULAR SYSTEMS

By
THONGAM GOMTI DEVI
DEPARTMENT OF PHYSICS

A Thesis
submitted in partial fulfilment of the
requirement of the Degree of
DOCTOR OF PHILOSOPHY
in
PHYSICS

of
NORTH-EASTERN HILL UNIVERSITY
SHILLONG
INDIA

THE NORTH-EASTERN HILL UNIVERSITY
May, 2005

DECLARATION

I, Th.Gomti Devi, hereby declare that the subject matter of this thesis is the record of work done by me, that the contents of this thesis did not form basis of the award of any previous degree to me or to the best of my knowledge to anybody else, and that the thesis has not been submitted by me for any research degree in any other University/Institute.

This is being submitted to the North-Eastern Hill University for the degree of Doctor of Philosophy in Physics.

(Thongam Gomti Devi)

Countersigned

17.5.05

(Dr. M.K. Parida)
Professor & Head
Department of Physics

Prof. & Head,
Physics Department,
N.E.H.U, Shillong-793022.

(Dr. Kamal Kumar)
Professor
Department of Physics

DEDICATED
TO
MY EMA AND BABA

ACKNOWLEDGEMENT

It gives immense pleasure and satisfaction in expressing my deep sense of gratitude to *Prof. Kamal Kumar*, Department of Physics, North-Eastern Hill University, Shillong for his keen guidance, constant encouragement and help during the entire course of my Ph. D. programme.

I am very much thankful to *Dr. A. L. Verma*, Professor (Retd.), Department of Physics, North- Eastern Hill University, Shillong for his interest in the work.

My special thanks are due to *Mr. Anil Kumar Rathore*, Senior Technical Assistant, Department of Physics for his help in recording Raman Spectra.

I am also thankful to the Head of the Department of Physics, NEHU for his encouragement during the course of work. Thanks are due to teachers and non-teaching staffs of the Department of Physics for their cooperation during the entire period of my research work.

I sincerely thank my friends *Soma Dutta, Dr.(Mrs.)Arpita Das, Nonibala, Urmila, Premabati, Romolus, Sandy, Tiken Singh, Sangeeta,* and other friends for their encouragement and cooperation during the entire period of work. I am deeply indebted to *Th. Somananda Singh* for his constant help, cooperation and encouragement during my entire research programme.

I owe my regards and love to my *parents, sisters (Indira, Geeta and Joymati) and brothers (Mahabir and Bikramjit)* who have been a constant source of inspiration throughout my life.

Lastly, I express my sincere thanks to CSIR, New Delhi for awarding the research fellowship during my research programme.

(Thongam Gomti Devi)

CONTENTS

CHAPTER 1

CHAPTER 1

INTRODUCTION

There has been a considerable interest in studying the molecular dynamics of liquids[1-5], which is of great importance for a large number of chemical, biological and physical phenomena. The knowledge of the structure and dynamics in liquids/solutions is expected to contribute significantly to the understanding of the condensed phases and the reactions that occur in solution. In liquids, the densely packed molecules exhibit strong mutual interactions in rapidly changing configurations due to random thermal motion of the molecules. Many attempts have been made in the past to analyze the Raman band shape in liquids to investigate which dynamic processes and interactions contribute in determining the shape of the band[1-2]. The relaxation, scattering and absorption spectroscopy provide useful information about the molecular motion in liquids. During the past several years, vibrational relaxation and molecular reorientational processes in liquids have been studied by analyzing [6-25] the band shape of the isotropic (I_{iso}) and anisotropic (I_{aniso}) components of the Raman band of the molecule. The full width at half maximum (FWHM) has been used for

the analysis of band shape. The sensitivity of Raman bandwidth (FWHM) on the environment has been demonstrated by the solvent dependent studies, which have been useful in obtaining the information on the dynamics of liquids.

A variety of theoretical models has been proposed to describe the influence of a solvent on vibrational frequencies and bandwidths. These theoretical models may often be applied to data obtained by different techniques such as Nuclear magnetic resonance (NMR), Electron Spin resonance (ESR) and vibrational spectroscopy (IR and Raman). Each model has adjustable parameters that can be used to fit the data. In these cases, the electromagnetic field causes a change of state in a reference system of nuclear spin or electronic spin states or the vibrational modes (vibrational energy levels) of molecules. The reference system (molecule) immersed in a liquid will have many degrees of freedom of the bath (rotational and translational). Thus, the states of the reference system will have a finite lifetime and energy width. This amounts to a decay of the time correlation function corresponding to the reference transition[10].

The band shape may provide valuable information about the interaction of the reference molecule with its environments and about the dynamics of the bath. The Laser Raman scattering experiments have been used to study the vibrational and rotational frequencies of molecules, which provides detailed information about the dynamic processes involved in

liquids. In case one wants to examine the reorientation and vibrational relaxation processes separately using vibrational (IR and Raman) spectroscopy, one has to study the well-isolated vibrational modes, which might provide good and clean spectra. From the experimentally observed I_{VV} and I_{VH} Raman band components (where I_{VV} and I_{VH} have their usual meanings)[24,26,27] , one can obtain the isotropic component $I_{iso}(\bar{\nu})$ and the anisotropic component $I_{aniso}(\bar{\nu})$ of the Raman spectrum. The isotropic and anisotropic components[11] are given by:

$$I_{iso}(\bar{\nu}) = I_{VV}(\bar{\nu}) - \frac{4}{3} I_{VH}(\bar{\nu})$$

$$I_{aniso}(\bar{\nu}) = I_{VH}(\bar{\nu})$$

where $\bar{\nu}$ denotes the frequency in cm^{-1}.

The peak frequencies of isotropic and anisotropic Raman bands of many molecules do not coincide in liquid state due to the orientationally dependent intermolecular forces [15, 16, 19-22]. The difference in peak position may sometimes be even more than 10 cm^{-1}. This is due to non-coincidence effect (NCE). The NCE is mostly associated with symmetric Raman active vibrational modes of polar molecules and is very pronounced for the modes, which are strongly infrared active. The solvent dependent studies have shown that the magnitude of the splitting decreases with increasing concentration of the solvent and tends to vanish in the limit of infinite

dilution. The effect has been observed in the CO stretches in carbonyls[12-15, 17, 24,25], CH stretches in chloroform[28] and CN in acetonitrile[29]. The NCE has been mainly attributed to the resonant transfer of vibrational excitation in the presence of local order due to strong interactions between permanent dipole moments. The most common source of resonant transfer relevant to the effect is due to transition dipole-transition dipole (TD-TD) coupling. This NCE has been interpreted as being due to the coupling between vibrations of neighbouring molecules, with strongly polar bonds by intermolecular dipole interactions in the liquid phase [6,11,12,30].

The vibrational Relaxation process consists of vibrational population relaxation and vibrational phase relaxation. The population (energy) relaxation involves vibrational inelastic processes and corresponds to what is called T_1 relaxation spin system, while phase relaxation (dephasing) involves only quasi-elastic interaction of the molecules with their surroundings leading to perturbation of the phase of the vibrational wave functions without changing their quantum states. It can be stated that in most cases vibrational lineshapes are mainly determined by dephasing, which corresponds to T_2 relaxation spin system in NMR. The study of vibrational phase relaxation has been an important endeavour of a chemical physicist in the attempt to understand and quantify the interaction of a chemical bond with the surrounding solvent molecule[1].

In liquids, the energy relaxation has longer lifetime in comparison with phase relaxation (dephasing). The vibrational phase relaxation process is responsible for the line broadening of the isotropic Raman band.

Different theoretical models on phase relaxation have been developed such as the hydrodynamic model[31-34], the isolated binary collision (IBC) model[35-39], the cell model[40,41] and the model based on resonant energy transfer[42-47].

A hydrodynamic model[31,36] can provide a good qualitative and semi-quantitative description of dephasing in molecular liquids. It seems likely that pure dephasing has more contribution. Moreover, the relaxation time of the random force is responsible for the viscosity dependence of the diffusion coefficient.

In the Isolated binary collision (IBC) model, the transition rate is assumed as the product of the collision rate in the liquid and the transition probability per collision in the gas phase. The probability per collision may be obtained either from scattering calculations or by independent experiments on low-density gases. Various models[35, 36] have been proposed for the collision rate in liquid phase. Fischer and Laubereau[35] introduced a gas like IBC model for pure dephasing in the liquid phase and applied it to a series of simple liquids. Litovitz[40] approximated the time between collisions to an Enskog time for the rate of binary collision of hard spheres using cell model. Again, Bratos and co-workers [42-43] used a stochastic model to study

the contribution of pure dephasing while the theoretical and experimental work of Döge et al[44] involved studies of the resonant transfer effect as well. Several authors [31,44,48-50] had shown that pure dephasing and resonant transfer are not truly separable and that the cross correlation between them can contribute significantly to the line shape.

One of the most important mechanisms that may contribute significantly to dephasing processes in liquids is the coupling between the similar modes of identical molecules (resonant energy transfer process). The interaction responsible for this coupling usually depends strongly on the relative orientation of the molecules. In some theoretical models, long-range (attractive) forces are involved. The collisional events are those, which have too short time of action to influence considerably the dephasing time. Consider the case of molecular harmonic oscillator that couples to the heat bath through translational diffusion where the effects of coupling of rotations to vibrations or translations are neglected. When dipole-dipole interactions and dispersion forces are included, there are three contributions to line broadening[46]. The first 'Self term', the second 'exchange term' and the third is 'cross self exchange term', respectively. The exchange term is due to the transfer of vibrational quantum states between two identical molecules through corresponding normal modes. This mechanism is normally referred as resonant energy transfer. It is possible to single out this particular kind of dephasing by performing dilution measurements.

Another important coupling mechanism is transition dipole-transition dipole (TD-TD) type[15], which is possible when strongly infrared active transitions are present. The resonant transfer mechanism is identified by dilution experiments with solvents, which reduces the coupling. Such experiments may exhibit band narrowing when dilution studies are carried out [46].

Vibrational Raman band shapes observed in the spontaneous Raman scattering process are broadened by homogeneous and inhomogeneous line broadening mechanisms. The homogeneous broadening yields information about the rapidly varying dynamic modulation processes responsible for vibrational dephasing. On the other hand, the inhomogeneous line broadening gives information about slowly varying modulation processes, which lead to a distribution of vibrational frequencies. The basis of the detailed study of vibrational dephasing is band shape and solvent induced frequency shift, which are due to the competition between slowly varying attractive forces and rapid collisional forces in a weak coupling regime. Although the vibrational resonance coupling due to TD-TD interaction may be important in some modes of polar molecules, it has been pointed out by Wang and Mchale[7] that the vibrational resonance coupling may also originate from quadrupole-quadrupole interaction or any other type of intermolecular interactions.

The Hamiltonian which determines the time evolution of the dynamic variables, is written as

$$H = H_{osc} + H_B + H_{coupl}$$

where H_{osc} is the sum of harmonic oscillator Hamiltonian, H_B is the bath Hamiltonian and H_{coupl} is the part of the Hamiltonian, which couples the internal vibrational coordinates of the bath molecules.

There are different mechanisms that can contribute to the coupling potential: dispersion interaction, dipole and multipole interactions and repulsive forces etc. Hence, in order to understand the nature of the intermolecular interactions and molecular dynamics, there is a need of detailed studies on vibrational relaxation, reorientational motion, frequency shifts, bandwidths and band shapes in various liquids. Several models have been proposed to describe the influence of a solvent on vibrational frequencies and bandwidths. These models characterize the solute-solvent interactions ranging from empirical or macroscopic quantities such as solvent donor and acceptor numbers or the dielectric constant and index of refraction to models based on microscopic statistical mechanical theories, which incorporate solvent-solute interactions at the molecular level [50].

Schweizer and Chandler[51] developed those models based on microscopic systems. These particular treatments are based on a partitioning of intermolecular forces into repulsive and attractive components. It is consistent with the van der Waals'/Weeks-Chandler-Andersen (WCA)

picture of fluids, where the short-range repulsive forces determine the fluid structure and the longer-range attractive forces can be treated by perturbation theories. This approach allows one to relate the solvent contributions to the vibrational frequencies and bandwidths to intermolecular interactions involving repulsive and attractive forces [50].

Schiebe and Döge[46] have given a simple theoretical approach to the behaviour of various band shape parameters in terms of dipole-dipole interaction in the frequency domain. The structure effect seems to play an important role in influencing the band shape of polar Raman bands in liquids with dipole-dipole interaction energies of the order of thermal energy k_BT. The asymmetry of the I_{VV} component of the band was explained based on the change in the orientation probability distribution into the direction of energetically favourable orientation. However, the theoretical approach is too simple to allow more than a qualitative interpretation of the experimental data. When the dipole sizes are comparable with those of solvent molecules, the fundamental problem lies in the determination of an effective electric permittivity of the medium. The two interacting situations in pure solute and when dissolved in solvents, differ markedly at high dilution. The solvent electric field influences the band shape of a reference mode significantly. Moreover, a considerable amount of information about vibrational relaxation and non-coincidence can be obtained by analyzing the experimentally measured band shapes of the isotropic and anisotropic

components of the Raman band of molecular liquids. The band shape of the reference mode is influenced by the concentration fluctuations of the environment in liquid mixtures. The microscopic environment affects the behaviour of a reference molecule in a very significant manner. It is therefore necessary to study the vibrational relaxation and NCE in the complex molecular systems from microscopic point of view. Moreover, the solvent effects on the NCE (anisotropy shift) and variation of bandwidth in dipolar liquids may offer new information about strong inter and intra-molecular interactions. Therefore in the present work, we have studied the Raman band shapes of the C=O stretching vibration of o-chlorobenzaldehyde (OCBD) and Methyl isobutyl ketone (MIBK) molecules in different polar and non-polar solvents. The C=O stretching mode of the carbonyl containing molecules have been chosen for the present study because of the following particular characteristics.

(1) It lies at high frequencies, so the condition $\hbar\omega >> k_B T$ is always true.

(2) Usually it is little mixed and / or coupled with other vibrations, which means that its normal coordinate may be considered as a pure one.

(3) It is well isolated from other modes of vibration in the molecules under present study.

It is, therefore, particularly suitable for probing the molecular environment and is expected to give detailed information regarding the complex

molecular systems. Moreover, these molecules have applications in chemical and biological fields. The experimental results have been explained using the concept of microenvironment, the role of hydrodynamic forces, the effective van der Waals' volume and the effect of reaction field (solvent reaction field) on the solute. These molecules with strong interactions have not been investigated fully from the vibrational relaxation and microscopic point of view. A rigorous description of the solution should take into account both the separation between molecules and their orientation with respect to each other. In this work the potential function, which incorporates the repulsive and dispersion forces found in regular fluids and the contributions of multipolar moments, specifically dipole and /or quadrupole moments have been investigated. In polar liquids, the existence of local orientational order assists the intermolecular coupling between identical vibrations in nearby molecules and induces the transfer of vibrational energy between them. The phenomology associated with this process appears in the Raman bands of these vibrations through the non-coincidence of their isotropic and anisotropic profiles mentioned earlier. In fact, the non-coincidence of the peak frequencies of the isotropic and the anisotropic components in Raman spectra has always been considered an efficacious probe of the structure and dynamics of polar liquids. We have focussed on the NCE by taking into account the screening factor related to the permanent and transition dipoles. The study of the anisotropic

components of the Raman bands were undertaken by taking into account the van der Waals' volume of the interacting system in order to interpret the various interactions involved in solute-solvent interaction. The NCE for OCBD was studied in CCl_4, CH_3CN, $CH_3C_6H_5$ and C_6H_5Cl solvents. The anisotropic bandwidth and the effect of van der Waals' volume of solute-solvent systems were also studied for OCBD in different solvents in order to understand about the intermolecular interactions in liquid mixtures.

Vibrational dephasing of the C=O stretching mode of OCBD is very sensitive to the details of the interaction potentials and it can be used to probe the influence of the solvent. The dephasing processes have been studied using relaxation time obtained from the FWHM of the isotropic component of Raman band of C=O stretching mode of *o*-chlorobenzaldehyde (OCBD) using various polar and non-polar solvents.

The anisotropic component of the Raman band gives information about the angular dependent intermolecular forces. These forces could be attractive as well as repulsive and may arise due to multipolar interaction or dispersion forces. The anisotropic bandwidth of C=O stretching mode of Methyl Isobutyl Ketone (MIBK) has also been studied in benzene, carbon tetrachloride, methylbenzene, chlorobenzene, acetonitrile and chloroform solvents by taking into account the van der Waals' volume of the sphere of influence in solute dissolved in the solvents.

The choice of these solvents was such that the solvent molecules are of different size and shape, multipolar moments and dielectric constants. The benzene and substituted benzene molecules have significant effects in solute-solvent interactions from the point of view of quadrupole moment and plate like structure. The CH_3CN and CCl_4 molecules have dipole moment and octupole moment, respectively and different in shapes having cylindrical and spherical shapes. The $CHCl_3$ has a symmetric top structure and provides the possibility of hydrogen bonding through C-H bond as H is an acidic hydrogen / proton. These molecules, because of different size shape and electrical properties may be of considerable help in the study of the intermolecular forces.

REFERENCES:

1. D.W. Oxtoby, Adv.Chem.Phys. **40**, 1 (1979).
2. S. Bratos, Vibrational Spectroscopy of Molecular liquids and solids, edited by S. Bratos and R. M. Pick (Plenum, New York,1980).
3. H. D. Thomas and J. Jonas, J. Chem. Phys. **90**, 4632 (1989).
4. Ying-Te Lee, J. Raman Spectrosc. **28**, 45 (1997).
5. S. Nugent and B. M. Ladanyi, J. Chem. Phys. **120**, 874 (2004).
6. G. Fini and P.Mirone, Spectrochim. Acta, **32A**, 625 (1976).
7. C. H. Wang and J. Mchale, J. Chem. Phys. **72**, 4039 (1980).
8. J. L. Mchale, J. Chem. Phys. **75**, 30 (1981).
9. W. Schindler, P.T. Sharko and J. Jonas, J. Chem. Phys. **76**, 3493 (1982).
10. D. W. Oxtoby, J. Phys. Chem. **87**, 3028 (1983).
11. W. Schindler, T. W. Zerda and J. Jonas, J. Chem. Phys. **81**, 4306 (1984).
12. A. Purkayastha, and K. Kumar, Spectrochim. Acta, **42A**, 1379 (1986).
13. A. Purkayastha and K. Kumar, Spectrochim. Acta, **43A**, 1269 (1987).
14. A. Purkayastha and K. Kumar, J. Raman Spectrosc. **19**, 249 (1988).
15. T. F. Sun, J. B. Chan, S.L. Wallen and J. Jonas, J. Chem. Phys. **94**, 7486 (1991).
16. R. J. Bartholomew and D. E. Irish, J. Raman Spectrosc. **29**, 115 (1998).
17. A. Das and K. Kumar, J.Raman Spectrosc. **30**,563 (1999).

18. A. Morresi, P. Sassi, M. Ombelli, R. S. Cataliotti and G. Paliani, J. Raman Spectrosc. **31**, 577 (2000).

19. A. Morresi, M. Paolantoni, P. Sassi, R. S. Cataliotti and G. Paliani, J. Phys. Condens. Matter. **12**, 3631 (2000).

20. M. G. Giorgini, M. Musso, A. Asenbaum and G. Doge, Mol. Phys. **98,** 783 (2000).

21. M. G. Giorgini, M. Musso and P. Ottaviani, Mol. Phys. **99**, 1485 (2001).

22. M. Musso, H. Torii, P. Ottaviani, A. Asenbaum and M. G. Giorgini, J. Phys.Chem. **106A**, 10152 (2002).

23. N. Lebum, P. Dhamelincourt, C. Focsa, B. Chazallon, J. L. Destombes and D. Prevost, J. Raman Spectrosc. **34**, 459 (2003).

24. A. Das and K. Kumar, Spectrochim. Acta, **54A**, 793 (1998)

25. A. Sokolowska, J. Raman Spectrosc. **30,** 507(1999).

26. M. A. Ricci, G. Signorelli and V. Mazzacurati, J. Phys.Condens. Matter, **2**, 183 (1990).

27. C. J. Fecko, J. D. Eaves and A. Tokmakott, J. Chem. Phys. **117**, 1139 (2002).

28. G. Döge, D. Schneider and A. Morresi, Mol. Phys. **80**, 525 (1993).

29. G. Fini and P. Mirone, Spectrochim. Acta. **32A**, 625 (1976).

30. R. J. Bartholomew and D. E. Irish, J. Raman Spectrosc. **30**, 325 (1999).

31. D. W.Oxtoby, D. Levesque and J. J. Weis, J. Phys. Chem. **68**, 5528 (1978).

32. D.W.Oxtoby, J. Phys. Chem. **70**, 2605 (1979).

33. R. Ouillon, V. Sergiescu and R. J. D' Leon, Mol.Phys. **49**, 151 (1983).

34. P. S. Dardiaw, R. I. Culier, J. Chem. Phys. **89**, 4415 (1988).

35. S. F. Fischer and A. Laubereau, Chem. Phys. Lett. **35**, 6 (1975).

36. D. W. Oxtoby and S. A. Rice, Chem. Phys. Lett. **42**, 1 (1976).

37. E. W. Knapp and S. F. Fischer, J. Chem. Phys. **74**, 89 (1981).

38. E. W. Knapp and S. F. Fischer, J. Chem. Phys. **76**, 4730 (1982).

39. G. Moser, A. Asenbaum, J. Barton and G. Döge, J. Chem. Phys. **102**, 1173 (1995).

40. F. J. Bartoli and T. A. Litovitz, J. Chem. Phys. **56**, 404 (1972).

41. D. J. Diestler and J. Manj, J. Mol. Phys. **33**, 227 (1977).

42. S. Bratos, J. Rios and Y. Guissani, J. Chem. Phys. **52**, 439 (1970).

43. S. Bratos and E. Marechal. Phys. Rev. **A4**, 1078 (1971).

44. G. Döge, R. Arndt and A. Khuen, Chem. Phys. **21**, 53 (1977).

45. P. Mirone and G. Fini, J. Chem. Phys. **71**, 2241 (1979).

46. D. Schiebe and G. Döge, Ber. Bunsenges. Phys. Chem. **85**, 520 (1981).

47. M. G. Giorgini, G. Fini and P. Mirone, J. Chem. Phys. **79**, 639 (1983).

48. R. Lynden-Bell, Mol. Phys. **33**, 907 (1977).

49. R. Wertheimer, Mol. Phys. **35**, 257 (1978).

50. G. J. Remar and R. A. Macphail, J. Chem. Phys. **103**, 4381 (1995).

51. K. S. Schweizer and D. Chandler, J. Chem. Phys. 76, 2296 (1982).

CHAPTER 2

CHAPTER 2

THEORETICAL ASPECTS

INTRODUCTION

The analysis of the vibrational band shapes can provide valuable information about the interactions and structural dynamics in liquids. Our main aim is the study of molecular vibrations by the laser Raman scattering as it provides a detailed information about a specific dynamic process in the liquid. In Raman scattering, a photon is scattered by the molecular system. Most photons are elastically scattered and this process is called Rayleigh scattering. Raman spectroscopy is based on the inelastic scattering of photons by molecules. The energy of the scattered radiation is less than the incident radiation for the Stokes line and the energy of the scattered radiation is more than the incident radiation for the anti-stokes line. For a vibration to be Raman active there must be a change in polarizability of the molecule during the vibration.

Vibrational relaxation studies in liquids have made a considerable progress through experiment, theory and computer simulation towards a deeper understanding of the physical processes involved. Vibrational phase

and energy relaxation time can be as short as few picoseconds and may thus be comparable to bath relaxation time. This has important consequences for the dynamics of the coupled systems[1-5]. In small molecules, reorientation provides the primary relaxation mechanism for allowed transitions. For larger molecules, vibrational relaxation mechanisms play an increasingly important role.

When a vibrationally excited molecule collides with a ground state molecule of the same species, there are three possible outcomes:

(1) The vibrational energy could be transferred to translations, rotations or different vibrational degrees of freedom (population relaxation).

(2) The vibrational excitation could be transferred resonantly to the other molecule, giving no net change in vibrational population (resonant transfer).

(3) The collision could be vibrationally elastic, with only the phase of the wavefunction changing (pure dephasing).

In liquid phase, population relaxation events usually need relatively long lifetime in comparison with phase relaxation events. All three types of collisions will give rise to broadening of the isotropic Raman line. In most cases, the pure dephasing is found to have more contribution in vibrational band shape analysis.

The general approach [2-5] of the vibrational dephasing process is the partition of the degrees of freedom of the molecules and the surroundings

into two groups, the exchanging group and the reservoir. Vibrational frequencies correspond to larger range of frequencies (~ 500 - 4000 cm^{-1}) whereas at room temperature, the thermal energy k_BT corresponds to about 200 cm^{-1}. As a result, a few states are thermally populated. On the other hand, rotational and translational modes have lower frequencies so that more states are thermally populated and it is not meaningful to describe them as discrete levels. Vibrational dephasing then occurs through the coupling of a quantum vibrational system to a classical heat bath of rotational and translational degrees of freedom.

2.1 ORIGIN OF VIBRATIONAL RELAXATION PROCESSES IN MOLECULAR LIQUIDS

Vibrational relaxation in the condensed phase is relevant in many aspects of chemical behaviour and photophysical processes [6]. The study of this process can provide useful information about the molecular motion and various complex intermolecular interactions in liquids. Moreover, one can use this process to elucidate solute-solvent interactions and intra-molecular couplings. Vibrationally excited solute molecules relax due to interactions with the solvent environment. The vibrations of a molecule are sensitive probes of local structure and dynamics in molecular liquids and give microscopic information about the processes involved. The widths and

positions of spectral transitions provide a wealth of information about the intermolecular interactions of the solute with the solvent [7-11].

For a well-separated vibrational transition, there are various sources of line broadening. The three primary sources of line broadening and of vibrational phase relaxation are considered as lifetime broadening, environmental broadening (pure dephasing) and resonance transfer [5].

Lifetime broadening arises due to the uncertainty principle. This uncertainty broadening generally makes small contribution to the bandwidth.

Environment broadening which arises from the fact that the vibrational frequency of a molecule **i** is perturbed by its interaction with other molecules and therefore has a component $\Delta\omega_i$ (t) which fluctuates with time[2-5]. The isotropic Raman lineshape is dependent on the vibrational phase relaxation. The isotropic Raman band shape due to solvent induced frequency fluctuations is given by the Fourier transform of $< Q_i$ (t) Q_i (0)>, where the angular brackets define an ensemble average vibrational co-ordinates Q_i at time t and differs from $Q_i(0)$ by a phase factor $\exp[\phi_i(t) - \phi_i(0)]$ and thus provide direct information about the dephasing rates[4].

The phase difference is given by

$$<\phi_i(t) - \phi_i(0)> = \varpi t + \int dt' \Delta\omega_i (t') \qquad \textbf{(2.1.1)}$$

where ϖ is the average vibrational transition frequency in the liquid and $\Delta\omega_i(t')$ gives the fluctuation in frequency due to the environment.

The vibrational phase relaxation is given by [12,13]

$$\langle Q_i(t)Q_i(0)\rangle = \mathrm{Re}\left\langle \exp\left[i\int dt'\Delta\omega_i(t')\right]\right\rangle e^{i\omega_0 t} \qquad (2.1.2)$$

where ω_0 is the gas phase transition frequency and $\hbar\Delta\omega_i(t) = V_{11}(t) - V_{00}(t)$ where $\mathbf{V}_{ii}$ is the unperturbed vibrational matrix element of the interaction Hamiltonian coupling the vibration to the bath of classical translational and rotational degrees of freedom. If we consider the autocorrelation function of $\Delta\omega_i(t)$ i.e.$\langle\Delta\omega_i(t)\Delta\omega_i(0)\rangle$, the bath relaxation time may then be defined [4,5] through

$$\tau_c = \int_0^\infty dt \frac{\langle \Delta\omega_i(t)\Delta\omega_i(0)\rangle}{\langle \Delta\omega_i(0)\Delta\omega_i(0)\rangle} \qquad (2.1.3)$$

The nature of the band shape depends on the relative magnitude of the two characteristic frequencies $\langle\Delta\omega_i^2\rangle^{1/2}$ and τ_c^{-1}. We may define a modulation regime depending on the value of $\langle\Delta\omega_i^2\rangle^{1/2}\tau_c$. When $\langle\Delta\omega_i^2\rangle^{1/2}\tau_c \gg 1$, the active molecule undergoes a perturbation for a long time. If it was possible to freeze the environment at a particular time, one would observe a distribution of frequency shift and a broadened vibrational band shape

(Gaussian) is obtained. This is referred to as static limit. While when$<\Delta\omega_i^2>^{1/2}\tau_c<<1$, we have the rapid modulation limit where there is a perturbation for a short time on the active molecule and the band is narrowed to a Lorentzian curve with full width at half maximum (in cm^{-1}) given by

$$\mathbf{fwhm} = <\Delta\omega_i^2>^{1/2}\tau_c \qquad \mathbf{(2.1.4)}$$

The contribution to vibrational line broadening is resonance transfer, or excitonic broadening which usually appears in pure liquids. If two identical molecules are brought together, the energy levels, which were earlier degenerate, will now split with one moving higher and the other lower. If a large number of molecules are brought together this splitting gives rise to a broad excitonic band.

When a molecule is surrounded by isotopically substituted molecules, the potential will change slightly while the vibrational frequency may be shifted sufficiently out of resonance to eliminate the excitonic broadening. The resonance energy transfer (RET) and environmental broadening are dependent. In fact, the resonance transfer may even lead to a narrowing of the isotropic Raman band. It has been experimentally verified that the position of the peak frequencies for isotropic and anisotropic Raman band components do not coincide for the case of vibrational modes involving RET. This is termed as non-coincidence effect (NCE) or anisotropy shift. The

I_{aniso} (ν) and I_{iso} (ν) give information about the angular dependent and the angular independent (spherically symmetric average value) of the potential respectively. Due to these different dependences, the two components exhibit not only different shapes but the peak positions are also shifted to a different extent leading to a non-vanishing splitting factor

$$\delta\nu = \nu\,(\text{aniso}) - \nu\,(\text{iso}) \qquad (2.1.5)$$

The NCE for polar liquid molecules provide valuable information about the liquid coupling mechanisms of short range orientational order which arise from intermolecular resonant vibrational interactions between neighbouring molecules that give rise to delocalization of vibrational modes. It is influenced by the molecular local order in the liquid itself. The orientational dependent intermolecular forces are also responsible for the NCE in liquids. NCE is considered as an efficacious probe for the dynamics of polar liquids[14-18]. Hence, a detailed knowledge about the perturbing coupling potential between the molecules and the bath is required in order to explain the mechanism of the vibrational relaxation and NCE.

(a) Isolated binary collisional model:

Fischer and Laubereau[19] proposed a model based on semi-classical collision theory to describe the dephasing of vibrationally excited molecules in a liquid. In this model, both the energy dissipated and the pure dephasing

are considered to be independent processes and the dephasing time τ is written as

$$\tau^{-1} = \tau_{ph}^{-1} + \tau_E^{-1} \qquad (2.1.6)$$

where τ_{ph}^{-1} is the dephasing term due to pure dephasing caused only by quasi-elastic collisions and τ_E^{-1} is the energy relaxation time.

However, this model does not reflect the whole complexity of the liquid environment because of difficulties in estimating some parameters for complex molecules. The values of anharmonicity and the reduced mass of the molecules were neglected in this model, which has been rectified by the hydrodynamic model proposed by Oxtoby [6].

(b) The Hydrodynamic model:

A hydrodynamic model can provide a good qualitative and semi-quantitative description of dephasing in molecular liquids. In hydrodynamic approach, a vibrating molecule is modelled as a macroscopic body embedded in a viscoelastic continuum. Oxtoby[12] presented a hydrodynamic model for the dephasing of molecular vibrations in liquids, which included the effects of vibrational anharmonicity. This model has correctly predicted the shortcomings of the hydrodynamic model [20] including the sphere in a viscous continuum with slip boundary condition and the negative minimum

in the velocity autocorrelation function. The expression for the dephasing rate of polyatomic system is of the form

$$\tau_v^{-1} = \eta T \qquad (2.1.7)$$

showing the dependence on viscosity η and temperature T. It has been found that the pure dephasing is playing a major contribution in the isotropic bandwidth study.

The model constructed by Schweizer and Chandler[21] shows the effects of repulsive and spatially slowly varying attractive forces on the vibrational frequency and dephasing of polyatomic molecular liquids. This model simultaneously examines both the broadening mechanisms and the frequency shifts. The theory of Schweizer and Chandler is more illustrated by the theory proposed by Ben Amotz et al [22]. The short-range repulsive and long-range attractive forces compete with each other to produce solvent and pressure-induced frequency shifts. A cavity distribution function was introduced to describe the repulsive frequency shift, while a van der Waals' mean field approximation was used for the attractive contribution.

(c) Resonant Energy Transfer:

The resonant energy transfer (RET) process occurs due to the interaction between the identical molecules[5]. In this process, the microscopic local order in liquid phase permits the coupling between the vibrational

states of the molecule through neighbouring transition dipoles and leads to anisotropy shift or non-coincidence effect (NCE).

The coupling potential V can be expanded in a Taylor series [4,23-24] as a function of normal co-ordinates **Q**

$$V = V_0 + \left(\frac{\delta V}{\delta Q_j}\right)_0 Q + \frac{1}{2}\left(\frac{\delta^2 V}{\delta^2 Q_j}\right)_0 Q^2 + \frac{1}{2}\sum_{ij}\left(\frac{\delta^2 V}{\delta Q_i \delta Q_j}\right)_0 Q_i Q_j + \qquad \textbf{(2.1.8)}$$

The first three terms are similar to the potential of a harmonic oscillator corresponding to a normal coordinate $\mathbf{Q_j}$. By choosing the energy of the equilibrium configuration to be zero, $\mathbf{V_o}$ may be eliminated. The last term is responsible for resonant energy transfer from one oscillator to another and leads to NCE.

Since $\mathbf{V} \leq \mathbf{H_o}$, the first order perturbation calculation for the frequency difference between the ground and first excited states can be performed leading to the expression

$$\Delta E = \left(\frac{\delta V}{\delta Q}\right)_0 \left(\langle 1|Q|1\rangle - \langle 0|Q|0\rangle\right) + \frac{1}{2}\left(\frac{\delta^2 V}{\delta^2 Q}\right)_0 \left(\langle 1|Q^2|1\rangle - \langle 0|Q^2|0\rangle\right) + \left(\frac{\delta^2 V}{\delta Q_i \delta Q_j}\right)_0 \left(\langle 1|Q|0\rangle\right)^2 \qquad (2.1.9)$$

In the above equation, the first term corresponds to mechanical anharmonicity, the second term to electrical anharmonicity and the last term

to resonance interaction. $<1|Q|1> - <0|Q|0>$ vanishes for a harmonic oscillator, but in real molecules we deal with anharmonic oscillators.

The electrical anharmonicity is the nonlinear part of the variation of the dipole moment with normal coordinates. It can give intensity to overtones and combination tones. The change in the electric dipole moment of a diatomic molecule during a vibration can be expressed in a Taylor series

$$\mu = \mu_0 + \left(\frac{\delta \mu}{\delta Q}\right)_0 Q + \left(\frac{\delta^2 \mu}{\delta Q^2}\right)_0 Q^2 + \qquad \textbf{(2.1.10)}$$

where μ_0 is the permanent dipole moment of the molecule and the sum of the terms higher than linear terms is called electrical anharmonicity.

The third term in equation (2.1.9) is the resonance interaction term given by

$$\Delta E_{res} = \left(\frac{\delta^2 V}{\delta Q_i \delta Q_j}\right)_0 \left(<1|Q|0>\right)^2 \qquad \textbf{(2.1.11)}$$

The most common source of resonant transfer relevant to the NCE is due to the transition dipole-transition dipole coupling[25].

Considering the interaction potential between two identical molecules

$$V = (\mu^2 / R_{ij}^3)\, K_{ij} \qquad \textbf{(2.1.12)}$$

where μ is the dipole moment of the molecule, $\mathbf{R_{ij}}$ is the distance between the two dipoles and $\mathbf{K_{ij}}$ is the geometric factor describing the relative orientation of the two dipole moments.

For point dipoles, $K_{ij} = 2\cos\theta_i \cos\theta_j + \sin\theta_i \sin\theta_j \cos\Phi_{ij}$

where θ_i is the angle between the dipole moment vector of molecules i and the ij vector which connects molecules i and j, Φ_{ij} is the angle between the perpendicular components of the dipole moments of the molecules i and j. The equation (2.1.11) can therefore be written as

$$\Delta E_{TD\text{-}TD} = \left(\frac{\delta \mu}{\delta Q}\right)^2 \left\langle \frac{K_{ij}}{R_{ij}^3} \right\rangle \left(< 1|Q|0 > \right)^2 \qquad \textbf{(2.1.13)}$$

For the dipole-dipole coupling, the splitting factor is given by

$$\delta\nu = \nu \text{ (out of phase)} - \nu \text{ (in phase)}$$

$$\propto \left\langle \frac{K_{ij}}{R_{ij}^3} \right\rangle \left(\frac{\delta \mu}{\delta Q}\right)^2 \qquad \textbf{(2.1.14)}$$

The brackets indicate an ensemble average for different relative orientations where the anisotropic component of the band is shifted in various degrees depending on the magnitude of the orientational factor K_{ij}.

At infinite dilution, the splitting factor reduces to zero i.e. the isotropic and anisotropic Raman components tend to coincide. The quantity $\left\langle \frac{K_{ij}}{R_{ij}^3} \right\rangle$ is difficult to calculate and hence the equation (2.1.14) reduces to proportionality as

$$\delta \nu \infty \left(\frac{\delta \mu}{\delta Q} \right)^2 \qquad (2.1.15)$$

The quantity $\left(\frac{\delta \mu}{\delta Q} \right)^2$ is proportional to the infrared absorption coefficient for a given vibration. Hence, the Raman bands studied corresponding to the strong IR absorption exhibit the non-coincidence effect.

Logan[25] presented a theory based on the NCE and according to it, the NCE has been attributed to resonant transfer of vibrational excitation in the presence of local order due to strong interaction between permanent dipoles. In this resonant excitonic transfer process, the main interaction is due to transition dipole-transition dipole coupling. Thus the Logan's theory satisfied the RET (resonant energy transfer) process; however it does not always give good approximation for the dispersion effect. Logan's approach assumes only point dipoles whereas it is necessary to account for the dipoles of finite length and repulsive interactions should be considered. According to Wang and Mchale[26], the NCE can be explained by the induced dipole-induced dipole interaction mechanism. Giorgini et al [27] studied the Logan's theory and found valuable information regarding the NCE based on thermodynamic state.

(d) Kubo method of Correlation function:

Kubo[28] developed a general theory of relaxation mechanism that has been adapted by several workers to explain the vibrational relaxation. This theory has been applied to vibrational dephasing via resonant energy transfer due to modulation of long-range dipolar potentials and to other dephasing mechanisms involving short-range potentials[29]. Using this theory, the correlation functions, which involve the process of pure dephasing, are given by the expression,

$$\Phi_{pp}(t) = \exp[-\langle\Delta\omega_i^2\rangle\{\tau_c^2(e^{-t/\tau c} - 1) + t\tau_c\}] \qquad \textbf{(2.1.16)}$$

where τ_c is the correlation time describing the fluctuations in the intermolecular potential, $\langle\Delta\omega_i^2\rangle$ is the root mean square frequency displacement of the instantaneous transition frequency. It measures the range of frequency distribution due to various molecular interactions. The τ_c and $\langle\Delta\omega_i^2\rangle$ contain valuable information about the nature of the intermolecular potential. In the slow modulation limit, where $\langle\Delta\omega_i^2\rangle >> \tau_C^{-1}$, the broadening of the vibrational band is inhomogeneous and the linewidth and lineshape reflect the width and shape of the static probability distribution for the frequency fluctuations which is often assumed to be Gaussian.

In the fast modulation limit, $<\Delta\omega_i^2> << \tau_C^{-1}$, the broadening is homogeneous and the lineshape is narrowed to a Lorentzian [30].

$$\left\langle \Delta\omega_i^2 \right\rangle = \frac{\int_{band} I_{iso}(\omega)\omega^2 \, d\omega}{\int_{band} I_{iso} \, d\omega} \qquad \textbf{(2.1.17)}$$

The above expression (2.1.17) can be modified into two extreme cases of short and long times[31]. In the slow modulation limit, the phase relaxation functions are described by the vibrational second moment $<\Delta\omega_i^2> = (M_2)_v$ and in the rapid modulation limit, the vibrational relaxation rate is taken to be directly proportional to the product of parameters $(M_2)_v$ and τ_c and thus the relaxation rate [32] is given by

$$\tau_v^{-1} = (M_2)_v \tau_c \qquad \textbf{(2.1.18)}$$

$$= <\Delta\omega_i^2> \tau_c \qquad \textbf{(2.1.19)}$$

The vibrational relaxation time can be defined as

$$\tau_v = \int_0^\infty \phi_{pp}(t) dt \qquad \textbf{(2.1.20)}$$

This is for the case of long approximation.

For the fast modulation regime,

$$\tau_v = (\pi c FWHM)^{-1} \qquad \textbf{(2.1.21)}$$

where FWHM= full width at half maximum of I_{iso} and c is the velocity of light.

For the slow modulation limit, from (2.1.19)

$$\tau_v^{-1} = \langle \Delta\omega_i^2 \rangle \tau_c$$

$$\tau_v = (\langle \Delta\omega_i^2 \rangle \tau_c)^{-1} \qquad \textbf{(2.1.22)}$$

Therefore depending upon the rate of modulation process, one may predict the band profile. Thus, the Kubo lineshape theory is appropriate in determining the vibrational dephasing. In case of long-range dipolar interaction, τ_c is directly proportional to dynamic viscosity and hence the vibrational relaxation rate is expected to depend on the viscosity of the medium. The band shapes considered so far are of well-isolated transitions present nearby or overlap; there can be further contributions to phase relaxation and spectral broadening[33].

(e) Screening effect on vibrational relaxation:

The difference between the peak frequencies of the isotropic and anisotropic Raman spectra is termed as anisotropy shift or non-coincidence effect. According to Mirone et al[34], the anisotropy shift is the result of vibrational coupling of transition dipoles in microscopic local order due to the strong interaction between permanent dipoles. They proposed empirical equations involving the macroscopic properties to elucidate the behaviour of I_{iso} and I_{aniso} in the pure liquid.

$$\Delta\nu = \Delta\nu_{neat}\frac{\varepsilon_1}{1-\phi_0}\frac{\phi-\phi_0}{\varepsilon_1\phi-\varepsilon_2(1-\phi)} \quad ,\phi > \phi_0 \qquad (2.1.23)$$

$$= 0 \qquad ,\phi < \phi_0$$

where $\Delta\nu_{neat}$ is the isotropic and anisotropic separation of a pure liquid solute, ε_1 and ε_2 are the static dielectric constants of pure solute and solvent, ϕ is the volume fraction of the solute and ϕ_0 is the value of the volume fraction at which $\Delta\nu$ becomes zero. If $\phi < \phi_0$, energy relaxation mechanisms are assumed to be active, whereas $\phi > \phi_0$, resonance intermolecular vibrational coupling is playing an important role.

Wang and Mchale[26,35] developed a general expression for a coupling Hamiltonian and concluded that short- range reorientational order is not the fundamental mechanism for the non-coincidence effect (NCE). The NCE is given by

$$\Delta\nu_{NCE} = \nu_{aniso} - \nu_{iso} \qquad (2.1.24)$$

$\Delta\nu_{NCE}$ can be taken positive or negative depending on the physical properties involved. The angular dependent resonance coupling interaction potential is the main factor for exhibiting the NCE.

In transition dipole coupling model, the expression [34-36] for $\Delta\nu_{NCE}$ is given by

$$\Delta\nu_{neat} = \frac{2\mu^2\left(\frac{\delta\mu}{\delta Q}\right)^2}{25\pi^2 c^2 \nu_0 \, kTd^3} \frac{N_0}{V_M}\phi S \qquad (2.1.25)$$

where μ is the dipole moment, Q and ν_0 are the normal co-ordinates and wavenumber of the vibrational mode under consideration, $\frac{\delta\mu}{\delta Q}$ is the dipole moment derivative, d is the minimum intermolecular distance, N_0 is Avogadro's number, V_M is the molar volume of the solute, ϕ is the volume fraction of the solute, c is the velocity of light and S is the screening factor for the interaction energy of two dipoles.

The screening factor S comprises of two factors S_p, screening factor due to permanent dipoles and S_t, screening factor due to transition dipoles.

Following the Onsager-Fröhlich model, which treats the dielectric as a continuum and the dipoles as point dipoles, the screening factor due to permanent dipoles S_p has the form

$$S_p = \left(\frac{n^2+2}{2\varepsilon+n^2}\right)^2 \varepsilon$$

where n is the refractive index of the solute and ε is the dielectric constant.

According to Giorgini et al[36], the value of S_p and S_t are given as follows

$$S_p = \left(\frac{n^2+2}{2\varepsilon+n^2}\right)^2 \varepsilon \quad \text{and} \quad S_t = \frac{(n^2+2)^2}{9n^2} \tag{2.1.26}$$

Comparing S_p and S_t, the screening factor S_t does not vary much with the variation of the solvent as the variation of refractive index is very less.

Therefore using equation (2.1.25)

$$\Delta\nu = \frac{2\mu^2\left(\frac{\delta\mu}{\delta Q}\right)^2}{25\pi^2 c^2 \nu_0 kTd^3} \frac{N_0}{V_M} \phi \left(\frac{n^2+2}{2\varepsilon+n^2}\right)^2 \varepsilon$$

That is,

$$\Delta\nu(2\varepsilon+n^2)^2\varepsilon^{-1} = \frac{2\mu^2\left(\frac{\delta\mu}{\delta Q}\right)^2 (n^2+2)^2}{25\pi^2 c^2 \nu_0 kTd^3 V_M} N_0\phi \tag{2.1.27}$$

This is another form of expressing the anisotropy shift using the simple dielectric model of Onsager-Fröhlich.

2.2 INTERMOLECULAR INTERACTION IN LIQUIDS:

Consider the interacting system of the molecules, which are located in such a way that the separation is large enough to avoid the overlapping of electronic orbital. In this range of large separations, we can consider different types of interaction depending on the presence of the interacting molecules. They are

1. Keesoms forces or dipole-dipole effect:

These forces arise due to the interaction between the permanent dipole moments of the molecules and are dependent on temperatures. The strength of a dipole-dipole interaction depends on both the dipole centers separation and their relative orientation [37].

In a generalized form, the interaction potential between two molecules of dipole moments μ_i and μ_j at positions r_i and r_j which tend to align both molecules [38] is

$$V_{or}(r_{ij}) = \mu_i \nabla_i \nabla_j \left| r_i - r_j \right|^{-1} \mu_j \qquad (2.2.1)$$

The orientation giving the lowest energy is the parallel alignment of the two molecules along the joining vector $r_{ij} = r_i - r_j$.

The interaction energy [39] for such system can be written as

$$V_{or} = -\frac{2\mu_i\mu_j}{r_{ij}^3} \text{ for } k_BT << \frac{\mu_i\mu_j}{r_{ij}^3}$$

$$= -\frac{2\mu_i^2\mu_j^2}{3k_BT\,r_{ij}^6} \text{ for } k_BT >> \frac{\mu_i\mu_j}{r_{ij}^3} \qquad (2.2.2)$$

where the orientation effect of both the dipoles have been considered leading to the doubling of interaction energy. This orientation effect is for the molecule, which possesses permanent dipoles. However, at high temperature, any alignment vanishes due to the thermal motion. The dipole-dipole interaction is relatively weak over the large distances of separation because of the $1/r^6$ distance dependence. However, over short distances of separation, dipole-dipole interaction is quite important.

2. Debye forces or the dipole-induced dipole effect:

Forces which result from the interaction of a permanent dipole and induced dipoles are known as Debye forces. Debye pointed out that molecules having permanent dipole moments not only align but also polarize each other. An induced dipole rotates simultaneously with the inducing dipole, so that a temperature independent energy gains results.

If a molecule i exhibits a permanent dipole μ_i, then the dipole induced at molecule j is $\mu_i \nabla_i \nabla_j r_{ij}^{-1} \alpha_j$.

The interaction potential of two dipoles[38] is given by

$$V_{ind}(r_{ij}) = \left(-\frac{1}{2}\right)\mu_i \nabla_i \nabla_j r_{ij}^{-1} \alpha_j \nabla_i \nabla_j r_{ij}^{-1} \mu_j \qquad \textbf{(2.2.3)}$$

The factor (1/2) arises due to dipole μ_j induced by μ_i and α_j is the polarizability of molecule j.

At high temperature, all orientations contribute according to Boltzmann statistics,

$$\Delta E_{ind} = -\frac{\left(\alpha_j \mu_i^2 + \alpha_i \mu_j^2\right)}{r_{ij}^6} \qquad \textbf{(2.2.4)}$$

This induction effect yields an attraction proportional to r_{ij}^{-6}. With the increase in temperature, the induction effect decreases but does not vanish its value. The dipole-induced dipole interaction exists only when the distance of separation is very small and therefore the energy involved for large distance of separation is extremely low.

3. London forces or dispersion effect:

The interaction of electric moments arising from fluctuations in the charge distributions of the molecules at large separations leads to the well-known London dispersion energy, which is present even if the molecules do

not possess permanent moments. The London forces or the dispersion effects are based on the quantum mechanics [38]. According to it, photons are moving randomly in space and these photons are constantly scattered by any particles, which are present so that instantaneous induced dipoles are able to produce rapidly fluctuating fields. This in turns polarizes the other molecules, thereby lowers the energy of the instantaneous dipole.

Suppose each instantaneous dipole P_i^{inst} of molecule i induces a dipole P_j^{ind} of molecule j , then the interaction potential of both molecules has the form

$$V_{dis}(r_{ij}) = \left(-\frac{1}{2}\right) < P_i^{inst} \nabla_i \nabla_j r_{ij}^{-1} X_j \nabla_j \nabla_i r_{ij}^{-1} P_i^{inst} >_{av} \qquad \textbf{(2.2.5)}$$

where, $\mathbf{X_j}$ is the molecular polarizability, the coupling parameter between photons and molecules.

The average polarization $< P_i^{inst} P_i^{inst} >_{av}$ of molecule i is proportional to the number of photons which is obtained from Planck's distribution.

The dispersion energy expression derived by London is

$$\Delta U(r)_{dis} = -\frac{3}{2}\frac{h\nu_i h\nu_j}{h(\nu_i+\nu_j)}\frac{\alpha_i \alpha_j}{r_{ij}^6} \qquad \textbf{(2.2.6)}$$

which is in the form of $\Delta U(r)_{dis} = -\frac{C_6}{r^6}$, where $\mathbf{C_6}$ is called the van der Waals' coefficient.

The dispersion energy occurs between any two molecules and it increases with the increase in temperature. At long range the interaction energy can be classified as multipolar (electrostatic), dispersion and induction energy and at short range as overlap (electrostatic and exchange) energy. The dispersion type of interaction can explain the general additive attraction between arbitrary atoms or molecules. The orientation effect and the induction effect require an alignment of permanent dipoles along the vector r_{ij} joining the interacting molecules. The orientation effect is not necessarily added between three molecules and in many cases repulsion of the third molecule rather than attraction is to be expected. Similarly, the induction effect is greatly reduced if many molecules superimpose their polarizing field from different sides. Hence, the dispersion type of interaction is more applicable in explaining the van der Waals' interaction comparing the other two effects.

Now let us consider two molecules or atoms, which are of rigid and perfectly elastic sphere interacting to each other. These molecules follow the gas laws and hence they attract to each other at longer distances and repel each other at shorter distances. When two molecules or atoms are sufficiently close to each other, then the two nuclei and the two electron clouds tend to vibrate together thereby leading to attraction between different molecules. The functional form of the intermolecular potential [40-42] is given by

$$V = 4\varepsilon\left[\left(\frac{\sigma}{r}\right)^{12} - \left(\frac{\sigma}{r}\right)^{6}\right] \qquad (2.2.7)$$

where ε is the well depth, σ is the distance between atoms or molecules. This is called the Leonard-Jones potential.

In general terms, $V = 4\varepsilon\left[\left(\frac{\sigma}{r}\right)^{m} - \left(\frac{\sigma}{r}\right)^{n}\right], m > n$ (2.2.8)

where **m** and **n** are the integers.

The potentials are zero at **r** = ∝ and **r** = σ and have a minimum at

$$\sigma_{min} = r\left(\frac{n}{m}\right)^{1/m-n} \qquad (2.2.9)$$

For larger values of **r**, the Leonard-Jone potential is asymptotic to an r^{-6} curve and therefore it has correct form to reproduce the long-range dispersion energy between closed shell atoms and molecules.

Another expression for intermolecular potential combined with the exponential repulsion $Ae^{-\alpha r}$ is given by

$$V = Ae^{-\alpha r} - \frac{B}{r^{6}} \qquad (2.2.10)$$

where **A**, **B** and α are constants.

2.2.1 Multipolar interactions:

In space-fixed axes, the dipole-dipole term V_{11} is given by

$$V_{11} = -\frac{\mu_1 \mu_2}{r^3}(3C_1C_2 - C_{12}) \qquad (2.2.11)$$

where C_i is the cosine angle between μ_i and r, C_{12} is the cosine of the angle between μ_1 and μ_2. The direction of r is chosen from molecule 1 and 2 in the intermolecular frame with polar axes along r.

For axially symmetric molecules (for molecules with at least threefold symmetry axes), the dipole-quadrupole term V_{12} in the space fixed axes [39] is

$$V_{12} = \frac{3}{2}\left(\frac{\mu_1 Q_2}{r^4}\right)\left[C_1(5C_2^2 - 1) - 2C_{12}C_2\right] \qquad (2.2.12)$$

The quadrupole-quadrupole term V_{22} in the space fixed axes as

$$V_{22} = \frac{3}{4}\left(\frac{Q_1 Q_2}{r^5}\right)\left(1 - 5C_1^2 - 5C_2^2 + 2C_{12}^2 + 35C_1^2C_2^2 - 20C_1C_2C_{12}\right) \qquad (2.2.13)$$

The minimum energy orientations for the three orientations V_{11}, V_{12} and V_{22} are shown in Fig.2.1.

The two linear quadrupoles prefer a T configuration which can be understood using a point charge model such as + = +. These minimum energy configurations are of importance for orientational structures of gas dimers, liquids and solids.

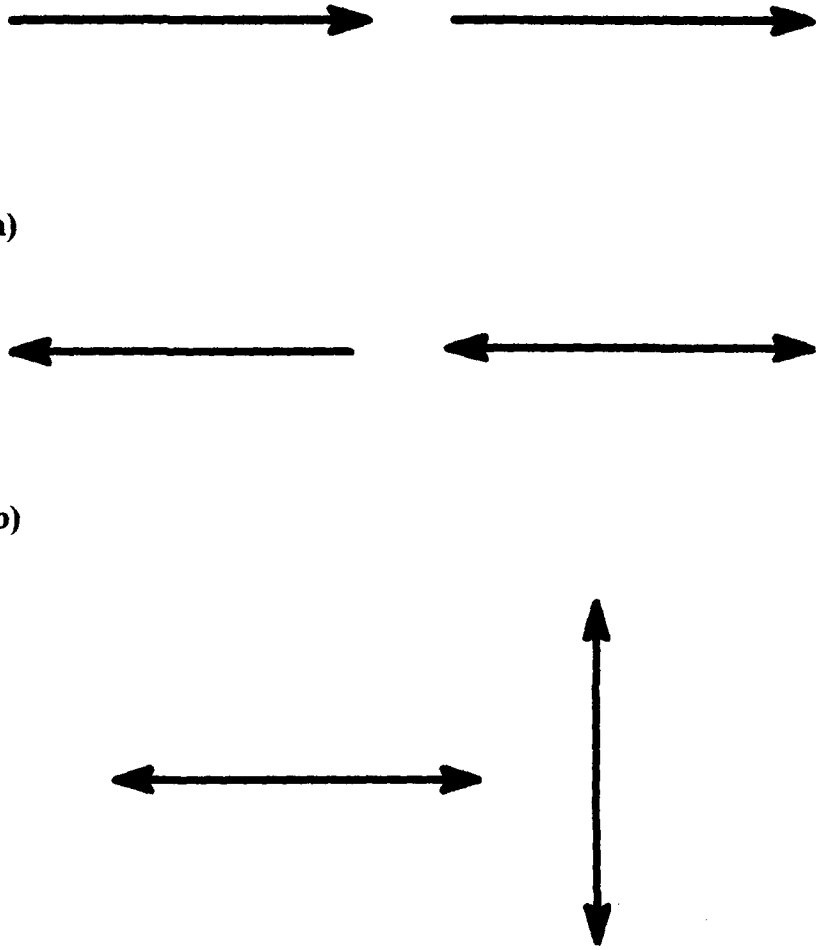

Fig. 2.1 Minimum energy orientation for
(a) dipole-dipole
(b) dipole-quadrupole
(c) quadrupole-quadrupole interactions

2.2.2 Van der Waals' volume and Radii :

The theory of van der Waals' attraction has a wide variety of applications. The van der Waals' attraction implies for particles whose separation is large enough to exclude overlap of electronic orbital. Here it is worth to mention the well-known van der Waals' equation [43]of state which implies for a fluid composed of particles that have a non-zero size and a pair wise attractive inter-particle force known as van der Waals' force. It exhibits a first order phase transition between a liquid phase and a gaseous phase. The van der Waals' equation is

$$\left(P + \frac{a}{v^2}\right)(v - b) = RT \qquad \textbf{(2.2.14)}$$

where **P** is the pressure of the fluid, a is a measure of the attraction between the particles, v is the volume of the fluid per particle, b is the total volume enclosed within the particle, **R** is the gas constant and **T** is the absolute temperature.

The above equation also indicates that the individual gas molecules do not have access to the total volume v since the remaining molecules already occupy volume b. The correction term $\frac{a}{v^2}$ at the pressure **P** implies that the kinetic energy with which the molecules hit the volume boundary is less than their kinetic energy in the interior, owing to the attractive force of

the molecules. The attractive correction term in kinetic energy, velocity and pressure is proportional to $\frac{1}{v^2}$ i.e. proportional to $\frac{1}{r^6}$ if r is the mean separation of the gas molecules.

The van der Waals' radii can study the van der Waals' force (intermolecular attraction) which is responsible for the attraction between any two atoms or molecules. Van der Waals' radius is the distance of closest approach between non-bonded atoms and defines the volume and surface of an atom or molecule. These intermolecular radii are assembled together to calculate the van der Waals' volumes[44]. Van der Waals' volume (V_w) is defined as the volume occupied by a molecule, which is impenetrable for other molecules with thermal energies at ordinary temperatures. The van der Waals' volume acts as a reducing parameter in the study of the physical properties of condensed phases. The calculation of V_w assumes a knowledge of bond distance, bond angles, the contact distances which is the intermolecular van der Waals' radii(r_w) and shapes characteristic of atoms in various molecular configurations [44]. It has been observed that the van der Waals' radius for heavy atoms is invariant under the most drastic environmental changes i.e. irrespective of its chemical composition and of its nearest non-bonded neighbours as well as of the phase state in which it is found. Hence, the van der Waals' radius can be estimated from the point of view of the electron density distribution around an atom.

The electron density Ψ^2 at a distance r from the core of a hydrogenic one-electron atom is given by

$$\Psi^2 = C^2 \exp\left\{ -\frac{2(\sqrt{2m_e I_0})r}{\eta} \right\} \qquad \textbf{(2.2.15)}$$

where m_e is the rest mass of the electron, I_0 is the first ionization potential of the atom and C is a normalization constant chosen such that $\int \Psi^2 dw = 1$, the integration is carried out over the whole space w.

As two atoms approach each other from $r = \infty$ their electron clouds interpenetrate more and more. According to Pauli-exclusion principle, there will be repulsion of the two atoms in direct proportion to the electron density in the interpenetrating region. Then the van der Waals' radius can be defined in terms of that distance r at which this repulsion just balances the attraction forces between the two atoms. It is difficult to formulate a critical electron density and calculation of r_w from it due to the low degree of accuracy. However, equation (2.2.15) contains a parameter $h/(me\ I_0)^{1/2}$, the De- Broglie wavelength λ_B of the outermost balance electron of an atom which might be related to the van der Waals' radius (r_w) which has the correlation form r_w = (constant) λ . The constant has the value 0.61 for the rare gas atoms, 0.53 for the halogens and 0.48 for the remainder of the non-

metallic elements. The correlation is deviated for the lightest elements having too large diameter.

The van der Waals' volume can be calculated from bond distances l and from r_w using the method of Bondi [44] given below (Fig.2.2):

In the figure (2.2),

r_1, r_2 = van der Waals' radii

l = covalent bond distance

m = auxiliary parameter

h_1, h_2 = height of the sphere segments

$$m = \frac{r_2^2 - r_1^2 + l^2}{2l}, \quad h_1 = r_1 + l - m, \quad h_2 = r_2 - m$$

$$V_1 = \pi h_1^2 \left(r_2 - \frac{h_1}{3} \right), \quad \Delta V_{2\text{-}1} = \pi h_2^2 \left(r_2 - \frac{h_2}{3} \right), \quad V_2 = \frac{4}{3} \pi r_2^3$$

Again the V_w of the atom having the high packing density and size compatible with the sphere obtained by application of kinetic gas theory is given by

$$V_w = N_A \left(\frac{\pi}{6} \right) \sigma^3 \qquad \textbf{(2.2.16)}$$

where N_A = 6.023 X 10^{23} molecules/mole.

σ = distance between like atoms at steepest ascent of repulsion branch of potential energy well.

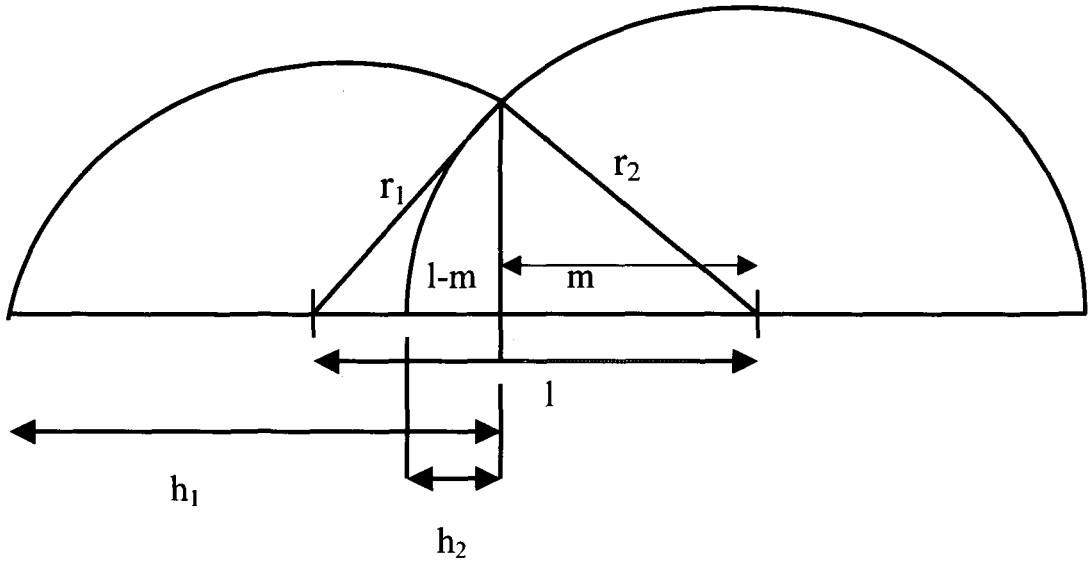

Fig. 2.2 Representative diagram for the calculation of van der Waals' volume

2.3 DIELECTRIC THEORY:

When an electric field is applied to a dielectric, the material is polarized through the alignment of permanent dipoles or the induction of molecular dipoles. For large field, the permanent dipoles are aligned better. The polarization **P** and the macroscopic field **E** are related [45,46] as

$$\mathbf{P} = \varepsilon_0 \chi \mathbf{E} \qquad \textbf{(2.3.1)}$$

where χ is the dielectric susceptibility.

The relation showing the dependence of polarization [47] on electric field strength is given by

$$\mathbf{D} = \varepsilon \mathbf{E} = 4\pi \mathbf{P} + \mathbf{E}$$

i.e.
$$\mathbf{P} = \left[\frac{\varepsilon - 1}{4\pi}\right]\mathbf{E} \qquad \textbf{(2.3.2)}$$

where **D** is the electric displacement.

If the material consists of non-polar molecules, the induced dipole moment **p** in a molecule of the dielectric is given by

$$\mathbf{p} = \alpha \mathbf{E}_i \qquad \textbf{(2.3.3)}$$

where $\mathbf{E}_i$ is called the internal field, which is equal to the total electric field at the position of the molecule minus the field due to the molecule itself.

If the material contains **N** dipoles per unit volume, using equation (2.3.3)

$$\mathbf{P} = N\mathbf{p} = N\alpha \mathbf{E}_i \qquad \textbf{(2.3.4)}$$

From equation (2.3.1) and (2.3.4), the dielectric susceptibility is

$$\chi = \left(\frac{N\alpha E_i}{\varepsilon_0 E} \right) \qquad (2.3.5)$$

Equation (2.3.2) is valid for liquids and gases in static or low frequency fields of moderate intensity. The electric field at moderate intensity gives rise to dipole density by translation (deformation) and rotation (reorientation) effect. In the translation effect, two types of phenomena are encountered. First, the electrons are shifted relative to the positive charge, which is known as electric polarization. The second one is the atomic polarization where atoms or atom groups are displaced relative to each other.

In the rotation effect, the electric field tends to direct the permanent dipoles. This effect is strongly dependent on temperature due to counter action by the thermal motion of the molecules. On the contrary, the translation effects being intra-molecular phenomena are slightly dependent on the temperature.

At higher field intensities, the field tends to direct an isotropic particle to an orientation such that its axis of highest polarizability coincides with the direction of the external field. The electric field shifts the chemical equilibrium between components with different permanent dipole moments in favour of the component with high permanent dipole moments.

The polarization **P** is assumed to be divided into two parts as

$$\mathbf{P} = \mathbf{P}_\alpha + \mathbf{P}_\mu \qquad (2.3.6)$$

where $\mathbf{P}_\alpha$ is the induced polarization caused by the translation effects and $\mathbf{P}_\mu$ is the dipole polarization caused by the orientation of the permanent dipoles.

The equation (2.3.2) can be written as

$$\mathbf{P}_\alpha + \mathbf{P}_\mu = \left[\frac{\varepsilon - 1}{4\pi}\right]\mathrm{E} \qquad \textbf{(2.3.7)}$$

Consider the electric field acting on a single molecule where the environment of the molecule is considered a continuum with the macroscopic properties of the dielectric.

The induced[47] polarization ($\mathbf{P}_\alpha$) may be written as

$$\mathbf{P}_\alpha = \sum_k \mathrm{N}_k \alpha_k (\mathrm{E}_i)_k \qquad \textbf{(2.3.8)}$$

where **N** is the number of particle per cm^3.

α is the scalar polarizability of a particle and $\mathbf{E}_i$ is the average field strength acting upon that particle. The index **k** refers to the $\mathbf{k}^{th}$ kind of particle.

The orientation polarization $\mathbf{P}_\mu$ can be written as

$$\mathrm{P}_\mu = \sum_k \mathrm{N}_k \bar{\mu}_k \qquad \textbf{(2.3.9)}$$

where $\bar{\mu}_k$ is the value of the permanent dipole vector arranged over all orientations. The value of $\bar{\mu}_k$ can be computed from the energy of the

permanent dipole, which depends on the part of the electric field $\mathbf{E}_d$ tending to direct the permanent dipoles.

The average moment per dipole in the direction of the applied field is given by

$$\bar{\mu} = \left(\frac{\mu^2}{3k_B T} \right) E_d \qquad \textbf{(2.3.10)}$$

Equation (2.3.9) can be written as

$$P_\mu = \sum_k N_k \frac{\mu_k^2 (E_d)_k}{3k_B T} \qquad \textbf{(2.3.11)}$$

Using equations (2.3.8) and (2.3.11) in equation (2.3.7), we get

$$\sum_k N_k \left[\alpha_k (E_i)_k + \frac{\mu_k^2 (E_d)_k}{3k_B T} \right] = \frac{(\varepsilon - 1)E}{4\pi} \qquad \textbf{(2.3.12)}$$

This equation is the fundamental equation for the dielectric constant for various polar and non-polar dielectrics.

When a molecule with permanent dipole strength μ is surrounded by the other particles, the inhomogeneous field of the permanent dipole polarizes its environment. In the surrounding particles, moments proportional to the polarizability are induced. If these particles have a permanent dipole moment, their orientation is influenced. Bell [47] introduced a better model for the dipole in a molecule, which is an ideal dipole in the centre of a spherical cavity to calculate the consequences of the effects cited

above. The field of the dipole in such a cavity polarizes the surrounding matter, and the resulting inhomogeneous polarization of the environment will give rise to a field **R** at the dipole, which is called the reaction field. **R** will have the same direction as the dipole vector μ due to symmetry and **R** will be proportional to μ as long as no saturation effects occur [47]. Hence

$$\mathbf{R} = \mathbf{f}\mu \tag{2.3.13}$$

where the factor **f** is called the factor of the reaction field.

Using Onsager approximation

$$\frac{4}{3}\pi \mathrm{Na}^3 = 1 \tag{2.3.14}$$

where **N** is the number of particles per cm^3, **a** is the radius of the spherical cavity where the ideal dipole moment μ is placed. The value of **a** is generally considered to be approximately equal to the molecular radius.

The reaction field of a non-polarizable point dipole is given by

$$\mathrm{R} = \frac{1}{\mathrm{a}^3}\frac{2(\varepsilon - 1)}{2\varepsilon + 1}\mu \tag{2.3.15}$$

Comparing this equation with (2.3.13), we conclude that the factor of the reaction field is given by

$$\mathrm{f} = \frac{1}{\mathrm{a}^3}\frac{2(\varepsilon - 1)}{2\varepsilon + 1} \tag{2.3.16}$$

The field in the dielectric can be described as the field of a virtual dipole μ_e at the centre of the cavity, which was called by Onsager as the external moment of the immersed dipole and is given by

$$\mu_e = \frac{3\varepsilon}{2\varepsilon+1}\mu \qquad \textbf{(2.3.17)}$$

For the case of polarizable permanent dipole, the reaction field induces a dipole $\alpha\mathbf{R}$ and hence satisfies the equation

$$\mathbf{R} = \mathbf{f}\,(\mu + \alpha\mathbf{R}) \qquad \textbf{(2.3.18)}$$

where μ is the permanent dipole moment.

α is the average polarizability

Therefore,
$$\mathrm{R} = \frac{\mathrm{f}}{1 - \mathrm{f}\alpha}\mu \qquad \textbf{(2.3.19)}$$

Eliminating the value of **f** from equation (2.3.16), we get

$$\mathrm{R} = \frac{1}{\left[\dfrac{2\varepsilon+1}{2(\varepsilon-1)} - \dfrac{\alpha}{\mathrm{a}^3}\right]}\frac{1}{\mathrm{a}^3}\mu \qquad \textbf{(2.3.20)}$$

In order to find the value of **R** in the case of liquids containing one kind of particle, we use the Onsager's approximation (2.3.14) and the equation

$$\frac{\alpha}{\mathrm{a}^3} = \frac{\mathrm{n}_\mathrm{D}^2 - 1}{\mathrm{n}_\mathrm{D}^2 + 2} \qquad \textbf{(2.3.21)}$$

where $\mathrm{n_D}$ is the index of refraction.

Now equation (2.3.20) becomes

$$R = \frac{4\pi}{3} N \frac{2(\varepsilon - 1)}{2\varepsilon + n_D^2} \frac{n_D^2 + 2}{3} \mu \qquad \textbf{(2.3.22)}$$

N is the number of particles per cm^3 and can be computed from

$$N = \left(\frac{d}{M}\right) N_A$$

where **M** is the molecular weight of the substance

d is the density and N_A is the Avogadro's number.

Under the influence of the reaction field **R**, the dipole moment is increased considerably and the increased moment [47,48] is given by

$$\mu^* = \mu + \alpha R \qquad \textbf{(2.3.23)}$$

Substituting the value of **R** from (2.3.19) to (2.3.23), we get

$$\mu^* = \left(\frac{\mu}{1 - f\alpha}\right) \qquad \textbf{(2.3.24)}$$

Using the value of **f** from (2.3.16) to the above equation, we have

$$\mu^* = \frac{\mu}{1 - \frac{\alpha}{a^3} \frac{2(\varepsilon - 1)}{2\varepsilon + 1}} \qquad \textbf{(2.3.25)}$$

Again substituting the value of $\frac{\alpha}{a^3}$ from equation (2.3.21) to equation (2.3.25), we have

$$\frac{\mu^*}{\mu} = \frac{2\varepsilon + 1}{2\varepsilon + n_D^2} \frac{n_D^2 + 2}{3} \qquad \textbf{(2.3.26)}$$

When the dipole is not surrounded by molecules of the same kind, the reaction field and the ratio $\frac{\mu^*}{\mu}$ are changed. From equation (2.3.22), N and n_D refer to the pure dipole compound, whereas ε is the dielectric constant of the mixture. Thus the changes in **R** and $\frac{\mu^*}{\mu}$, when the environment of the dipole is changed, result in a change of the factor $\frac{2(\varepsilon-1)}{2\varepsilon+n_D^2}$ in equation (2.3.22) and a change of the factor in $\frac{2\varepsilon+1}{2\varepsilon+n_D^2}$ equation (2.3.26) respectively.

2.4. THE ONSAGER EQUATION FOR POLAR AND NON-POLAR DIELECTRICS IN INTERNAL AND DIRECTING FIELDS

For a non-polar system, the fundamental equation [47] for the dielectric constant (2.3.12) simplifies to

$$\frac{\varepsilon-1}{4\pi}E=\sum_k N_k\alpha_k(E_i)_k \qquad (2.4.1)$$

The internal field E_i is also influenced by the cavity field E_c and the reaction field **R** of the induced dipole and hence considering both the effects of the fields, E_i can be written as

$$E_i = E_c + R \qquad (2.4.2)$$

where the cavity field E_c is given by

$$E_c = \left[\frac{3\varepsilon}{2\varepsilon + 1}\right] E \qquad (2.4.3)$$

The internal field for the case of polar molecules can also be built up from the cavity field and the reaction field. In this case, the reaction field is taken as field of the total dipole moment of the molecule. In the spherical cavity, the permanent dipole moment and the reaction field caused by it will have the same direction, as the angle between them will be constant during the movement of the molecule. Therefore, the reaction field **R** does not influence the direction of the dipole moment of the molecule and does not contribute to the directing field $\mathbf{E}_d$. On the other hand, the reaction field polarizes the molecule, contributes to the internal field $\mathbf{E}_i$. As a result, there is a difference between the internal field $\mathbf{E}_i$ and the directing field $\mathbf{E}_d$ and this difference gives the value of the reaction field averaged over all orientations of the polar molecule

$$\mathbf{E}_i - \mathbf{E}_d = \bar{\mathbf{R}} \qquad (2.4.4)$$

where $\bar{\mathbf{R}}$ is the total reaction field connected with the permanent part of the dipole moment.

For finding the value of $\mathbf{E}_d$, the polarizability of the molecule must be taken into account. The directing field $\mathbf{E}_d$ can be obtained by removing the permanent dipole of a molecule without changing its polarizability. In this case, we have eliminated the contribution of **r** to $\mathbf{E}_i$. The field $\mathbf{E}_d$ causes a

dipole α E_d with reaction field $f\alpha$ E_d, where **f** is the reaction field given by equation (2.3.16). Thus, E_d is given by the equation

$$E_d = E_c + f\alpha E_d$$

Therefore,
$$E_d = \left[\frac{1}{1-f\alpha}\right]E_c \qquad \textbf{(2.4.5)}$$

where E_c is the cavity field given by equation (2.4.3)

f is the reaction field factor and α is the polarizability.

Substituting the value of E_c from (2.4.3) to equation (2.4.5), we get

$$E_d = \frac{1}{1-f\alpha}\frac{3\varepsilon}{2\varepsilon+1}E \qquad \textbf{(2.4.6)}$$

If the dielectric consists of different kinds of molecules, then the directing field for each kind of molecule must be calculated separately.

For the k^{th} kind of molecule, the directing field is given by

$$(E_d)_k = \frac{1}{1-f_k\alpha_k}\frac{3\varepsilon}{2\varepsilon+1}E \qquad \textbf{(2.4.7)}$$

with
$$f_k = \frac{1}{a_k^3}\frac{2(\varepsilon-1)}{2\varepsilon+1} \qquad \textbf{(2.4.8)}$$

where ε is the dielectric constant of the mixture and a_k is the radius of the cavity belonging to the particle of the k^{th} kind.

Then from equation (2.4.4), the internal field can be written as

$$E_i = E_d + \bar{R}$$

from equation (2.3.19), we have $\bar{R} = \frac{f}{1-f\alpha}\bar{\mu}$

where $\bar{\mu}$ is the value of the μ averaged over all orientations and is given as

$$\bar{\mu} = \frac{\mu^2}{3k_BT}E_d$$

Hence $$E_i = \left(1+\frac{f}{1-f\alpha}\frac{\mu^2}{3k_BT}\right)\frac{1}{1-f\alpha}\frac{3\varepsilon}{2\varepsilon+1}E \qquad \textbf{(2.4.9)}$$

For a mixture of different kinds of molecules, the internal field at the $\mathbf{k}^{th}$ kind of molecule is

$$(E_i)_k = \left(1+\frac{f_k}{1-f_k\alpha_k}\frac{\mu_k^{\,2}}{3k_BT}\right)\frac{1}{1-f_k\alpha_k}\frac{3\varepsilon}{2\varepsilon+1}E \qquad \textbf{(2.4.10)}$$

Now substituting equations (2.4.7) and (2.4.10) in the fundamental equation (2.3.12), we have

$$\frac{(\varepsilon-1)(2\varepsilon+1)}{12\pi\varepsilon} = \sum_k N_k \frac{1}{1-f_k\alpha_k}\left[\alpha_k + \frac{1}{3k_BT}\frac{\mu_k^2}{1-f_k\alpha_k}\right] \qquad \textbf{(2.4.11)}$$

Taking Onsager's approximation for the radius of cavity

$$\frac{4}{3}N_k a_k^3 = 1 \qquad \textbf{(2.4.12)}$$

and the polarizability is given by

$$\frac{(\varepsilon_\infty)_k - 1}{(\varepsilon_\infty)_k + 2} = \frac{4}{3}\pi N_k \alpha_k \qquad \textbf{(2.4.13)}$$

where ε_∞ is the dielectric constant characteristic for the induced polarization, we obtained for the ratio $\frac{\alpha_k}{a_k^3}$ as

$$\frac{\alpha_k}{a_k^3} = \frac{(\varepsilon_\infty)_k - 1}{(\varepsilon_\infty)_k + 2} \tag{2.4.14}$$

Using equations (2.4.8) and (2.4.14), we find the value of $\frac{1}{1 - f_k \alpha_k}$ as

$$\frac{1}{1 - f_k \alpha_k} = \frac{((\varepsilon_\infty)_k + 2)(2\varepsilon + 1)}{3(2\varepsilon + (\varepsilon_\infty)_k)} \tag{2.4.15}$$

Hence equation (2.4.11) can be written as

$$\frac{\varepsilon - 1}{4\pi\varepsilon} = \sum_k N_k \frac{(\varepsilon_\infty)_k + 2}{2\varepsilon + (\varepsilon_\infty)_k} \left[\alpha_k + \frac{((\varepsilon_\infty)_k + 2)(2\varepsilon + 1)}{3(2\varepsilon + (\varepsilon_\infty)_k)} \frac{\mu_k^2}{3k_B T} \right] \tag{2.4.16}$$

For pure dipole liquids, we find

$$\frac{\varepsilon - 1}{4\pi} = \frac{3\varepsilon}{4\pi} \frac{\varepsilon_\infty - 1}{2\varepsilon + \varepsilon_\infty} + \frac{(\varepsilon_\infty + 2)^2 (2\varepsilon + 1)\varepsilon}{(2\varepsilon + \varepsilon_\infty)^2} \frac{N\mu^2}{9k_B T} \tag{2.4.17}$$

after substituting α_k and using equations (2.4.12) and (2.4.14)

Hence $$\mu^2 = \frac{9k_B T}{4\pi N} \frac{(\varepsilon - \varepsilon_\infty)(2\varepsilon + \varepsilon_\infty)}{\varepsilon(\varepsilon_\infty + 2)^2} \tag{2.4.18}$$

Equation (2.4.18) is called the Onsager equation. The permanent dipole moment of a molecule can be computed from the dielectric constant of the pure dipole liquid if the density and ε_∞ are known. Moreover, for most

dielectrics the dielectric constant ε_∞ is equal to the square of the index of refraction n , as followed from Maxwell's relation.

$$\varepsilon_\infty = n^2 \qquad \textbf{(2.4.19)}$$

In Onsager equation, the particles are assumed spherical and it takes into account the local field due to molecules within distances large compared to molecular dimensions but small compared to the thickness of the material. However, it neglects the local directional forces on the molecules due to their neighbours[48]. For the case of dilute solutions of a dipolar solute in a non-polar solvent, the polar molecules are far apart so that the interactions between them can be neglected. However, there will be an interaction between the polar molecules and the solvent molecules and this interaction can be taken into account approximately by using the form of Lorentz local field.

2.5 THEORIES OF KIRKWOOD AND FRÖHLICH:

Fröhlich [47] developed a model which represents a dielectric with dielectric constant ε, consisting of polarizable molecules with a permanent dipole moment. In this model, he introduced a continuum with dielectric constant ε_∞ in which point dipoles with a moment μ_d are embedded. Each molecule is replaced by a point dipole μ_d having the same non-electrostatic

interactions with the other point dipoles, while the polarizability of the molecule can be assumed to form a continuum with dielectric constant ε_∞.

The polarization **P** can be divided into two parts as

$$\mathbf{P} = \mathbf{P}_{in} + \mathbf{P}_{or} \qquad (2.5.1)$$

where $\mathbf{P}_{in}$ is the induced polarization and $\mathbf{P}_{or}$ is the orientation polarization. The induced polarization is equal to the polarization of the continuum with dielectric constant ε_∞, hence we can write

$$P_{in} = \left[\frac{\varepsilon_\infty - 1}{4\pi}\right]E \qquad (2.5.2)$$

The orientation polarization is given by the dipole density, which is due to dipoles μ_d. Consider a sphere with volume **V** containing **N** dipoles, then

$$P_{or} = \frac{1}{V} < M_d.e > \qquad (2.5.3)$$

where
$$M_d = \sum_{i=1}^{N} (\mu_d)_i \qquad (2.5.4)$$

$<\mathbf{M}_d.\mathbf{e}>$ is the average component of the moment due to dipoles in the sphere, in the direction of the field and is expressed as

$$< M_d.e > = \frac{\int dx^N M_d.e \exp\left(-\frac{U}{k_B T}\right)}{\int dx^N \exp\left(-\frac{U}{k_B T}\right)} \qquad (2.5.5)$$

where **U** is the energy of the dipoles in the sphere and consists of three parts namely the energy of the dipoles in the external field, the electrostatic interaction energy of the dipoles and the non-electrostatic interaction energy between the molecules. The third kind of energy is responsible for the short-range correlation between orientations and positions of the molecules.

The external field in this model is equal to the field situated in a spherical cavity which is filled with a continuum with dielectric constant ε_∞, and this field is called the Fröhlich field E_F. In this case the spherical cavity is situated in a dielectric with dielectric constant ε.

The Fröhlich field[47] is given by

$$E_F = \frac{3\varepsilon}{2\varepsilon + \varepsilon_\infty} E \qquad \textbf{(2.5.6)}$$

The general expression for the dielectric constant can be written as

$$\frac{\varepsilon - 1}{4\pi} = \left(\frac{\partial}{\partial E} (P_{in} + P_{or}) \right)_{E=O} \qquad \textbf{(2.5.7)}$$

After substituting equations (2.5.2) and (2.5.3) in equation (2.5.7), we get

$$\varepsilon - \varepsilon_\infty = \frac{4\pi}{V} \left(\frac{\partial}{\partial E} < M_d . e > \right)_{E=O} \qquad \textbf{(2.5.8)}$$

Now rewriting E_F instead of E as the independent variable, we have

$$\varepsilon - \varepsilon_\infty = \frac{4\pi}{V}\left(\frac{\partial E_F}{\partial E}\right)_{E=O}\left(\frac{\partial}{\partial E_F} < M_d.e >\right)_{E_F=O} \qquad \textbf{(2.5.9)}$$

Since in this case, $$\frac{\partial U}{\partial E_F} = -M_d.e$$

We obtain,

$$\varepsilon - \varepsilon_\infty = \frac{4\pi}{V}\left(\frac{\partial E_F}{\partial E}\right)_{E=O}\frac{< M_d^2 >_o}{3k_B T} \qquad \textbf{(2.5.10)}$$

which is the expression for the dielectric constant in Fröhlich's model.

Using the value of E_F from (2.5.6) to the above equation, we can write

$$\varepsilon - \varepsilon_\infty = \frac{4\pi}{V}\frac{3\varepsilon}{2\varepsilon + \varepsilon_\infty}\frac{< M_d^2 >_o}{3k_B T} \qquad \textbf{(2.5.11)}$$

i.e. $$< M_d^2 >_0 = \frac{k_B TV}{4\varepsilon}\frac{(\varepsilon - \varepsilon_\infty)(2\varepsilon + \varepsilon_\infty)}{\varepsilon} \qquad \textbf{(2.5.12)}$$

Evaluating the average $< M_d^2 > 0$ which is equal to $N'\mu_d^2 \sum_{j=1}^{N'} < \cos\theta_{ij} >$, we get

$$\frac{(\varepsilon - \varepsilon_\infty)(2\varepsilon + \varepsilon_\infty)}{12\pi\varepsilon} = \frac{N}{3k_B T} g\mu_d^2 \qquad \textbf{(2.5.13)}$$

where $N = \frac{N'}{V}$, $\mathbf{g}$ = the correlation factor = $\sum_{j=1}^{N'} < \cos\theta_{ij} >$

This correlation factor takes into account the correlation between the orientations due to the short-range order.

The permanent dipole moment μ_d in the centre is given by

$$\mu_d = \frac{\varepsilon_\infty + 2}{3}\mu \qquad \textbf{(2.5.14)}$$

where μ is the moment of the molecules in the gas phase.

Substituting the value of μ_d from (2.5.14) to (2.5.13), we have

$$g\mu^2 = \frac{9k_BT}{4\pi N}\frac{(\varepsilon - \varepsilon_\infty)(2\varepsilon + \varepsilon_\infty)}{\varepsilon(\varepsilon_\infty + 2)^2} \qquad \textbf{(2.5.15)}$$

This equation (2.5.15) is called the Kirkwood-Fröhlich equation. Equations (2.4.18) and (2.5.15) are compared and it is cleared that Kirkwood -Fröhlich equation is the generalization of the Onsager equation. The Kirkwood-Fröhlich equation gives the relation between the dielectric constant ε, the dielectric constant of induced polarization ε_∞, the temperature, the density and the permanent dipole moment.

The correlation factor **g** is a measure of the local ordering in the material. Positive deviation of **g** from unity results when short range hindering torques favour parallel orientation of the dipoles of neighbouring molecules, while negative deviations result from antiparallel orientation. If **g**

is unity, it means that fixing the position of one dipole does not influence the positions of the others except through the long-range electrostatic forces.

For the evaluation of the undetermined parameters in the model, it is useful to determine **g** as a function of the concentration when the compound is dissolved in a nonpolar solvent. However, the equation (2.5.15) is valid only for pure dipole liquids.

The equation, which is valid for solutions of polar compounds in non-polar solvents is given by

$$g\mu^2 = \frac{9k_BT}{4\pi N_A x_P}\frac{(2\varepsilon+\varepsilon_\infty)^2}{(\varepsilon_\infty+2)^2(2\varepsilon+1)}\left[\frac{\phi(\varepsilon-1)}{\varepsilon} - \frac{3x_0M_0(\varepsilon_0-1)}{(2\varepsilon+\varepsilon_0)d_0} - \frac{3x_PM_1(\varepsilon_\infty-1)}{(2\varepsilon+\varepsilon_\infty)d_1}\right]$$

(2.5.16)

where $\mathbf{d_1}$ and $\mathbf{d_0}$ are the densities of the polar and non-polar compounds in the pure state. x_0 and x_P are the molar fractions for the non-polar and the polar component respectively. $\mathbf{M_0}$ and $\mathbf{M_1}$ are the molecular weight of the non-polar solvent and the polar solvent. $\phi = \frac{x_0M_0 + x_PM_1}{d}$ is the molar volume of the mixture and $\mathbf{N_A}$ is the Avogadro's number.

Equation (2.5.16) helps in calculation of the Kirkwood correlation function g from experimental data for solutions of associating compounds in non-polar solvents.

2.6 RAMAN ACTIVITY:

The Raman effect arises from the interaction of the incident light with the electrons in the illuminated molecule. It is an inelastic scattering phenomenon in which the illuminated sample absorbs a photon and simultaneously emits another photon of different frequency. The photons present in the incident light has energy $h\nu_o$. On collision with molecules, photons may be elastically scattered which gives rise to the phenomenon of Rayleigh scattering. However, collision of photons with the molecules may be inelastic resulting the molecules to undergo a transition to a higher energy level resulting the photon lose energy and are scattered with a lower frequency and the process is termed as Stokes Raman Scattering [49]. The molecules, which are already in a higher vibrational energy state, may undergo a transition to a lower energy level. In this case, the photons are scattered with increased frequency and the process is termed as Anti-Stokes Raman Scattering. Fig.2.3 shows the diagrammatic presentation of these three types of light scattering.

Raman Spectroscopy is generally carried out in the visible and near-UV range of excitation frequencies. The theory of Raman effect shows that the amount of Raman scattering from a sample is directly proportional to the intensity of the incident radiation at the sample, to the fourth power of the incident frequency and to the concentration of the scattering species. Furthermore, the Raman scattered radiation is incoherent since the phase of

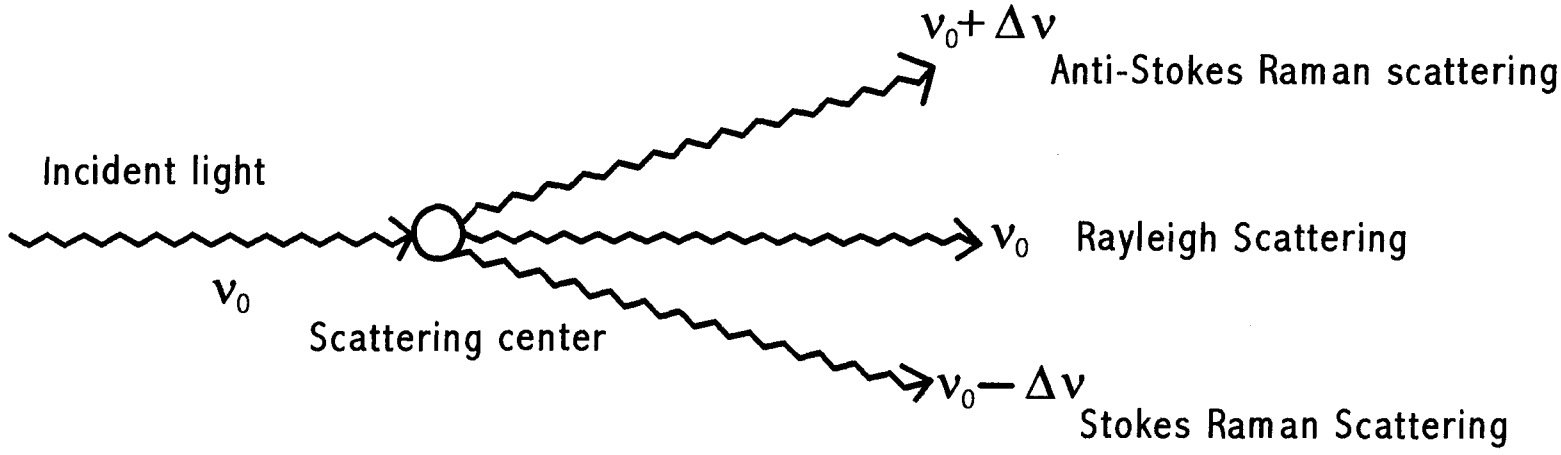

Fig. 2.3 Diagrammatic presentation of Anti-Stokes Raman scattering , Rayleigh scattering and Stokes Raman scattering

Raman scattering varies arbitrarily from molecules to molecules. Thus, the intensity of Raman scattering is proportional to the number of scattering species i.e. to the concentration of the sample.

When the electric field of the incident radiation is very large, the non-linear contributions to the molecular polarizability become significant. Due to non-linear interaction of a molecular system with an intense laser radiation, many new phenomena arise which changes the wave number of the laser exciting line. The effects reflecting these phenomena are namely ,the hyper-Raman effect, the stimulated Raman effect, the inverse Raman effect and coherent Anti-Stokes Raman Scattering (CARS) respectively. The CARS is an important tool for the study in chemical physics , biological samples and in analyzing the molecular structure. This technique has the advantage of spectral and spatial discrimination against fluorescence and does not require a spectrometer.

The phenomenon of the Raman effect arises because molecular vibrations modulate the frequency of the induced dipole in a molecule by an incident field. The induced electric dipole moment by the electric field **E** can be expanded [50] as

$$\mu = \alpha_1 \mathbf{E} + \alpha_2 \mathbf{E}^2 + \alpha_3 \mathbf{E}^3 \qquad \textbf{(2.6.1)}$$

where the **E** and μ are the electric field and induced dipole moment of the molecule. α_1 is the polarizability tensor of rank 2 while α_2 and α_3 are the hyperpolarizabilities of rank 3 and 4 etc.

The linear term in the equation (2.6.1) represents the Spontaneous Raman Scattering.

Although a quantum mechanical treatment is necessary for a complete explanation of Raman scattering phenomenon, but many aspects of the phenomenon can be described reasonably well by the classical electromagnetics of the induced dipole and the molecular vibration. The variation of the polarizability with vibrations of the molecule can be expressed by expanding each component α_{ij} of the polarizability tensor in a Taylor series with respect to the normal coordinates of vibration [51] as

$$\alpha_{ij} = (\alpha_{ij})_0 + \sum_k \left(\frac{\partial \alpha_{ij}}{\partial Q_k}\right)_0 Q_k + \frac{1}{2}\sum_k \left(\frac{\partial^2 \alpha_{ij}}{\partial Q_k \partial Q_\lambda}\right)_0 Q_k Q_\lambda + \qquad \textbf{(2.6.2)}$$

where **Q** is the vibrational normal co-ordinate, $(\alpha_{ij})_0$ is the polarizability tensor of the molecule in its equilibrium position. The subscript '$_0$' indicates that the expansion is centered at the equilibrium molecular configuration. The summations are over all normal co-ordinates.

For normal linear Raman effect, the polarizability of the molecule is related to the normal coordinate $\mathbf{Q_k}$ by the equation

$$(\alpha_{ij})_k = (\alpha_{ij})_0 + \left(\frac{\partial \alpha_{ij}}{\partial Q_k}\right)_0 Q_k \qquad \textbf{(2.6.3)}$$

neglecting the higher terms

This equation holds for each of the six polarizability components. Raman transitions invariably arise from the ground vibrational state, which belongs to a totally symmetric representation. Furthermore, the induced dipoles responsible for Raman scattering associated with the molecular frequency $\boldsymbol{\omega k}$ will be zero unless one of the components of the derived polarizability tensor $\left(\frac{\partial \alpha_{ij}}{\partial Q_k}\right)_0$ is non-zero. Hence, for a particular vibrational mode to be Raman active, at least one component of the polarizability tensor, a plot of that component against the normal coordinate must have a non-zero gradient at the equilibrium position. Both in the infrared and Raman spectrum [52], we have the selection rule $\Delta v_i = \pm 1$ for each normal vibration v_i. Only those vibrations that are connected with a change in dipole moment can have $\Delta v_i = \pm 1$ for an infrared transition and only those vibrations that are connected with a change of polarizability can have $\Delta v_i = \pm 1$ for a Raman transition.

REFERENCES:

1. R. G. Gordon, J. Chem. Phys. **40**, 1973 (1964).
2. D. W. Oxtoby, Adv. Chem. Phys. **40**, 1078 (1971).
3. D. W. Oxtoby, Chem. Phys. Lett. **52**, 224 (1977).
4. D. W. Oxtoby, D. Levesque and J. J. Weis, J. Chem. Phys. **68**, 528 (1978).
5. D. W. Oxtoby, J. Phys. Chem. **87**, 3028 (1983).
6. E. L. Sibert III and R. Rey, J. Chem. Phys. **116**, 237 (2002).
7. R. J. Gordon, Adv. Magn. Reson. **3**, 1 (1968).
8. W. G. Rothschild, G. J. Rosasco and R. C. Livingston, J. Chem. Phys. **62**, 1253 (1975).
9. D. W. Oxtoby, Adv. Chem. Phys. **40**, 1 (1979).
10. A. Morressi, L. Mariani, M. R. Distefano and M. G. Giorgini, J. Raman Spectrosc. **26**, 179 (1995).
11. R. Rey and J. T. Hynes, J. Chem. Phys. **108**, 142 (1998).
12. D.W. Oxtoby, J. Chem. Phys. **70**, 2605 (1979).
13. K. S. Schweizer and D. Chandler, J. Chem. Phys.**76**, 2296 (1982).
14. T. F. Sun, J. B. Chan, S. L. Wallen and J. Jonas, J. Chem. Phys. **94**, 7486 (1991).
15. M. Musso, H. Torii, P. Ottaviani, A. Asenbaum and M. G. Giorgini, J. Phys. Chem. **106A**, 10152 (2002).

16. A. Morresi, M. Paolantoni, P. Sassi, R. S. Cataliotti and G. Paliani, J. Phys. Condens. Matter. **12,** 3631 (2000).

17. R. J. Bartholomew and D. E. Irish, J. Raman Spectrosc. **29,** 115 (1998).

18. M. G. Giorgini, M. Musso and P. Ottaviani, Mol. Phys. **99**, 1485 (2001).

19. S. F. Fischer and A. Laubereau, Chem. Phys. Lett. **35**, 6 (1975).

20. R. Zwanzig and M. Bixon, Phys. Rev. **2A**, 2005 (1970).

21. K. S. Schweizer and D. Chandler, J. Chem. Phys. **76**, 2296(1982).

22. D. Ben Amotz, M. R. Lee, S. Y. Cho and D. J. List, J. Chem. Phys. **96**, 8781 (1992).

23. G. Doge, R. Arndt and J. Yarwood, Mol. Phys. **52**, 399 (1984).

24. W. Schindler, T. W. Zerda and J. Jonas, J. Chem. Phys. **81**, 4306 (1984).

25. D. E. Logan, Chem. Phys. **103**, 215 (1986).

26. C. H. Wang and J. Mchale, J. Chem. Phys., **72**, 4039 (1980).

27. M. G. Giorgini, M. Musso, A. Asenbaum and G. Doge, Mol. Phys. **98**, 783 (2000).

28. R. Kubo, in fluctuations, relaxation and resonance in magnetic systems, edited by D. ter Haar, pp.23, Oliver and Boyd, Edinburgh (1962).

29. R. Arndt and R. E. D. McClung, J. Chem. Phys. **69**, 4280 (1978).

30. G. J. Remar and R. A. Macphail, J. Chem. Phys. **103**, 4388 (1995).

31. A. Purkayastha and K. Kumar, J. Raman Spectrosc. **19**, 249 (1988).

32. J. Yarwood and R. Arndt, in Molecular Association, edited by R. Foster, vol. **2**, pp. 287, 297-300, Academic Press, London (1979).

33. R. M. Shelby, C. B. Harris and P. A. Cornelus, J. Chem. Phys. **70**, 34 (1979).

34. P. Mirone and G. Fini, J. Chem. Phys. **71**, 2241 (1979).

35. J. L. Mchale, J. Chem. Phys. **75**, 30 (1981).

36. M. G. Giorgini, G. Fini and P. Mirone, J. Chem. Phys. **79**, 639 (1983).

37. Raymond Gabler, Electrical Interactions in Molecular Biophysics, PP. 157, Academic Press, INC. New York (1978).

38. D. Langbein in "Springer Tracts in Modern Physics: Van der Waals attraction" Vol. **72**, PP.4, Edited by G.Höhler, Springer-Verlag, Berlin, (1974).

39. C. G. Gray and K. E. Gubbins, Theory of Molecular fluids, Vol **1**: Fundamentals, International Series of Monographs on Chemistry, Clarendon Press, Oxford (1984).

40. M. Karplus and R. N. Porter, Atoms and Molecules, An Introduction for students of Physical Chemistry, PP. 262-267, The Benzamin/Cummings Publishing Company, California (1970).

41. H. Margenau and N. R. Kestner, Theory of Intermolecular Forces, Pergamom Press, Oxford (1979).

42. Charles Kittel, Introduction to Solid State Physics, PP. 56-63, John Wiley and Sons, Inc., Singapore(1995).

43. F. Daniels and R. A. Alberty, Physical Chemistry, Fourth Edition. PP-87, John Wiley and Sons, New York (1975).

44. A. Bondi, J. Phys. Chem. **68**, 441 (1964).

45. David J. Griffiths, Introduction to Electrodynamics, Prentice Hall of India Pvt. Ltd., New Delhi (1997).

46. S. Bone, J. Eden, P. R. C. Gasloyne and R. Pethig, J. Chem. Soc. Faraday Trans., 1 , 77, 1729 (1981).

47. C. J. F. Bottcher, Theory of electric polarization, Vol **1**, Elsevier Amsterdam (1973).

48. C. P. Smyth in "Molecular interaction" **Vol 2**, edited by H. Ratajczak and W. J. Orville-Thomas, John Wiley and Sons, Chichester (1981).

49. Anthony T. Tu, Raman Spectroscopy in Biology, Principles and Applications, John Wiley and Sons, New York (1982).

50. L. J. Radziemski, R. W. Solarz and J. A. Paisner, Laser spectroscopy and its Applications, edited by Marcel Dekker, pp.514, New York (1987).

51. D. A. Long, Raman Spectroscopy, Mcgraw-Hill International Book Company, London (1977).

52. G. Herzberg, Molecular spectra and molecular structure, *II Infrared and Raman spectra of polyatomic molecules*, pp-249, D. Van Nostrand Company INC. New York (1945).

CHAPTER 3

CHAPTER 3

EXPERIMENTAL ASPECTS

INTRODUCTION

In this chapter, we present a brief discussion of the experimental techniques and the instruments used to obtain the laser Raman spectra for the study. The Raman Scattering is a weak phenomenon compared to Rayleigh scattering ($\approx 10^{-6}$ of the intensity of Rayleigh light) and only a small fraction of photons are scattered by the Raman scattering. The majority of the scattered light is similar to the original incident light in terms of photon energy. In a standard Raman experiment, the intense monochromatic radiation is focussed onto the sample. The scattered light is gathered by the collecting optics and is directed to a dispersive system (usually a double monochromator) which selects the scattered light of particular frequency range. At the exit port of the monochromator, the Raman spectrum is displayed in the form of a series of faint lines. The signals are detected by a photomultiplier tube and are recorded by a DATAMATE (Fig.3.1) using DM-3000 software.

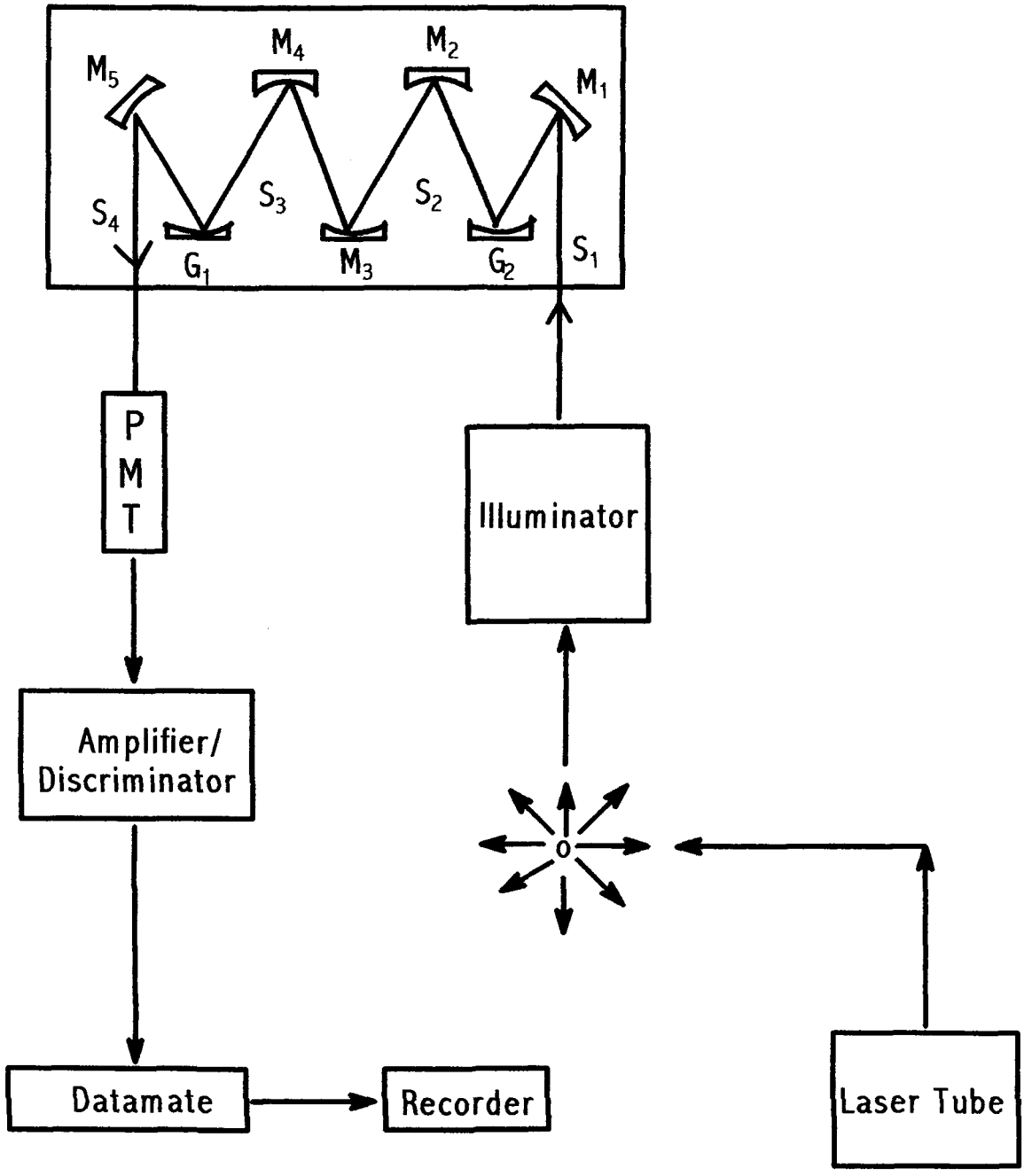

Fig. 3.1 Block diagram of a Raman instrument used in recording spectra

3.1 VIBRATIONAL RELAXATION TIME AND ANISOTROPY SHIFT MEASUREMENTS

It is a common practice in Raman scattering experiment to have the incoming light polarized normal to the scattering plane (= vertical, V) and to register both, the normal and the in plane (=horizontal, H) components of the scattered light $I_{VV}(\bar{\nu})$ and $I_{VH}(\bar{\nu})$. These components of Raman spectrum can be used[1] to get the isotropic and anisotropic components using the following relationship:

$$I_{iso}(\bar{\nu}) = I_{VV}(\bar{\nu}) - \frac{4}{3} I_{VH}(\bar{\nu}) \qquad (3.1.1)$$

$$I_{aniso}(\bar{\nu}) = I_{VH}(\bar{\nu}) \qquad (3.1.2)$$

where $I_{VV}(\bar{\nu})$ and $I_{VH}(\bar{\nu})$ are also represented as the polarized and depolarized components of Raman Spectra[2-5] respectively. $\bar{\nu}$ is the wavenumber in cm^{-1}.

The I_{VV} and I_{VH} components are defined as follows:

Consider the laser light travelling along the Y-direction and if X is the direction of observation, then X-Y plane forms the scattering plane (Fig.3.2). The direction of polarization of the laser light is normally taken perpendicular to this plane i.e. parallel to z-plane. The scattered radiation is detected in two orientations by rotating the analyzer parallel to the direction

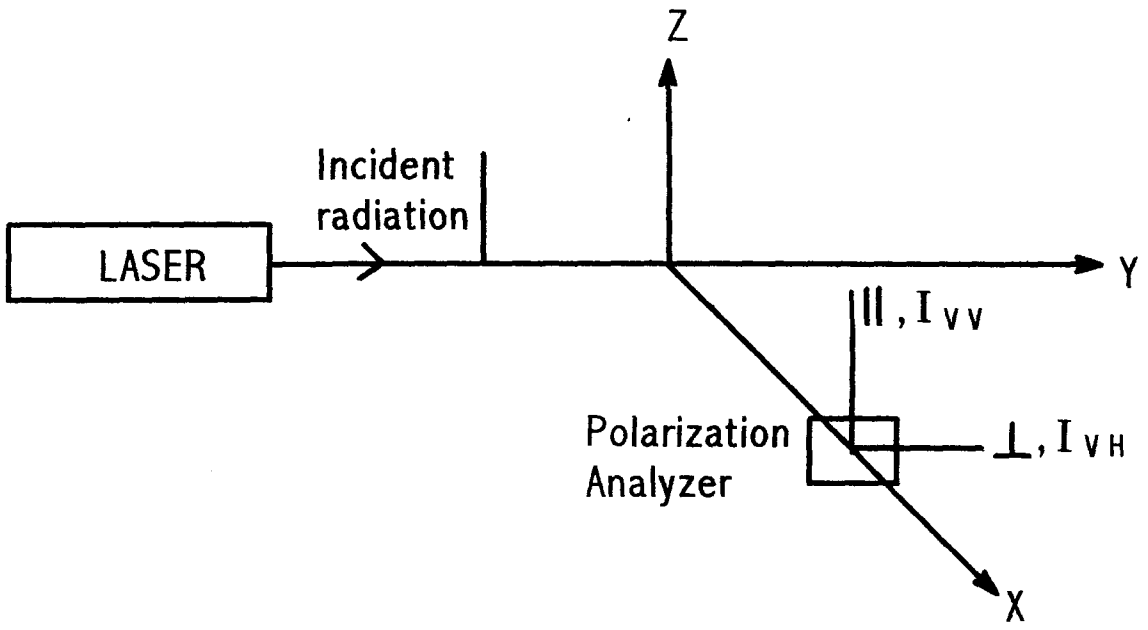

Fig. 3.2 Optical diagram showing the two Raman components I_{VV} and I_{VH} of scattered intensity

of the incident radiation (I_{zz}= I_{VV}) and perpendicular to the direction of the polarization of the incident radiation (I_{zy}=I_{VH}).

Assuming the band profile to be Lorentzian in shape, the vibrational relaxation time (τ_v) can be calculated as,

$$\tau_v^{-1} = \pi c \Gamma_{iso} \qquad \textbf{(3.1.3)}$$

where Γ_{iso} is the full width at half maximum (FWHM) of the isotropic component and c is the velocity of light. In order to accurately determine these quantities one must record the band profile with as high spectral resolution as possible.

The effect of finite slitwidth on Raman linewidth can be corrected by using the equation[6]

$$\Gamma_t = \Gamma_a [\, 1 - (S/\Gamma_a)^2] \qquad \textbf{(3.1.4)}$$

where Γ_t and Γ_a are the true and apparent Raman linewidth (FWHM) respectively, and S is the spectral slitwidth in cm^{-1}.

For the case of Lorentzian linewidth, the effect of finite slitwidth on the observed Raman linewidth can be corrected by the method of Singh et al.[7]

Here, observed Raman linewidth = $(\Delta\nu_{1/2})_R$

True Raman linewidth = Γ_L which is to be calculated.

Spectral slit width = S

$X = S/(\Delta\nu_{1/2})_R$

$Y = 0.998 + 0.020X - 1.160X^2 + 0.143X^3$

$$\Gamma_L = Y\,(\Delta\nu_{1/2})_R$$

Hence using all these mathematical expressions, the value of the true Raman Lorentzian linewidth has been measured.

The anisotropy shift ($\delta\nu$) can be obtained from the difference between peak positions of isotropic and anisotropic Raman components given by

$$\delta\nu = \nu(\text{aniso}) - \nu(\text{iso})$$

3.2 SOURCE OF EXCITATION:

The spectra physics model 165 Ar^+ laser is used for recording the Raman spectra.

The specification of Spectra Physics model 165 Ar^+ laser is presented below:

Noise, light control RMS, 10 Hz - 20 MHz	0.2%
Noise, Current control RMS, 10 Hz - 2 MHz	1%
Frequency stability	60 MHz/°C
Beam Diameter	1.25 mm
Beam Divergence (full angle)	0.69 mrad
Cavity configuration	long radius, output, flat high reflector
Cavity length w/o prism	1 + 0.003 meter
W/ prism	1.05 + 0.003 meter
Folded cavity	N/A

Polarization		Vertical
Mode-spacing	w/o prism	149.6-150.5 MHz
	W/ prism	142.5-143.3 MHz
Folded cavity		N/A

3.2.1 SPECTRA PHYSICS MODEL 165 Ar^+ LASER:

The spectra Physics model 165 Ar^+ laser is a continuous wave (CW) laser. It essentially consists of a laser head and an exciter (spectra physics model 265). The laser head consist of a Berryllium oxide plasma tube closed at each end by the Brewster angle windows, a solenoid and an optical resonator. A reflector (spherical) at the output end, together with a prism assisted by a flat reflecting mirror at the back end forms the optical resonator. The prism is placed in the optical path of the resonator in such a way that it selects the correct wavelength. The plasma tube is positioned exactly along the central line of the mirror. External thumb wheel controls are provided for the selection of wavelength of the emitted radiation and for changing the intra-cavity aperture. The emitted light from this laser source is polarized and the plane of polarization can be changed to any desired plane by using the $\lambda/2$ plate.

The spectra physics model 265 Exciter contains the necessary electric and electronic circuits in order to create, sustain and monitor the ionic discharge in the plasma tube. It also monitors and controls the output power and

regulates the solenoid current of the 165 Ar^+ laser head. The 265 Exciter runs on 230 volts three phase power line, which is provided by a power transformer supplied with a three phase 400 volts stabilized power from the main line. The input stabilization was achieved with the help of three single-phase 8.3 KVA (each) Nelco voltage stabilizers connected in the star (Y) configuration. Both the 165 Ar^+ laser and the 265 exciter are continuously cooled by flowing chilled de-ionized distilled water at a constant temperature of 15^0 C and at a pressure of 40 PSIG from the Neslab HX-500 (air cooled) water chilled plant.

3.3 OPTICS AROUND THE SAMPLE

A laser filter or the lasermate is kept in the light path before it enters the focussing system. The laser filter is a small grating monochromator, which allows the excitation wavelength to pass through but blocks weaker non-lasing lines from the laser plasma. It is therefore able to provide a clean Raman spectrum uncluttered by the laser-plasma lines, especially for a strong scattering sample[8].

The filtered laser beam is deflected upward through 90^0 by a mirror and is focussed onto the sample to a spot of diameter of around 10 μm by the fused silicon-condensing lens. Scattered radiation from the sample passes through a polarization analyzer, a device based on birefringence and total reflection or on dichroism. The polarization analyzer transmits light of

a particular polarization depending on the orientation of the polarizer. Use of polarization analyzer therefore provides direct information regarding the state of polarization of the observed plasma band. The scattered radiation is collected by an elliptical mirror, which ascertains a large solid angle about the focal volume and hence collects the optimum amount of scattered light. Fig.3.3 shows the optical diagram of the light scattering systems.

3.4 THE SPECTROMETER: SPEX RAMALOG MODEL 1403 DOUBLE MONOCHROMATOR:

The function of the spectrometer is to separate the spatially scattered photons from the sample based on their frequency. The light dispersing process is repeated by linking two single monochromators to form a double monochromator. The double monochromator also separates the Raman photons from the overwhelming number of Rayleigh photons.

All the Raman Spectra in the present study have been recorded with the help of SPEX Ramalog 1403 double monochromator coupled with a water-cooled photomultiplier tube RCA C-31034-02.

The SPEX Ramalog 1403 double monochromator is f/7.8 instrument with a spectral coverage from 3.1 X 10^4 cm^{-1} to 1.1 X 10^4 cm^{-1}. An accuracy of ± 1cm^{-1} in the 10,000 cm^{-1} range, a resolution of 0.15 cm^{-1} and a spectral

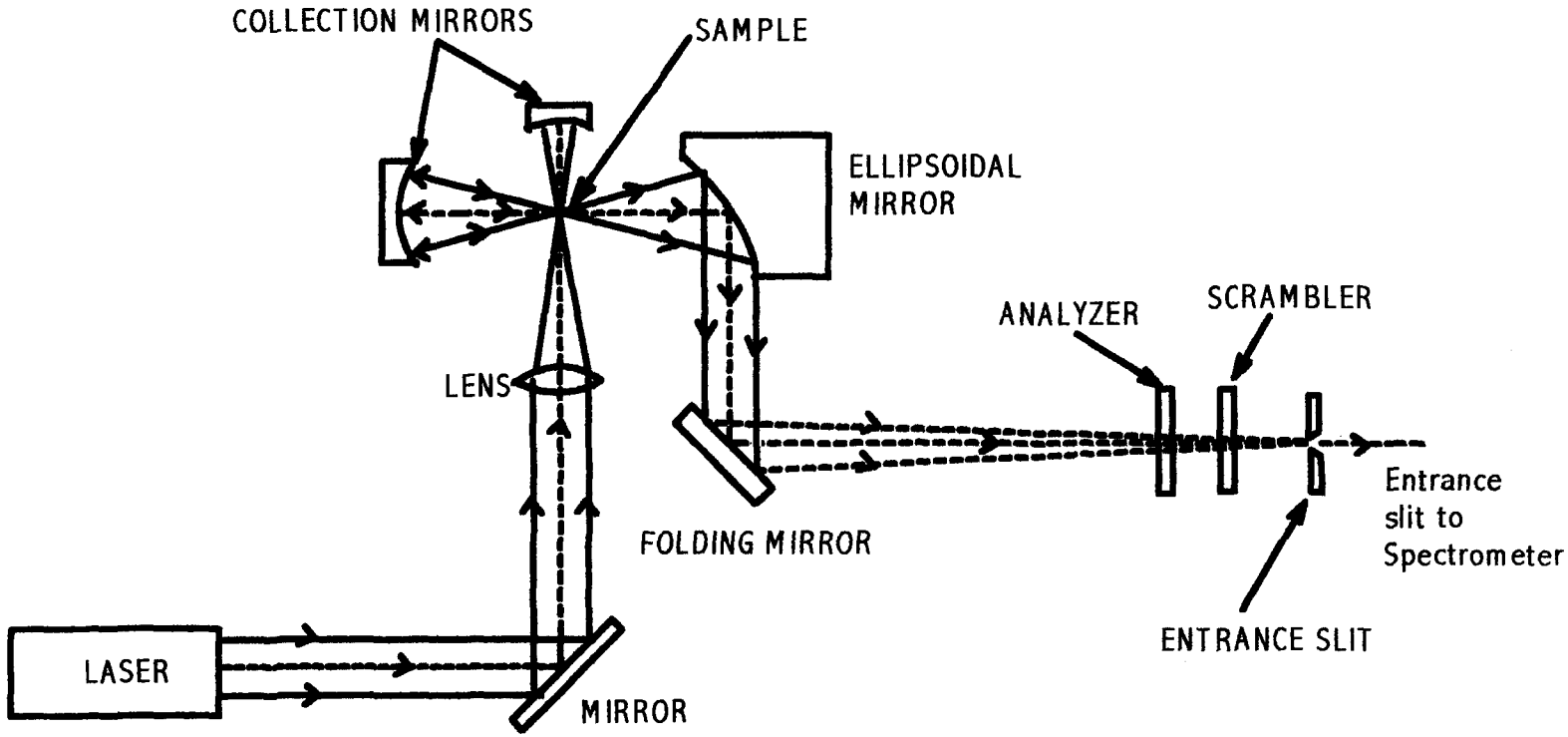

Fig. 3.3 Optical diagram of the light-collecting system of a Raman instrument

repeatability of ± 0.2 cm^{-1} can be achieved by this instrument. The 1800 grooves/mm holographic gratings are used in this instrument.

The gratings are mounted on a modified Czerny- Turner mount as shown in Fig.3.4. The fundamental grating equation[9] as applied to Czerny-Turner mount is

$$d\,(\sin\alpha + \sin\beta) = m\lambda \qquad \textbf{(3.4.1)}$$

where m = order, λ= wavelength, d= grating spacing, α = angle of incidence, β = angle of diffraction.

In case of 1403 instrument this formula may be expressed as

$$2d\sin\theta\cos\phi = m\lambda \qquad \textbf{(3.4.2)}$$

where $\phi = 10^0$, hence $\cos\phi = 0.984$

θ = grating rotation measured from zero, its position at the direct image.

Equation (3.4.2) was obtained by substituting

$$\alpha = \theta + \phi$$

and

$$\beta = \theta - \phi$$

Here θ denotes the angle of rotation of the grating from zero as illustrated in the Fig.3.4 and ϕ represents the constant angle, which depends on the design of the instrument.

The 1800 grooves/mm holographic gratings disperse the scattered radiation focussed onto the entrance slit of the spectrometer. Nearly monochromatic radiation of frequency ν for a particular tuning of the

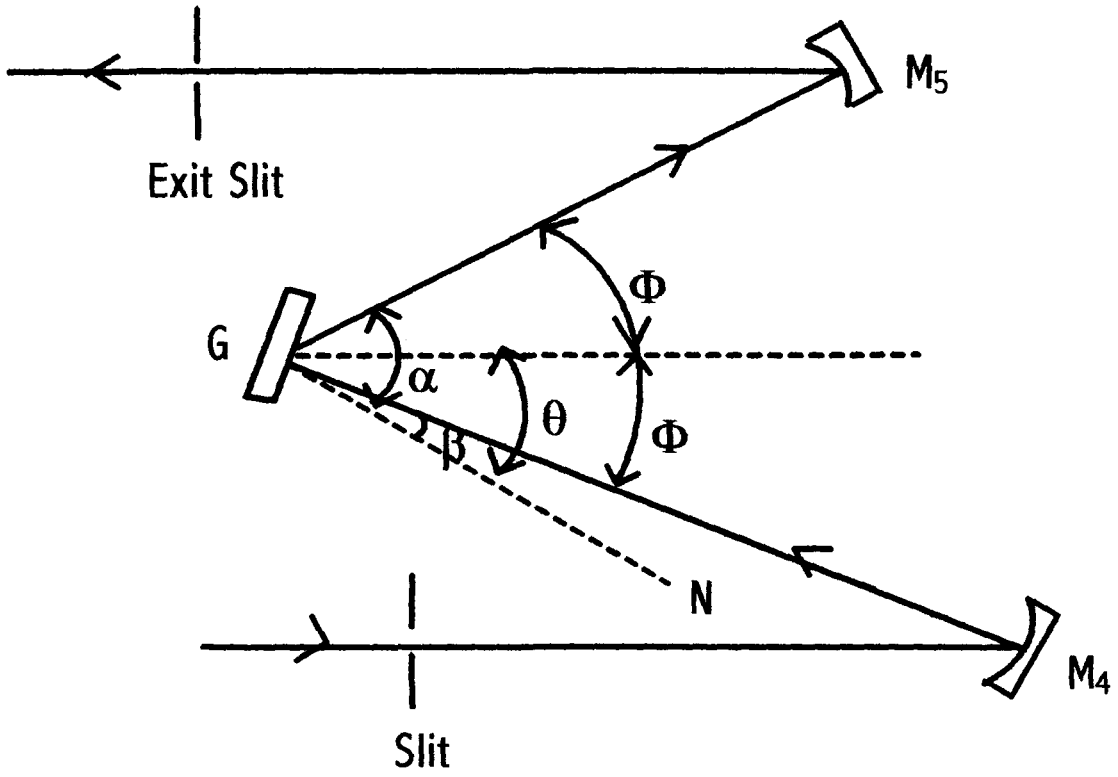

Fig. 3.4 Diagram showing the Czerny-Turner mount of gratings for the model SPEX Ramalog 1403 double monochromator

spectrometer reaches the exit slit of the double monochromator by the grating mirror combination.

The theoretical resolving power R_T is given by

$$R_T = \frac{\lambda}{\Delta\lambda} = \frac{\nu}{\Delta\nu} = 2\sin\theta\cos\phi\frac{W}{\lambda} = mN \qquad (3.4.3)$$

where λ= wavelength

ν= wavenumber

N= total number of grating grooves

W= width of grating ruling and

m= order of diffraction

Factors influencing resolution:

Source: From equation (3.4.1), since resolution depends linearly on the grating width (i.e. optical path difference), resolution deteriorates if the source illuminates less than the full width of the grating. Therefore, the source or condensing lens should fully illuminate the collimating mirror. This can usually be checked visually by opening the spectrometer or, in the case of energy outside the visible spectrum, by making certain that throughput is reduced when the edges of the collimating mirror are obstructed.

Slit width: Spectral bandpass is a function of the reciprocal linear dispersion, which, in turn depends on the wavelength, the grating constant, the focal length of the instrument and the spectral order.

Slit height: Increase in the heights of the straight slits reduces the instrumental resolution. As the height of the slits is increased, the ends of the exit slit begin to pass portions of adjoining wavelengths.

3.5 COLLECTION OF SCATTERED RADIATION:

A standard sampling platform is supplied with the SPEX 1459 illuminator. The Raman liquid cell of 1 ml capacity with 1431 M holder was used for holding the sample. The sample is illuminated with laser radiation and then the laser focus control is adjusted until the brightest image is observed at the sample. The image of the sample-scattered radiation is deflected on the target. An elliptical collection mirror (f/1.4) images the scattered radiation on the entrance slit of the spectrometer. The image is centered on the cross wires with the lateral adjustments and focus adjustment are turned until the sharpest image is achieved. By rotating the swing away mirror counter clockwise, the sample-scattered radiation is allowed to pass into the spectrometer. The signal is now peaked photo-electrically between the focus and lateral adjustments until the signal from the detector is maximized. In order to increase the scattering and collection efficiency, spherical mirrors may be mounted above and behind the sample

in the 1459 illuminator. Both mirrors increase the amount of scattered radiation that reaches the spectrometer entrance slit and therefore increase the signal from the detector. Two optical elements may be interposed in the beam, an analyzer and a scrambler, before it reaches the entrance slit. The scrambler is a wedge of birefringence materials. The two components of polarized light passing through it will be thrown out of phase as with a $\lambda/2$ plate. The retardation will vary from place to place and is not exactly $\lambda/2$; hence the emerging radiation will be depolarized. It cancels the variation in the spectrometer response, that results from polarization dependent efficiencies.

The laser output is polarized perpendicularly, whereas the Raman radiation from the sample is depolarized. The analyzer interposed in pathway may transmit the light either perpendicularly polarized or parallel polarized, depending on the orientation of the analyzer. In both the cases, the same scrambler is employed in front of the entrance slit of the monochromator to depolarize the radiation.

3.6 PHOTON COUNTING DETECTION

The detection system consists of a RCA C31034-02, II-stage QUANTACON type photomultiplier tube (PMT) with S-20 response in the photon-counting mode. The C31034-02 is designed specifically for use at

reduced temperatures, e.g., -30^0 C. Cooling reduces the dark count caused by the thermionic emission to ≈ 10 cps. Spex DATAMATE DM 3000 software were used for recording the spectra and for the acquisition of the data. The central processing unit (CPU) of the DATAMATE is an 8-bit microprocessor based ROM. The data can be processed in real time to subtract away background, take ratios, integrate or convert to logarithm for absorption states. DATAMATE photon counting results are expressed as and normalized to counts/sec. The DATAMATE also supplies high voltage (0-2000volts D.C. -ve) to the PMT. The high voltage is CPU selectable in 10 volts increment. The output current is variable from 0-2 mA. The linearity is better than 0.01% over full range. The noise level is 0.015% peak to peak at full load. The input in photon counting - DAM mode is -ve going pulse 0.1mV amplitude or greater. The gain of the amplifier is 400 and the rise time is 10 ns. The pulse pair resolution is less than 25 ns. The discriminator is internally adjustable from 5 mV to 200 mV. The maximum count rate for photon counting is $25X10^6$ Hz. The linearity and accuracy of the output data (Y-axis) is 0.3% full scale and resolution is one part in 4000.

3.7 THE PHOTOMULTIPLIER TUBE

RCA C-31034-02 photomultiplier tube, cooled to -30^0C by a thermoelectric cooling device was used for obtaining the Raman Spectral data. The photomultiplier tube having an almost linear, absolute,

responsivity 3000Å wavelength range was operated for a current gain of 10^6 with a maximum dark pulse summation of 12cps. The RCA C-31034-02 photomultiplier tube consists of a gallium arsenide chip placed at its photocathode, an ultraviolet transmitting glass window and an inline copper beryllium dynode structure consisting of eleven dynodes.

The raw data is obtained from the output of the preamplifier (pc Dam) of gain 400. The anode of the PMT is the input of the pc Dam. The high voltage of 1750 volts required for operating the PMT is supplied by the DATAMATE with a stability of +0.002% after 30 minutes of warm up.

3.8 SAMPLING TECHNIQUES

A laser beam, being a narrow and unidirectional, entity, can be manipulated in a variety of sample cell configurations thus providing considerable ingenuity in exercising the design and use of sample cells. A substantial advantage stemming from the geometric simplicity of the Raman experiment is that samples may be examined in any physical states. For liquid samples, which we have used more frequently, a cell consisting of around 1 cm path length is adequate, provided the cell bottom is transparent. In order to minimize the amount of scattered light from the interface reaching the spectrometer, the cell should be toped around the meniscus.

3.9 THE INTENSITY OF RAMAN SCATTERED LIGHT AND THE DEPOLARIZATION RATIO

In order to measure the depolarization ratio accurately, the polarization of the exciting laser beam is kept constant and the analyzer is placed after the sample[10]. Suppose the polarization of the laser beam is parallel to the Z- axis (Fig.3.2) and the direct transmission of the analyzer is turned from Y to Z direction to measure I_{VH} and I_{VV} respectively. The intensity of the I_{VH} component is proportional to

$$I_{VH} \alpha 3\gamma'^2$$

and that of I_{VV} component is proportional to

$$I_{VV} \alpha (45\alpha'^2 + 4\gamma'^2)$$

where the factors α'^2 and γ'^2 are defined by the derivatives of the polarizabilities as,

$$\alpha' = \frac{1}{3}(\alpha'_{XX} + \alpha'_{YY} + \alpha'_{ZZ})$$

$$\gamma'^2 = \frac{1}{2}[(\alpha'_{XX} - \alpha'_{YY})^2 + (\alpha'_{YY} - \alpha'_{ZZ})^2 + (\alpha'_{ZZ} - \alpha'_{XX})^2]$$

$$+ 6(\alpha'^2_{XY} + \alpha'^2_{YZ} + \alpha'^2_{ZX})$$

Since the constant factor is same for the fixed experimental conditions, the depolarization ratio is

$$\rho = \frac{I_{VH}}{I_{VV}} = \frac{3\gamma'^2}{45\alpha'^2 + 4\gamma'^2} \qquad (3.9.1)$$

If the Raman scatter is known for the directions X and Y, its intensity in any direction ϕ of the X-Z plane may be calculated from

$$I(\phi) = I_X \cos^2 \phi + I_Z \sin^2 \phi \qquad (3.9.2)$$

The angle dependent intensities after the analyzer are

$$I_{VH}(\phi) \propto 3\gamma'^2$$

$$I_{VV}(\phi) \propto (45\alpha'^2 + 4\gamma'^2)\cos^2\phi + 3\gamma'^2\sin^2\phi$$

$$= (45\alpha'^2 + \gamma'^2)\cos^2\phi + 3\gamma'^2$$

The observed depolarization ratio is

$$\rho_{obs} = \rho + \rho(1-\rho)\frac{\phi^2}{3} \qquad (3.9.3)$$

For $\rho << 0.75$, $\rho(1-\rho)\frac{\phi^2}{3}$ is of the order of magnitude of ϕ.

Thus the measured depolarization ratio ρ_{obs} will be larger than the true depolarization ratio, ρ.

If an angle $\phi = 10^0$ (= 0.175 rad) is needed to measure a depolarization ratio of $\rho = 0.01$, in the case of highly polarized band, this method will produce a systematic error of $(1-\rho^2)\frac{\phi^2}{3} \approx 10^{-4}$ or 1%

However, if a completely depolarized band is to be measured for which the depolarization ratio is $\rho = 0.75$, the systematic error by using the same collecting angle $\phi = 10^0$ will be

$$0.19 \text{ X } 10^{-2} \text{ or } 0.3\%$$

Therefore, we see that measured depolarization ratio is always larger than the theoretically expected value.

3.10 MULTIFREQUENCY LCR-METER, HP- 4263 B:

The multifrequency LCR-meter, HP-4263B was used for the measurement of capacitance. The measurements of capacitance were carried out[11] in the series equivalent circuit mode. The four terminal fixture HP-16089B was used for all measurements.

The salient features of this instrument are presented in the Table below:

Table

Few specification of multifrequency LCR-meter, HP- 4263 B

Measurement Circuit modes: Auto, Series and Parallel

Measurement terminals : Four terminal pair configuration with guard terminal

Range modes : Auto and Manual (up-down)

Measurement Frequencies : 100 Hz, 120 Hz, 200 Hz, 400 Hz, 1KHz, 2KHz, 4 KHz, 10 KHz, 20 KHz, 40 KHz and 100 KHz

Test signal level	: 1mv to 5Vrms continuously variable in 4 ranges
Offset Adjustment	: Stray capacitance, residual inductance, resistance and conductance of test fixture or test leads can be compensated for as follows:
	C: up to 20pF
	L: up to 2000nH
	R: up to 0.5Ω
	G: up to 5 sec
Operating temperature	: 0°C to 55°C at 90% RH (40°C) and humidity

REFERENCE:

1. W. Schindler, T. W. Zerda and J. Jonas J. Chem. Phys. **81**, 4306 (1984).
2. M. A. Ricci, G. Signorelli and V. Mazzacurati, J. Phys. Condens. Matter, **2**, 183 (1990).
3. A. Das and K. Kumar, Spectrochim. Acta, **54A**, 793 (1998).
4. Y. J. Kim, H-Chou Chang, V. S. Sullivan and J. Jonas, J. Chem. Phys. **111**, 9658 (1999).
5. C. J. Fecko, J. D. Eaves and A. Tokmakott, J. Chem. Phys. **117**, 1139 (2002).
6. K. Tanabe, Spectrochim. Acta, **40A**, 437 (1984).
7. R. K. Singh, S. N. Singh, B. P. Asthana and C. M. Pathak, J. Raman Spectrosc. **25**, 423 (1994).
8. Operation and maintenance instrumental manual for SPEX Model 1403 Spectrometer (1982).
9. H. A. Strobel, Chemical Instrumentation, pp. 320-327, Addition - Wesley, Mass (1973).
10. C. D. Allemand, Applied Spectrsc. **24**, 348 (1970).
11. Operation Manual HP 4263 B LCR meter (1996).

CHAPTER 4

CHAPTER 4

ANISOTROPY SHIFT AND RAMAN BANDWIDTH STUDIES IN O-CHLOROBENZALDEHYDE : ROLE OF REPULSIVE FORCES

1. Introduction

In liquid mixtures, the Raman band shape of the reference mode is influenced by the concentration fluctuations in the environment[1-3]. The dependence of the frequency and bandwidth of Raman vibrational bands on the environment provides useful information regarding the solute-solvent interactions and intermolecular forces. The analysis of the Raman spectra of several molecular liquids indicates that the peak frequencies of the isotropic and anisotropic components of totally symmetric mode do not coincide. This is termed as non-coincidence effect (NCE) or anisotropy shift[4-28]. The phenomenon of NCE was observed by Fini et al [4]. Later Fini and Mirone[5,6], Wang and Mchale [7,8], Logan[9-11] and Torii et al[12-14] developed various theoretical models for the explanation of NCE in dipolar liquids. According to Wang and McHale, any angular dependent resonance coupling mechanisms can give rise

to NCE such as dipole-dipole coupling, quadrupole-quadrupole coupling, transition dipole-transition dipole coupling and hydrogen bonding. The theory of Fini and Mirone is based on the macroscopic properties for studying the behaviour of isotropic and anisotropic Raman components on dilution of liquids. Logan developed a theory and attributed NCE to resonant excitonic transfer in the presence of local order owing to strong permanent dipoles. In this process, the main interaction is due to transition dipole-transition dipole coupling.

The non-coincidence of the peak frequencies of the isotropic and the anisotropic components in Raman spectra has always been considered an efficacious probe of the structure and dynamics of polar liquids. This NCE may be interpreted as being due to the coupling between vibrations of neighbouring molecules with strongly polar modes by intermolecular dipole interaction in the liquid phase[17,20,29-30] . In polar liquid molecules, the origin of the NCE is due to the orientationally dependent intermolecular forces. These forces modulate the vibration of a symmetrical mode; change the oscillator force constant of this mode and cause splitting of a vibration into an isotropic vibration and an anisotropic vibration. The isotropic vibration is governed by the angular independent inter- and intra-molecular potentials, whereas the anisotropic vibration by angular dependent inter- and intra-molecular forces. As a result,

there is a difference in the peak frequencies of these two components of the Raman band[31]. The spherically symmetric and asymmetric intermolecular forces play significant role in determining the band shape of isotropic and anisotropic components respectively. The isotropic component of the Raman band can be used to calculate the vibrational relaxation rate. This study is reported in the chapter 5.

Solvent dependent study of anisotropic component of the Raman band[1] has also provided information about the intermolecular interactions. However, further studies are required to get a better understanding of the complex molecular systems.

In the present chapter, we focus on the study of the non-coincidence effect by taking into account the screening factor related to the permanent and transition dipoles in order to interpret the various interactions involved in solute-solvent interactions. The van der Waals' volume of the interacting systems has been taken into account to study the solution phase and the anisotropic component has been used to probe the intermolecular forces. We have chosen the C=O stretching mode of o-Chlorobenzaldehyde (OCBD) as solute and CCl_4, CH_3CN, $CH_3C_6H_5$ and C_6H_5Cl as solvents for our study. The OCBD is a useful molecule having chemical and biological applications. The C=O stretching vibration of OCBD is well isolated from other normal modes of

vibration. Moreover, the OCBD, which contains Cl atom, is expected to give valuable information on the interacting nature with the surrounding solvents and the effect of steric hindrance in this microscopic environment.

2. Experimental

The measurements were carried out by means of a SPEX Ramalog 1403 double monochromator equipped with a cooled RCA C31034 photomultiplier and photon counting arrangement. The spectrometer control and data processing were achieved with the help of a Datamate using DM-3000 software. The 4880 Å line from the Spectra Physics model 165 Ar^+ laser was used as the excitation source. The spectral slitwidth was kept at 2 cm^{-1}. The compounds are commercial products and they were used without further purification. The accuracy of measurement is believed to be ± 0.5 cm^{-1}. The isotropic and anisotropic components were obtained as

$$I_{iso}(\bar{\nu}) = I_{VV}(\bar{\nu}) - \frac{4}{3} I_{VH}(\bar{\nu}) \qquad \textbf{(4.2.1)}$$

$$I_{aniso}(\bar{\nu}) = I_{VH}(\bar{\nu}) \qquad \textbf{(4.2.2)}$$

where $I_{VV}(\bar{\nu})$ and $I_{VH}(\bar{\nu})$ are the polarized and depolarized Raman spectra [1,32,33] respectively and $\bar{\nu}$ is the wave number in cm^{-1}.

The effect of finite slit width was corrected [34] by using the equation

$$\Gamma_t = \Gamma_a [\ 1 - (S/\Gamma_a)^2] \qquad \textbf{(4.2.3)}$$

where Γ_t and Γ_a are the true and apparent Raman linewidth (FWHM) respectively, and S is the spectral slit width in cm^{-1}.

3. Results and Discussion

The Raman Spectra of C=O stretching mode of OCBD were measured using CCl_4, CH_3CN, $CH_3C_6H_5$ and C_6H_5Cl solvents at different solvent concentrations ranging from 10% to 90% solvent concentration and the isotropic components were found out. The Raman spectrum of neat OCBD, which is exhibiting the anisotropy shift, is shown in Fig. 4.1. The anisotropic and isotropic Raman spectra of OCBD in four solvents are shown in Fig.4.2. The peak frequencies of isotropic and anisotropic components were found out. The anisotropy shift ($\delta\nu = \nu_{aniso} - \nu_{iso}$) was measured for different solvent concentrations ranging from 10% to 90% solvent concentrations using the above four solvents. The anisotropy shift decreases as the solvent concentration increases irrespective of the nature of the solvent (Fig. 4.3). This is due to the transition dipole-transition dipole (TD-TD) interactions of the vibrations of two adjacent molecules [12,20]. For the molecules having aromatic rings, the coupling mechanism responsible for the NCE must be associated with quadrupolar resonant coupling[23].

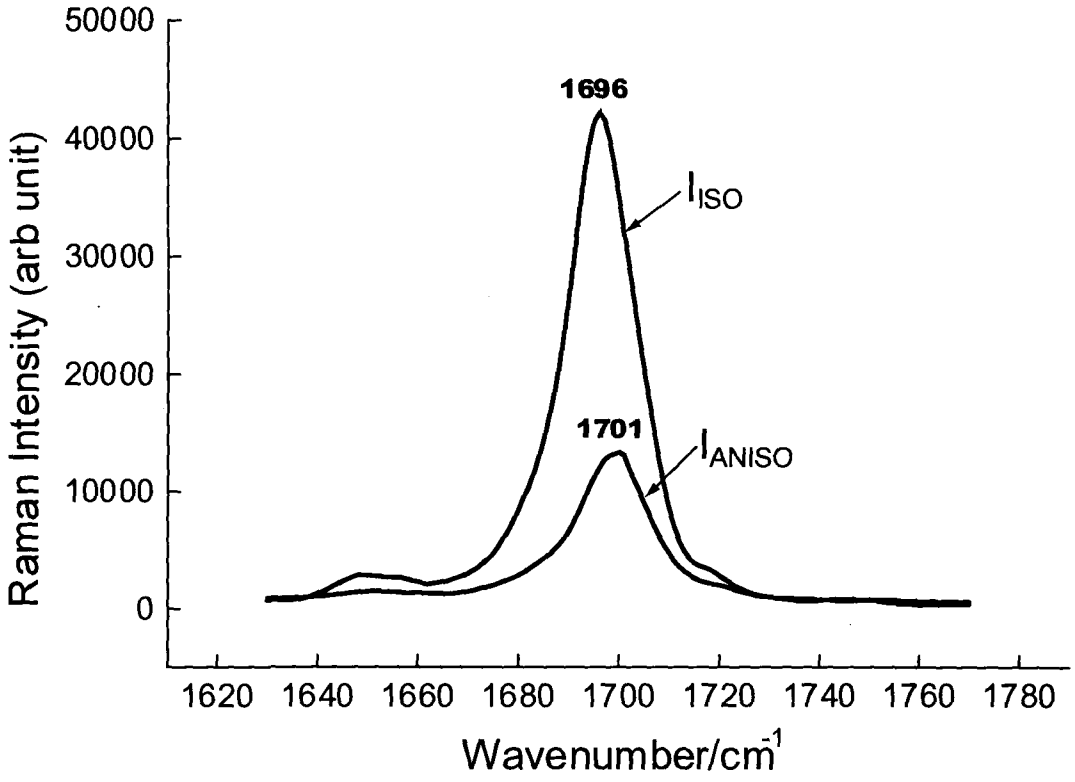

Fig. 4.1 Raman spectrum of Neat OCBD

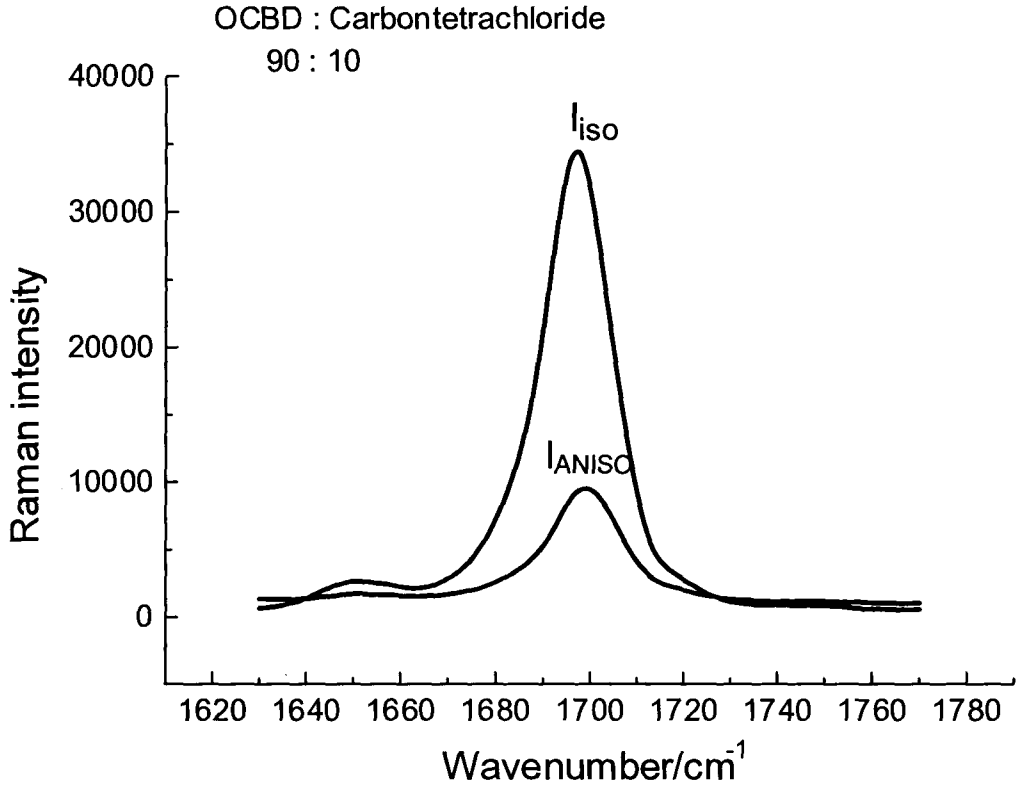

Fig. 4.2 (a) Raman spectrum of OCBD in Carbontetrachloride

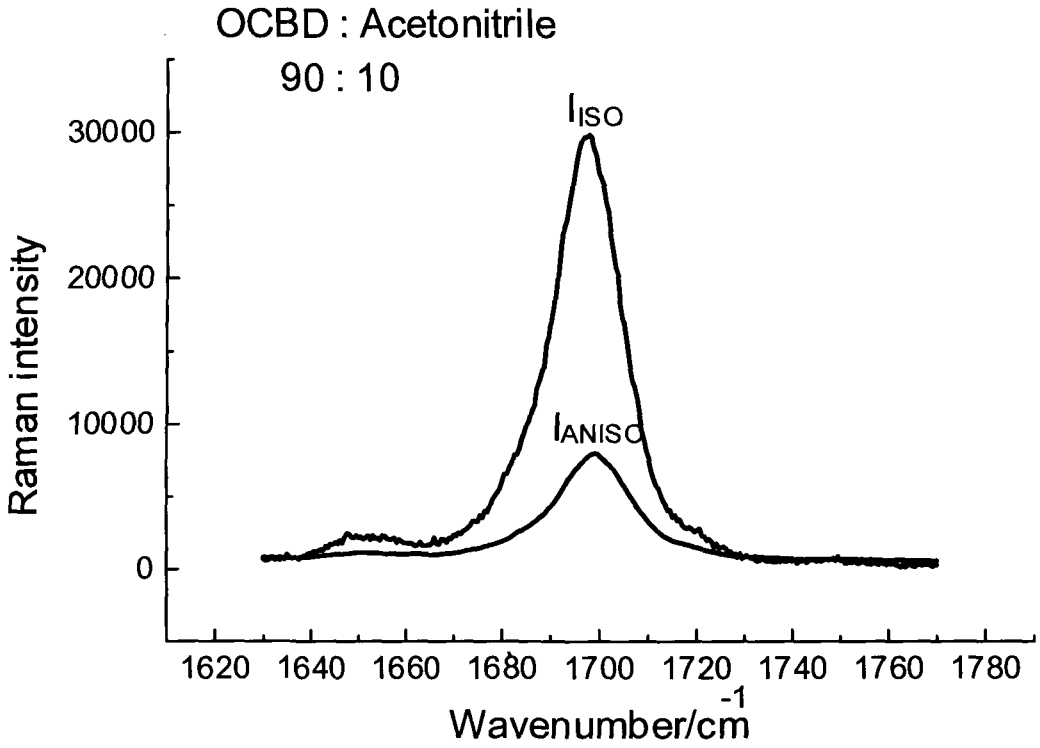

Fig. 4.2 (b) Raman spectrum of OCBD in Acetonitrile

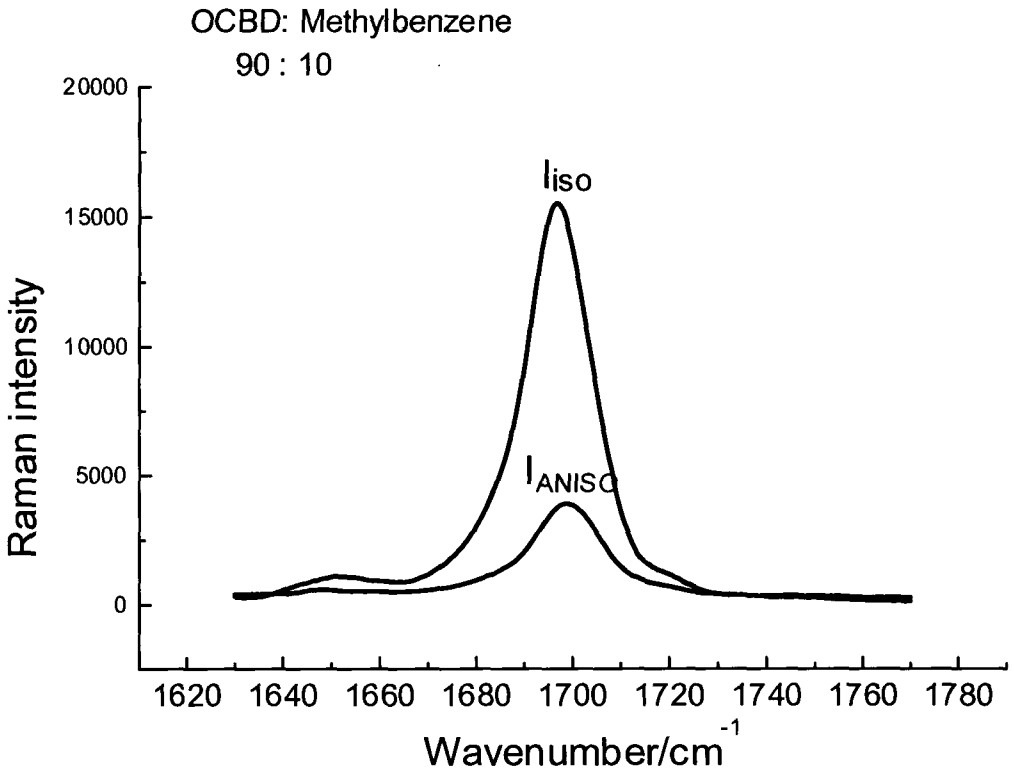

Fig. 4.2 (c) Raman spectrum of OCBD in Methylbenzene

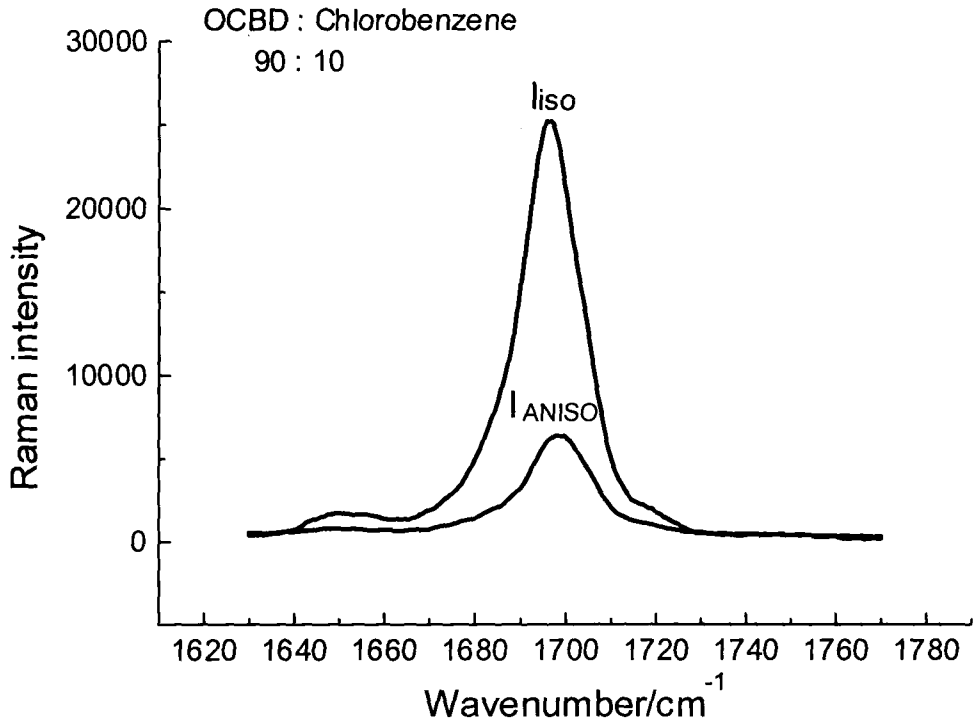

Fig. 4.2 (d) Raman spectrum of OCBD in Chlorobenzene

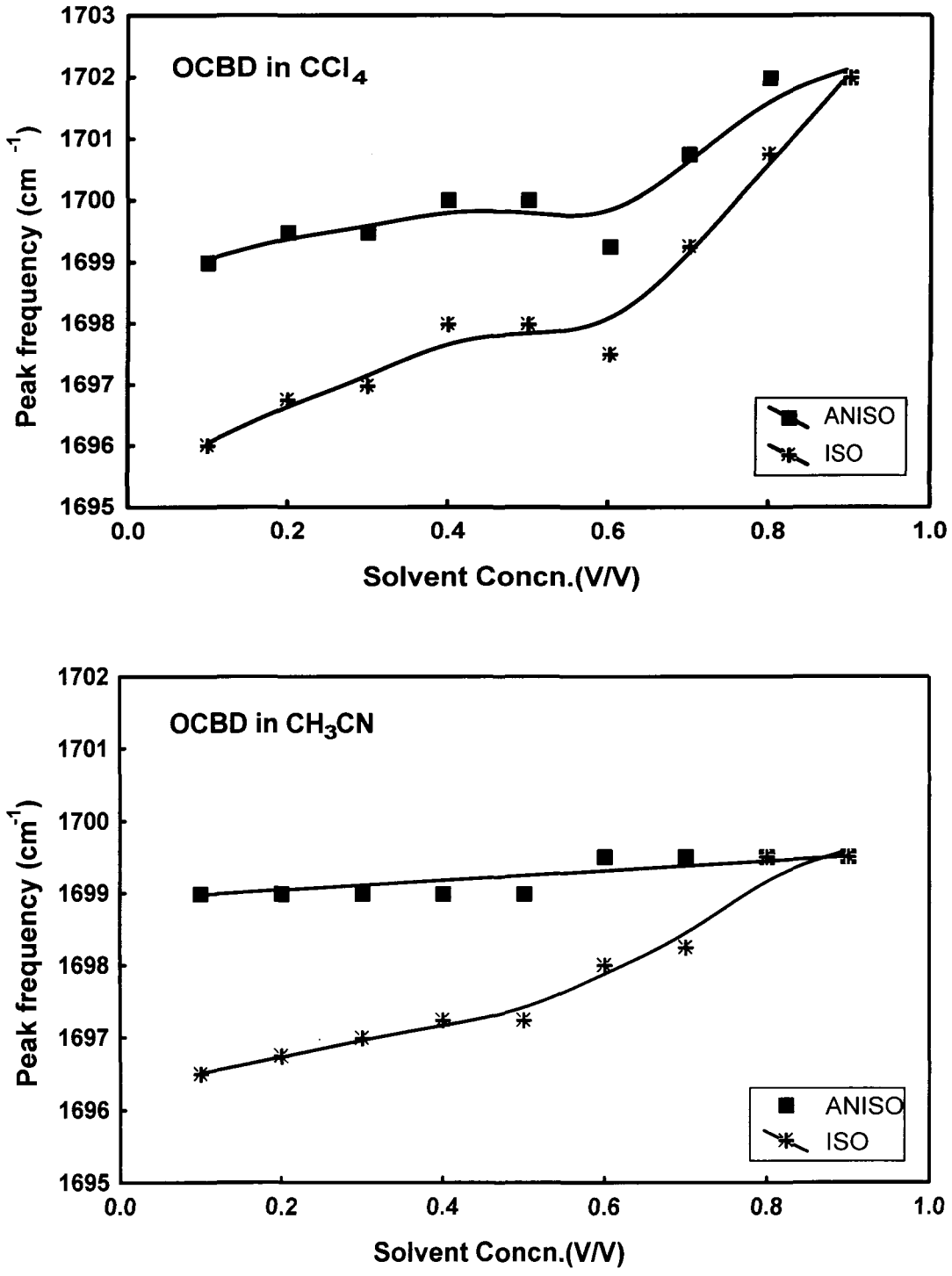

Fig. 4.3 (a) Variation of peak frequencies of isotropic and anisotropic components in different solvent concentrations

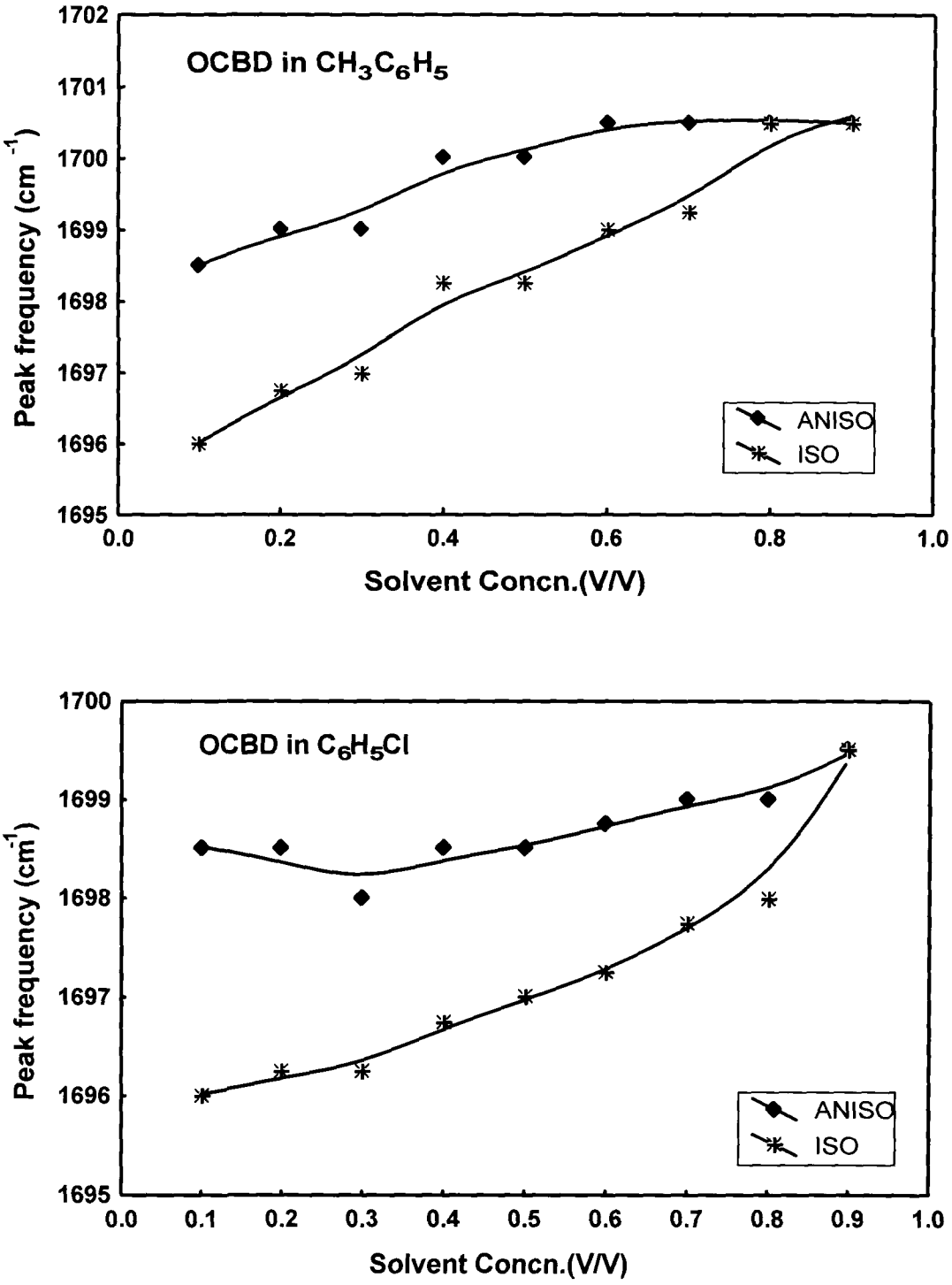

Fig. 4.3 (b) Variation of peak frequencies of isotropic and anisotropic components in different solvent concentrations

The coupling potential V can be Taylor expanded in the usual manner

$$V = V_0 + \left(\frac{\delta V}{\delta Q_j}\right)_0 Q + \frac{1}{2}\left(\frac{\delta^2 V}{\delta^2 Q_j}\right)_0 Q^2 + \frac{1}{2}\sum_{ij}\left(\frac{\delta^2 V}{\delta Q_i \delta Q_j}\right)_0 Q_i Q_j + \qquad \textbf{(4.3.1)}$$

and summation is performed over molecules i perturbing the vibration Q_j.

The third term is responsible for the resonance energy transfer and leads to NCE. The coupling potential due to dipole-dipole interactions is given by

$$V = \left(\frac{\mu_i \mu_j}{R_{ij}^3}\right) K_{ij} \qquad \textbf{(4.3.2)}$$

where μ is the dipole moment of the molecule, R_{ij} is the distance between the two dipoles and K_{ij} is the geometric factor describing the relative orientation of the two dipole moments.

The expression for TD-TD interactions which is responsible for the NCE in the liquid is given by

$$\Delta E_{TD-TD} = \left(\frac{\delta \mu}{\delta Q}\right)^2 \left\langle \frac{K_{ij}}{R_{ij}^3} \right\rangle \left(< 1|Q|0 > \right)^2 \qquad \textbf{(4.3.3)}$$

According to McHale, the splitting ($\Delta\nu$) in the transition dipole coupling model is given as

$$\delta\nu = \frac{2\mu^2\left(\frac{\delta\mu}{\delta Q}\right)^2}{25\pi^2 c^2 \nu_0 kTd^3} \frac{N_0}{V_M} \phi \; S \qquad \textbf{(4.3.4)}$$

where μ is the dipole moment, ν_0 and Q are the wave number and the normal coordinate of the vibrational mode under consideration, d is the minimum intermolecular distance, N_0 is Avogadro's number, V_M is the molar volume of the solute and S is a screening factor for the interaction energy of two dipoles.

Following the Onsager- Fröhlich dielectric model [20,29], which treats the dielectric as a continuum, the polarizability as isotropic and dipoles as point dipoles, the screening factor due to permanent dipole is $S_P = \left(\frac{n^2+2}{2\varepsilon + n^2}\right)^2 \varepsilon$ and the factor $S_t = \frac{(n^2+2)^2}{9n^2}$ is due to transition dipole where ε is the dielectric constant and n is the refractive index. The screening factor does not vary much with the variation of the solvent; hence, the term S_t may be considered constant.

Therefore, considering only S_P term, the equation [20] for $\delta\nu$ taken the form

$$\delta\nu\left(2\varepsilon + n^2\right)^2 \varepsilon^{-1} = \frac{2\mu^2\left(\frac{\delta\mu}{\delta Q}\right)^2\left[n^2+2\right]^2 N_0}{25\pi^2 c^2 \nu_0 kTd^3 V_M}\phi \qquad \textbf{(4.3.5)}$$

where N_o is the Avogadro's number, ϕ is the volume of the solute, ν_o is the vibrational frequency of the isolated molecule, d is the minimum intermolecular distance, V_M is the molar volume of the solute, kT is the thermal energy, μ is the dipole moment, Q is the mass weighted normal coordinate and $\frac{\delta\mu}{\delta Q}$ is the transition moment.

The dielectric constant of the solution was calculated by using the relation

$$\varepsilon_{solution} = \phi\, \varepsilon_{solute} + (1- \phi)\, \varepsilon_{solvent} \qquad \textbf{(4.3.6)}$$

Table 4.1 shows the molecular parameters for solute and solvent molecules. The value of the parameter $F=\delta\nu(2\varepsilon +n^2)^2\varepsilon^{-1}$ was found out and plotted as a function of the solute volume fraction ϕ for different solvents (Figs. 4.4(a) and 4.4(b)). The graph clearly shows that the data points fit well in exponential curves for all the solvents except CH_3CN. In case of OCBD- CH_3CN system, the data points are lying in a straight line, which indicates that the dielectric continuum theory holds better in this system. The high dielectric constant of CH_3CN solvent may be playing a significant role for such behaviour. The exponential curves for the three solvents (CCl_4, $CH_3C_6H_5$ and C_6H_5Cl solvents) show that the Onsager- Fröhlich dielectric continuum model does not hold good in these systems. Therefore, in these solvents, the discreteness of the medium exists and the screening effect may not be as effective as envisaged by

Table 4.1

Molecular parameters

Molecules	Dielectric Constant (ε)	Refractive Index (n)
C_7H_5ClO	23	1.57
CCl_4	2.24	1.457
CH_3CN	37.5	1.342
$CH_3C_6H_5$	2.4	1.494
C_6H_5Cl	5.7	1.523

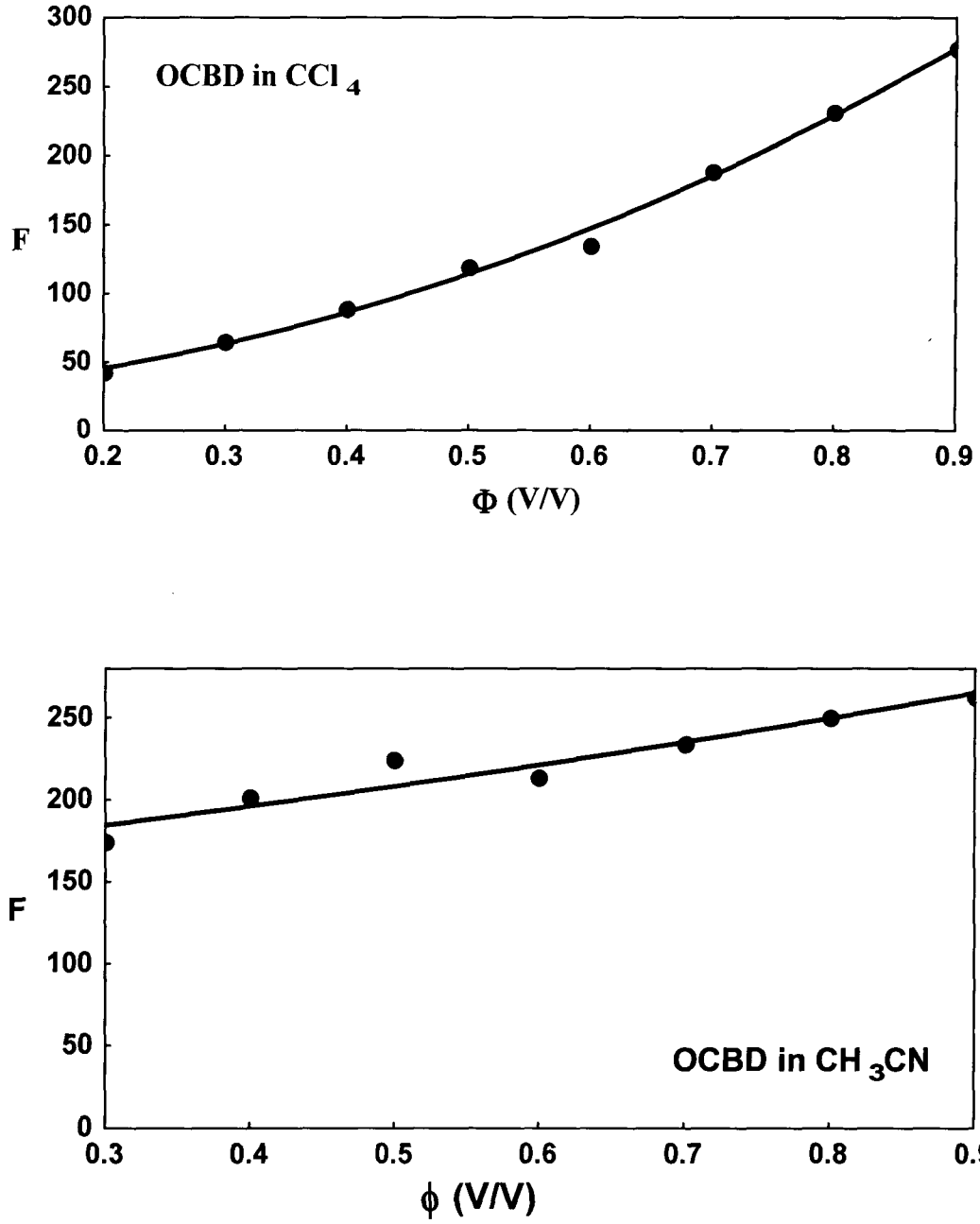

Fig. 4.4 (a) Variation of parameter F as a function of the solute volume fraction ϕ

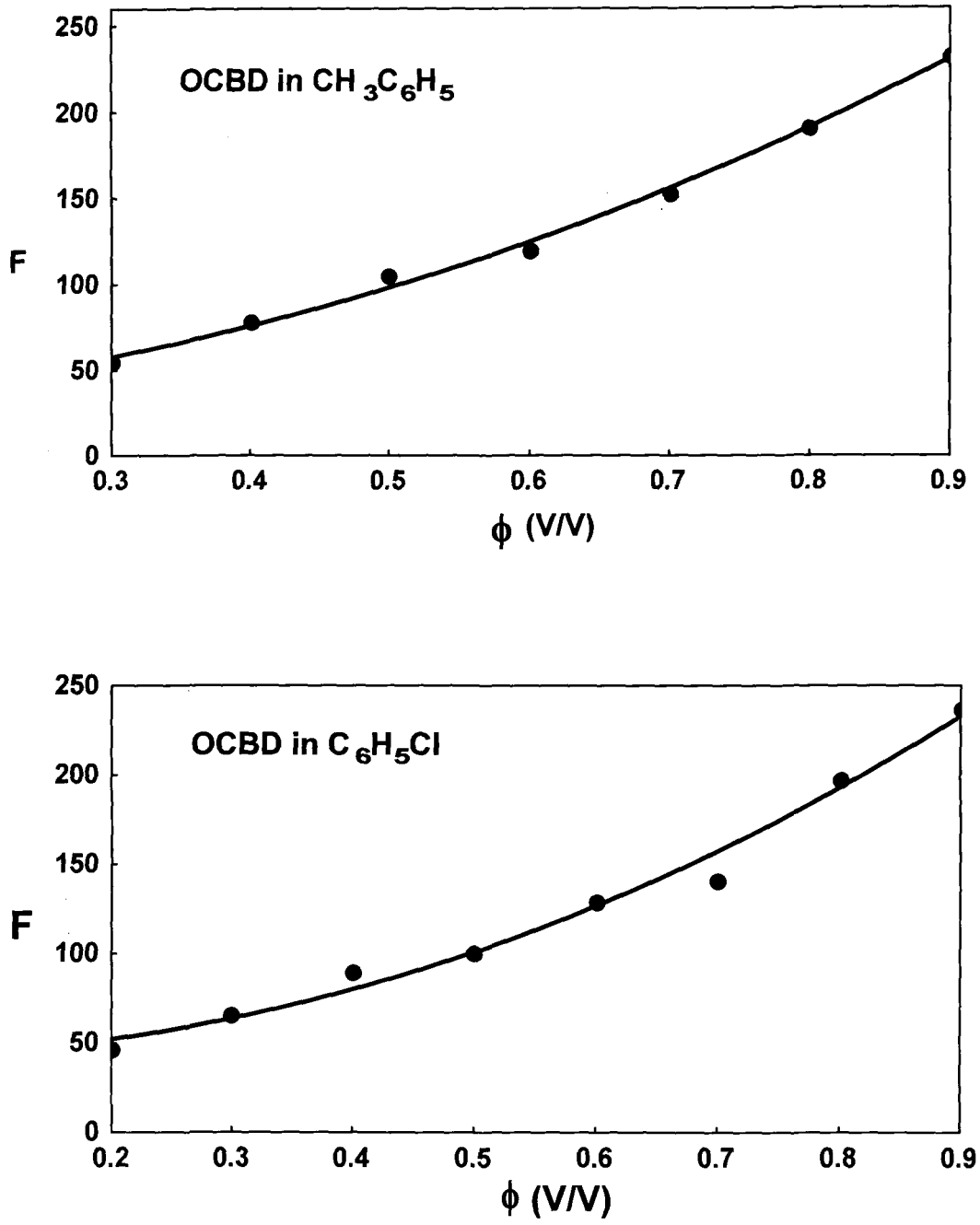

Fig. 4.4 (b) Variation of parameter F as a function of the solute volume fraction ϕ

the Onsager-Fröhlich model in such systems. However, the exponential curves indicate the repulsive nature of the interacting systems except in case of CH_3CN solvent.

For the case of OCBD-benzene substituted molecules, steric hindrance may also be contributing to the repulsive potential, which depends upon the position of the substituents in the aromatic ring, besides the presence of Chlorine atom. Considering the solvent effect of CCl_4 on the C=O stretching mode of OCBD, the C-Cl bond of CCl_4 molecule points to the carbonyl oxygen producing a strong electric field on C=O bond in the direction that the chlorine atoms look as if they had large positive charges [35]. The CH_3CN molecule may be visualized as a cylindrical structure. This cylindrical unit may come in close proximity with the benzenoid portion and may align with the plate likes structure of OCBD. The multipolar interactions may start playing a significant role. The dipole-quadrupole interactions, which are repulsive in nature[1], may not allow the close proximity of solute-solvent molecules.

In order to get more information about the intermolecular interactions in liquid mixtures, the anisotropic Raman components were studied for OCBD in different solvents. The bandwidths of the anisotropic component were measured. The anisotropic bandwidth in the neat liquid is 15.8 cm^{-1}. Fig.4.5 shows the plot of Γ_{aniso} as a function of solvent concentration. The plot of Γ_{aniso}

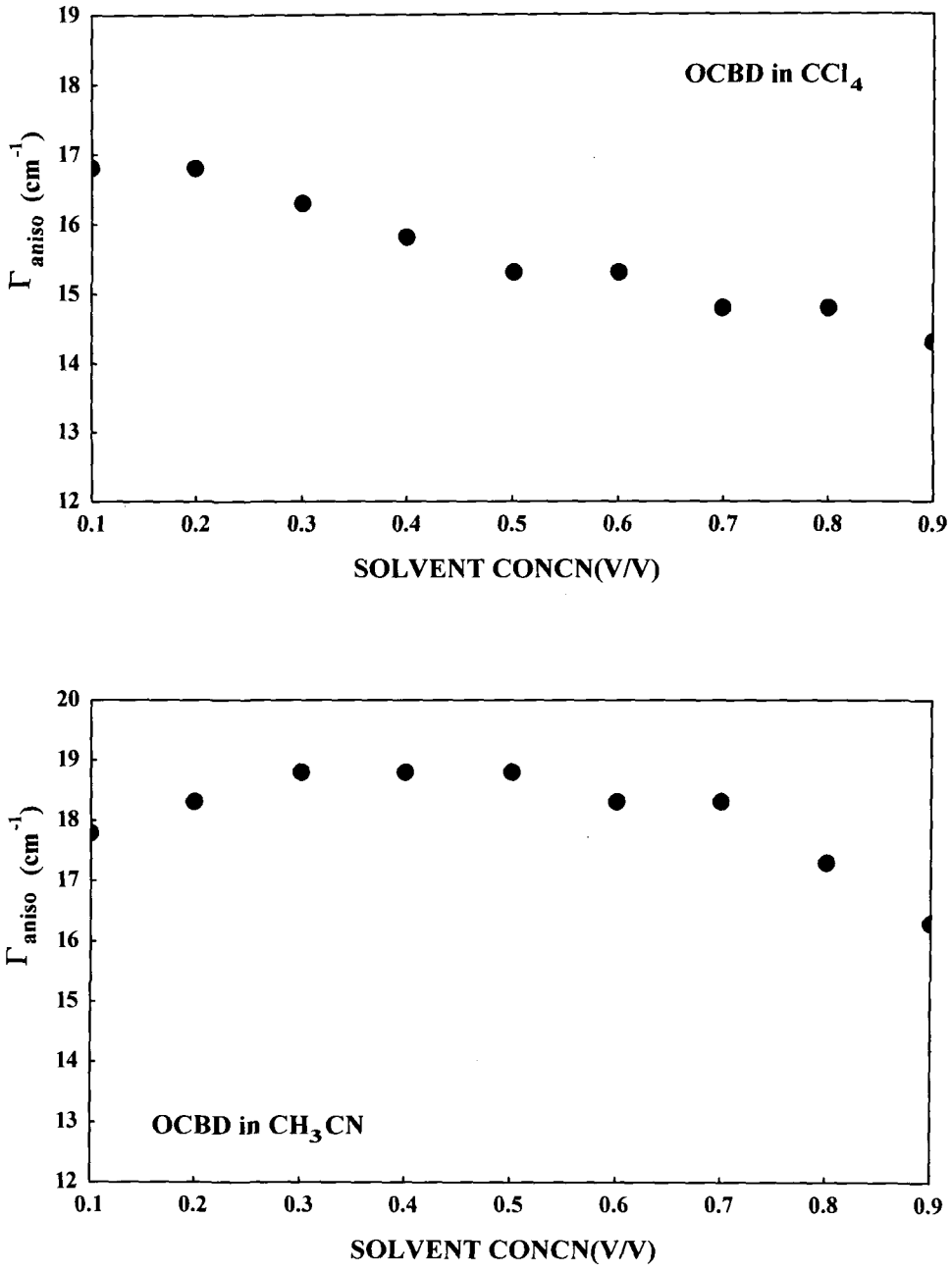

Fig.4.5(a). Variation of anisotropic bandwidth with solvent concentration in CCl_4 and CH_3CN solvents

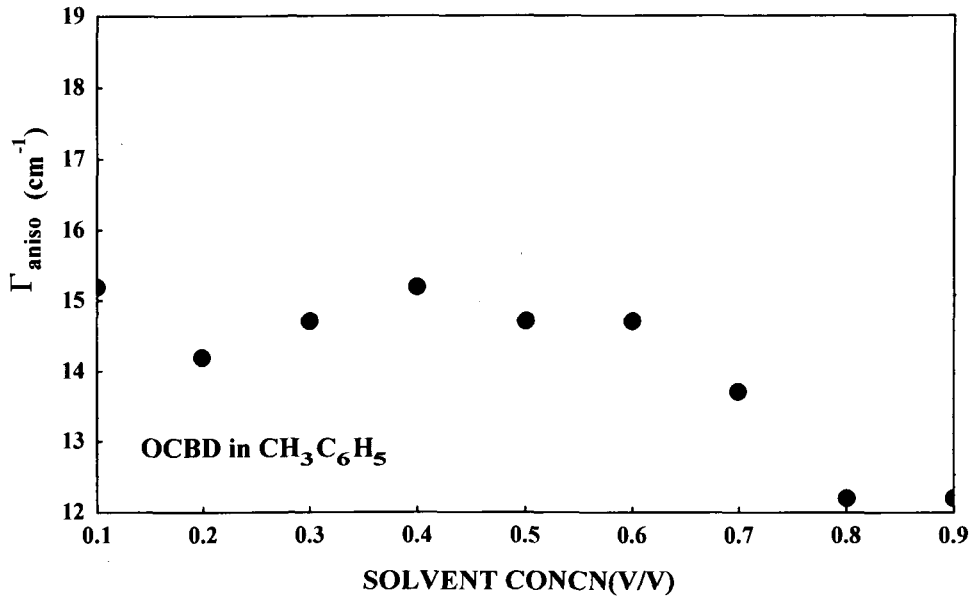

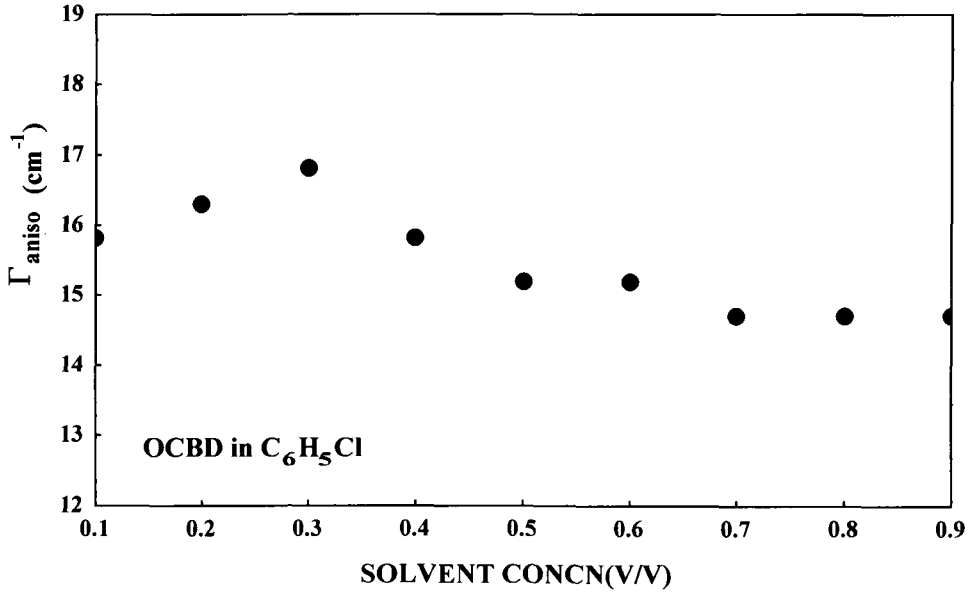

Fig.4.5(b). Variation of anisotropic bandwidth with solvent concentration in $CH_3C_6H_5$ and C_6H_5Cl solvents

as a function of solvent concentration shows that the data points are scattered and cannot be fitted into a single curve. For CCl_4 solvent, the data points show a decrease in the bandwidth while going from lower to higher solvent concentration, whereas for CH_3CN and C_6H_5Cl solvents, the data points show an initial increase and then a decrease in the bandwidth as the concentration increases. In case of $CH_3C_6H_5$ solvent, the data points show somewhat different pattern as compared to others. However, the bandwidth is found to decrease at high solvent concentration for all the solvents. The bandwidths of isotropic Raman component (Γ_{iso}) were also found out in order to see the changing pattern according to different solvent concentrations and plotted with respect to the solvent concentration (Fig.4.6). Interestingly, the isotropic bandwidths are also found to decrease at higher solvent concentration. The dramatic change in shape on going from lower to higher solvent concentration region reflects the changes in liquid dynamics brought about by solvent collisions[36,37]. Furthermore, the non-linearity of Γ_{aniso} showing in these plots from lower to higher solvent concentration may be due to the structural characteristics and the interacting nature of the substituents in the molecules. The interpretation of the data may require the knowledge of interacting nature of the molecular fragments. The theory proposed by Bratos and Tarjus [38-41] to interpret Raman band shapes of pure van der Waals' liquids that predict a different spectral

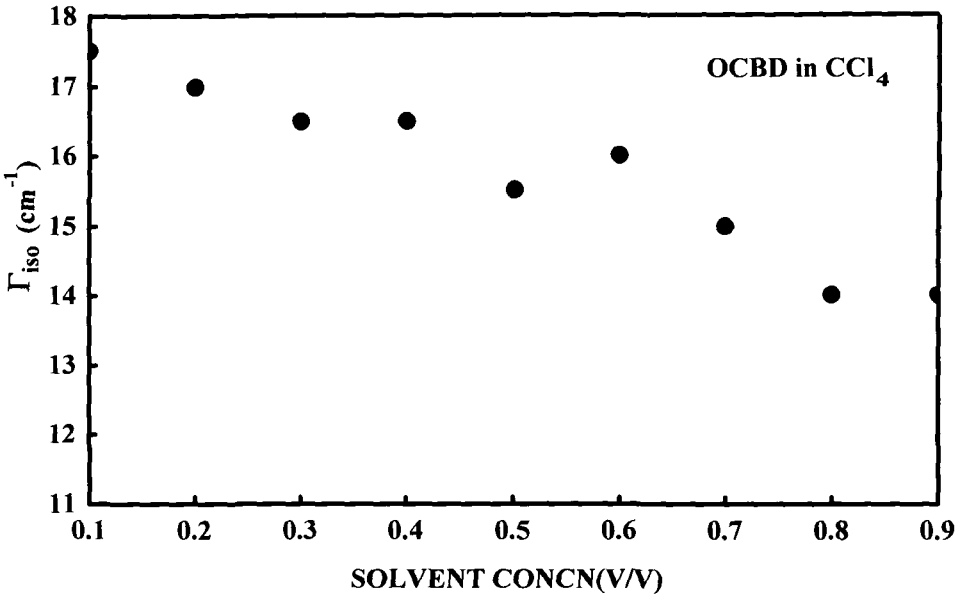

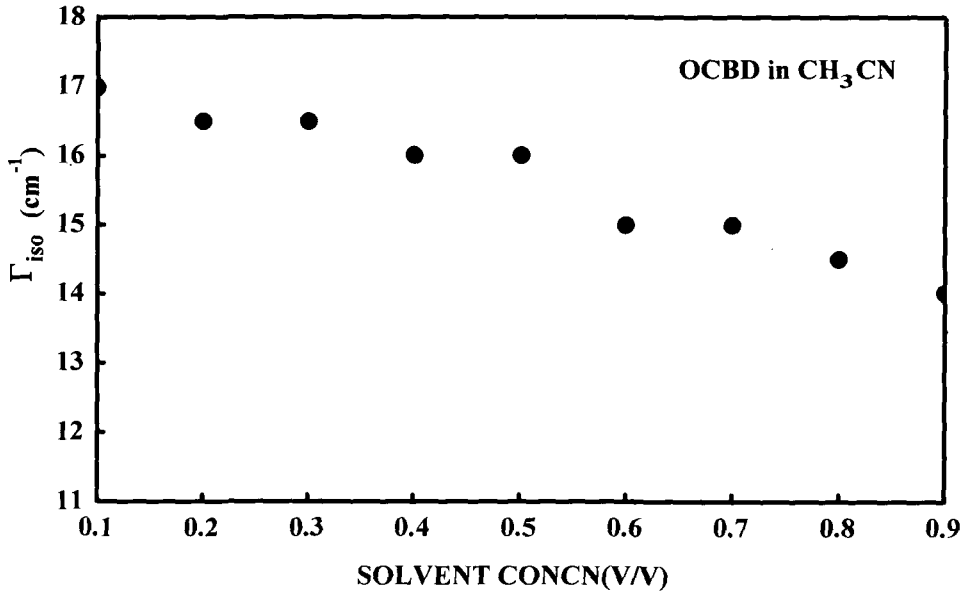

Fig.4.6 (a) Variation of isotropic bandwidth with solvent concentration in CCl_4 and CH_3CN solvents

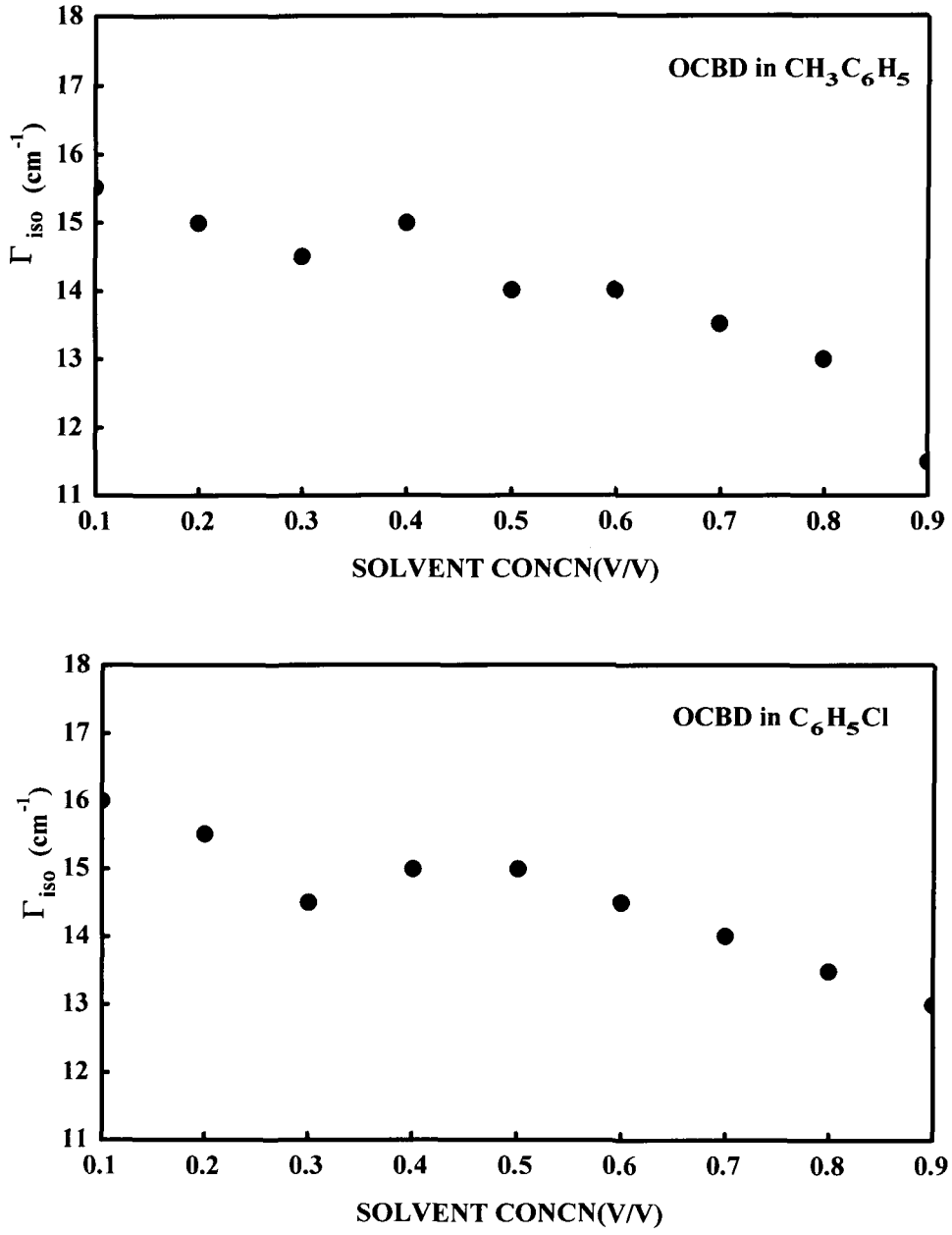

Fig.4.6(b). Variation of anisotropic bandwidth with solvent concentration in $CH_3C_6H_5$ and C_6H_5Cl solvents

behaviour for isotopic and chemical solutions. They show that for isotopic solutions (consisting of two different isotopes) the variation with concentration of the half width of an isotropic Raman band strongly depends on the speed of vibrational modulation. In the model developed by Bratos and Tarjus, the system consisting of N_A solute molecules and N_B solvent molecules was considered where the solvent molecules may be an active molecule or belong to an entirely different chemical species. The molecules of the species A execute anharmonic vibrations described by internal co-ordinates $r = (r_1, r_2,.....,r_N)$ which are governed by a semi-classical Hamiltonian

$$H(r,t)=\left[\frac{1}{2}\sum_{i=1}^{N_A}P_i^2+\frac{1}{2}\sum_{i=1}^{N_A}Kr_i^2+\frac{1}{6}\sum_{i=1}^{N_A}fr_i^3+.....\right]+[V(r,t)] \qquad \textbf{(4.3.7)}$$

where K and f are the harmonic and anharmonic force constants respectively, P_i represent the momentum co-ordinates.

$$V(r,t)=\sum_{i,j=1}^{N_A}V_{ij}^{(AA)}(r,t)+\sum_{i=1}^{N_A}\sum_{j'=1}^{N_B}V_{ij'}^{(AB)}(r,t) \qquad \textbf{(4.3.8)}$$

where the pair potentials $V_{ij}^{(AA)}$ and $V_{ij'}^{(AB)}$ describe the solute-solute and the solute-solvent interactions respectively. These potentials differ from each other for chemical, but coincide for isotopic solvents.

The molecules N_A and N_B are assumed to execute stochastic rotations and translations described by the co-ordinates

$$\theta = \left(\theta_1^{(A)}, \theta_2^{(A)}, \ldots\ldots, \theta_{N_A}^{(A)}, \theta_1^{(B)}, \theta_2^{(B)}, \ldots\ldots, \theta_{N_B}^{(B)}\right) \qquad \textbf{(4.3.9)}$$

and

$$R = \left(R_1^{(A)}, R_2^{(A)}, \ldots\ldots, R_{N_A}^{(A)}, R_1^{(B)}, R_2^{(B)}, \ldots\ldots, R_{N_B}^{(B)}\right) \qquad \textbf{(4.3.10)}$$

However, the correlation between vibrations and rotations, although present, is weak. Moreover, there is no collision-induced scattering and the direct vibrational interactions between the solute and solvent molecules are neglected in this model, instead the rotational-translational interactions are taken into consideration.

In case of isotopic solutions, it is seen from the work of Bratos and Tarjus [39] that the vapour-liquid frequency shift $\Delta\omega$ of an isotropic Raman band is a linear function of the concentration (ϕ_A) of the solute molecules. On the other hand, the position of an anisotropic Raman band is independent of concentration. The variation with concentration of the half-width of an isotropic Raman band strongly depends on the speed of vibrational modulation. The

expressions for the half width $\Delta\omega_{1/2}$ in the fast modulation (FM) and in the slow modulation (SM) limits are given by

$$\Delta\omega_{1/2}^{SM} = (2\ln 2)^{1/2}\{ [\ \langle(\Delta\Omega_{11})^2\rangle\ ] + \phi_A[2N(\langle\Delta\Omega_{11}\Delta\Omega_{12}\rangle) + N^2\langle(\Delta\Omega_{12})^2\rangle] + \phi_A^2[N^2\langle\Delta\Omega_{12}\Delta\Omega_{13}\rangle] + \ldots\ \}^{1/2} \quad \textbf{(4.3.11)}$$

$$\Delta\omega_{1/2}^{FM} = \{ [\ \langle(\Delta\Omega_{11})^2\rangle\tau_{11,11}\ ] + \phi_A[\ 2N\langle\Delta\Omega_{11}\Delta\Omega_{12}\rangle\tau_{11,12} + N\langle(\Delta\Omega_{12})^2\rangle\tau_{12,12}\ ] + \phi_A^2[N^2\langle\Delta\Omega_{12}\Delta\Omega_{13}\rangle\tau_{12,13}]\ \} \quad \textbf{(4.3.12)}$$

where τ is a representative correlation time,

$$\Omega_{ii} = \sum_{j=1}^{N_A}\omega_{ij}^{(AA)} + \sum_{j'=1}^{N_B}\omega_{ij'}^{(AB)}\ , \quad \Omega_{ij} = \frac{1}{2\mu\omega_0}\left[\frac{\partial^2 V^{(AA)}}{\partial r_i \partial rj}\right]_0 = \varpi_{ij}^{(AA)},\ i \neq j$$

and $\Delta\Omega_{ij} = \Omega_{ij} - \langle\Omega_{ij}\rangle$

In these equations, $\omega_{ij}^{(AA)}$ represents the frequency increment induced in the molecule i of the species A by a non-resonant interaction with a molecule j of the same species and $\omega_{ij'}^{(AB)}$ describes a similar meaning where the non-resonant

interaction is between two molecules i and j' of different species A and B. $\varpi_{ij}^{(AA)}$ denotes the frequency shift generated in molecules i and j of the species A by a resonant interaction between them.

Then one can conclude that the half-width $\Delta\omega_{1/2}$ is a quadratic function of ϕ_A if the vibrational modulation is fast. If the vibrational modulation is slow then the half-width depends on the square root of ϕ_A and it exhibits an intermediate behaviour for intermediate modulation speeds. The half-width of an anisotropic Raman band is, in practice, weakly concentration dependent.

On the other hand, spectral properties of solutions involving chemical solvents are much more difficult to analyze than the isotopic solutions. This is due to the variation of the chemical composition of the solvation shell surrounding the active molecule as well as to the presence of the structure-breaking processes influencing various probability distributions. In chemical solutions, the peak frequencies of isotropic and anisotropic Raman bands are concentration dependent. The expressions of frequency shifts for isotropic and anisotropic Raman band are

$$\Delta\omega_{iso}=\left[\ N\left\langle\omega_{12'}^{(AB)}\right\rangle\ \right]+\phi_A\left[\ \left(N\left\langle\omega_{12}^{(AA)}\right\rangle-N\left\langle\omega_{12'}^{AB}\right\rangle\right)+N\left\langle\varpi_{12}^{(AA)}\right\rangle\ \right] \qquad \textbf{(4.3.13)}$$

$$\Delta\omega_{\text{aniso}} = [\ N\langle\omega_{12'}^{(AB)}\rangle\ ] + \phi_A [\ (N\langle\omega_{12}^{(AA)}\rangle - N\langle\omega_{12'}^{AB}\rangle)\ ] \qquad \textbf{(4.3.14)}$$

which are in fact nonlinear in ϕ_A. The half-width of isotropic and anisotropic Raman bands is concentration dependent. However, this dependence is complex even in the slow and fast modulation limits. In chemical solutions, the solvent-induced effects on the band shape are of a similar magnitude in isotropic and anisotropic Raman spectra. Moreover, the environmental fluctuations of transition frequency and rotational fluctuations depend on ϕ_A, which is of different behaviour found in isotopic solutions.

It has been shown that for chemical solution, the halfwidth of isotropic and anisotropic Raman bands is concentration dependent and the solvent-induced effects on the band shape are of a similar magnitude in isotropic and anisotropic Raman spectra. At low solvent concentration region, the Raman band shape appears to derive its major contribution through the resonant energy transfer (RET) processes where the microscopic local order in liquid phase permits the coupling between the vibrational states of the solute molecule through neighbouring transition dipoles[42-47]. The intermolecular coupling through RET is a function of intermolecular separation and depends on the angular dependence spatial distributions of the interacting dipoles which

determines the relative alignment of the pair molecules. With the increase in solvent concentration, the changes incorporated in terms of spatial distribution of active molecule compounded with the diminution in the degree of microscopic local order by the solvent molecules result in the gradual fall of the contribution through RET mechanism. This type of interacting situations may be considered as the so-called solvent cage effect where the molecules of a solute are confined in a potential well, created by solvent molecules. Such interacting situations are expected to have a significant contribution in determining the Raman band shape in the intermediate solvent concentration region. The interaction energy due to solute-solvent interaction may arise due to the contribution from one or more coupling terms [3-4, 47-48], such as dipole-dipole, dipole-induced dipole, dipole-quadrupole and quadrupole-quadrupole, etc.

In order to interpret the complicated nature, the van der Waals' volume of the sphere of influence in a solute dissolved in four solvents CCl_4, CH_3CN, $CH_3C_6H_5$ and C_6H_5Cl solvents is taken into account. The calculation of van der Waals' volume assumes knowledge of bond distance, intermolecular van der Waals' radii[49] and shapes of atoms in various molecular configurations. Table 4.2 shows the van der Waals' radii of the molecules and (C-Cl) bond length. The centres of the atoms of the surrounding molecules are allowed to be placed near

Table 4.2

van der Waals' radii

C-Cl	C	Cl	H	N
1.77Å	1.6 Å	1.8 Å	1.2 Å	1.5 Å

Table 4.3

van der Waals' volume of the molecular parameters

C=O (cm^3/mole)	CCl_4 (cm^3/mole)	CH_3CN (cm^3/mole)	$CH_3C_6H_5$ (cm^3/mole)	C_6H_5Cl (cm^3/mole)
11.7	114.73	59.44	62.07	63.11

the probe (C=O) and the solvent accessible areas and volumes of molecules may be used to quantify their interaction with the solvent [50, 51]. Hence, the main interaction is considered to be between the dipole moment of C=O and the dipole, quadrupole and octupole moments of the solvents.

For the case of solute-CCl_4, the main interaction is expected between the C=O of the solute and C-Cl bond of the solvent molecule. In the solute molecule a quadrupole moment from the benzenoid portion is present in addition to the permanent dipole of C=O of the solute molecule. However, the benzenoid portion of OCBD being plate like structure the spherical CCl_4 molecule can easily roll over the planes of the solute molecule. The CCl_4 molecule is highly polarizable and has spherical shape; therefore, the solvent's van der Waals' volume was calculated by taking the radius of the sphere to be equal to the sum of C-Cl bond distance and the van der Waals' radii of the chlorine atom. The solvent CCl_4 molecule acquires electric charge due to polarization and as a result an electrostatic potential is developed in the vicinity of the molecule whose value decreases with the increasing distance between the molecules (solute and solvent).

For solute-CH_3CN system, the main interaction is likely between the dipole moment of C=O bond of the solute and the dipole moment of the solvent. When OCBD is dissolved in CH_3CN, the dipole-dipole interaction of

the solute-solvent system will affect the pair interaction. The dipole of CH_3CN molecule will interact with the dipole of the solute and align along the electric field of the solute dipole. Considering the Debye equation for dielectric behaviour[52] which involves the reorientation of the dipolar molecule by cooperative movement with the immediately surrounding molecules, it is possible to write the torque exerted on a dipolar molecule by a field F due to the dipole moment of the C=O bond of the solute

$$-\mu F\sin\theta = \xi\left(\frac{d\theta}{dt}\right) + I\left(\frac{d^2\theta}{dt^2}\right) \qquad \textbf{(4.3.15)}$$

where ξ is the frictional force constant and I is the molecular moment of inertia. A simplistic picture of the above solvent cage effect on a dipolar field [52] can be shown (Fig. 4.7). If a dipole of moment μ is located at the origin of a system of polar co-ordinates pointing along the Z-axis, then the field F at a point r,θ,ϕ where θ is the angle between r and Z-axis and ϕ is the angle between the projection of r in the XY plane and the X-axis has the components

$$F_x = \frac{3\mu}{r^3}\cos\theta\sin\theta\cos\phi$$

$$F_y = \frac{3\mu}{r^3}\cos\theta\sin\theta\sin\phi \qquad \textbf{(4.3.16)}$$

$$F_z = \frac{\mu}{r^3}\left(3\cos^2\theta - 1\right)$$

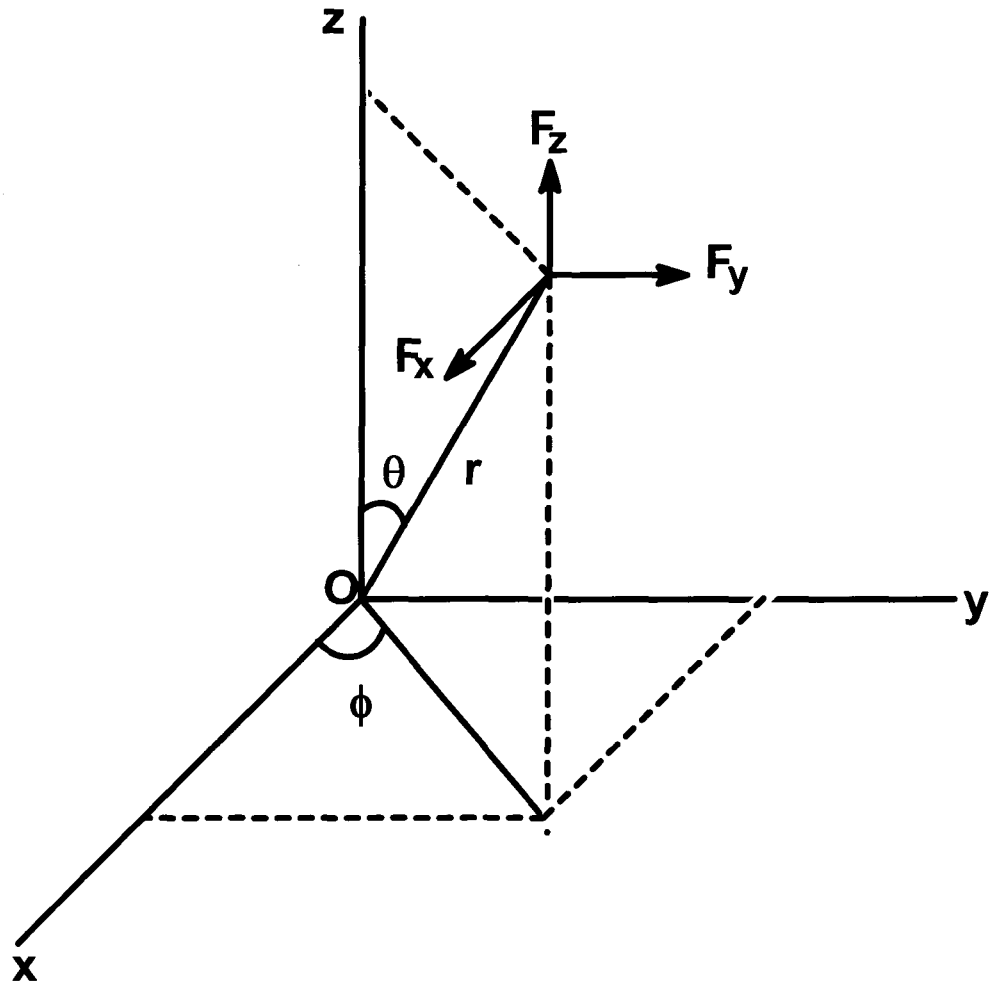

Fig. 4.7 Interacting situation is between the dipole moment of the C=O bond of the solute and the dipole moment of the solvent (acetonitrile).

The distance of closest approach in this case will be determined by the orientation of C-C≡N fragment of the solvent molecule. The dipole of CH_3CN will try to align along the **F** of the dipole of the solute molecule and thus an average component will be there along the director. Thus, the average component of the solvent will be along the solute dipole. In this case, the closest approach is determined by the orientation of the C-C≡N fragment of the solvent molecule. However, the benzene rings of solute molecules approach each other while still interacting through dipole-dipole interactions. These planar benzenoid structures lead to a repulsive quadrupole-quadrupole interaction[53], thereby weakening the pair interactions. However, the liquid nature of the system will maintain the smooth flow because the hydrodynamic forces may be dominant over the electrical forces. The cylindrical shape of the CH_3CN molecule may not hinder the smooth flow of the molecules; hence, the van der Waals' volume for the solvent has been taken for the entire molecule, which is the sum of van der Waals' volume of the C-C≡N fragment and the van der Waals' volume of CH_3 group[49].

However, for solute OCBD-benzene group compound, the main interaction is between the quadrupole moment of solvent benzene and the benzenoid fragment of the solute. If we consider the simple shear flow of a benzene molecule between two parallel planes constituted by the benzenoid

portions of the molecules, hydrodynamic properties are likely to play a significant role. The effective viscosity depends on the orientation of the dipole moment of the solute molecule (the director). The orientation of the director will not be fixed in a liquid; the equation of motion of the director will come into play in addition to the liquid flow [1]. Consider a simple shear flow of planar benzene molecule between two parallel planes of solute molecules along the z-axis normal to the x-axis (Fig.4.8). Hence the velocity gradient is along the x-axis, given by v=[0,0,u(x)]. The flow of the molecule depends on the angles with which the director makes with the flow direction and with the velocity gradient. The translational motions are coupled to inner and orientational motions of the molecules and hence the flow disturbs the alignment leading the rotation of the director. In this case, the effective viscosity is given as $\sigma_{xz} = \eta \frac{du}{\partial x}$ which depends on the orientation of the director (**n**). The angles θ and ϕ specify the direction of the director.

The equation of motion of the director [54] can be written as

$$I\left(\frac{d\Omega}{dt}\right) = \tau_F + \tau_{visc} \qquad \textbf{(4.3.17)}$$

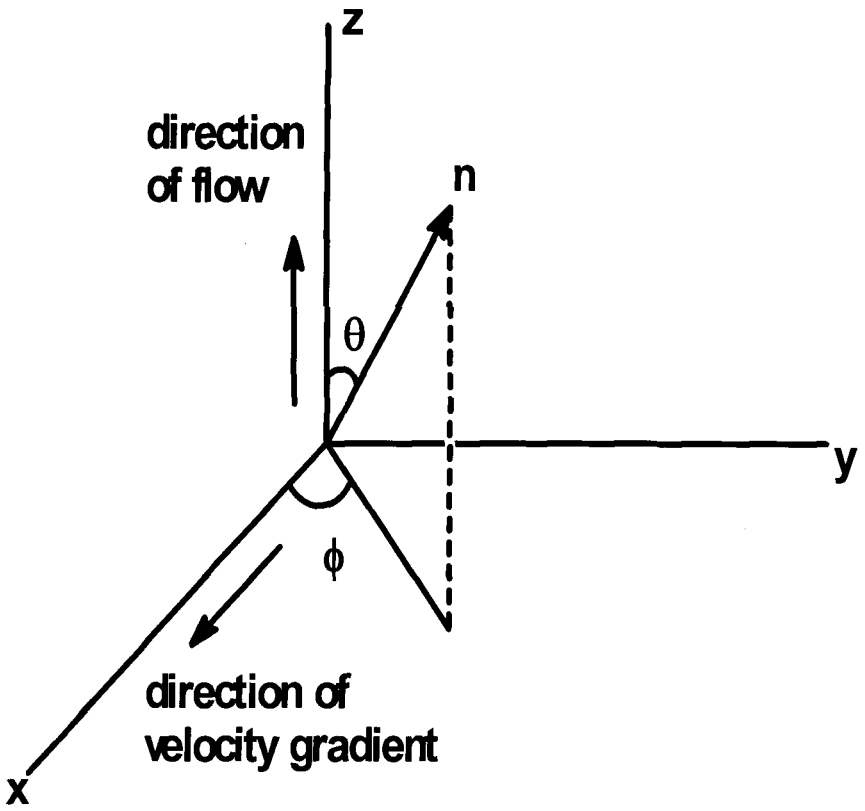

Fig. 4.8 Simple shear flow of planar benzene molecule between two parallel planes of solute molecules

where I is the moment of inertia per unit volume, Ω is the local angular velocity of the director, given by $\Omega = n \times \frac{dn}{dt}$ and τ_F is the torque per unit volume on the director due to the electric forces $\tau_F = \mathbf{n} \times \mathbf{h}$

h being the molecular field. **n** is the director. τ_{visc} is a torque on the director due to frictional forces relative to its surroundings. If n is perpendicular to the benzene plane ($\theta=\phi=90^o$), there is no torque and $\tau_{visc}=0$. For the case when the solvent is parallel to the director, one may find a torque which leads to change in the orientation of the C=O bond due to strong dipole-quadrupole repulsive type of interaction. Due to the changed orientation of one of the C=O bonds in the attracting pair, the interaction becomes weaker under the influence of the solvent. The orientation of the C=O bond of the solute systems comes in close proximity of the benzenoid portion of the solvent molecules. Hence, the van der Waals' volume of the solute is taken as that of C=O and that for the solvent the entire molecular structure is taken into account. For the case of OCBD-$CH_3C_6H_5$ system, the van der Waals' volume of the solvent molecule is taken as the sum of van der Waals' volume of the benzene ring and the van der Waals' volume of CH_3 group[49]. Similarly, for OCBD-C_6H_5Cl system, the van der Waals' volume of the C_6H_5Cl is taken as the sum of van der Waals' volume of the benzene ring and the van der Waals' volume of Chlorine atom.

Table 4.3 shows the calculated values of van der Waals' volume of solute and solvents using the data from Bondi [49] and the schematic diagram used by Bondi, which shows the method of calculation of the van der Waals' volumes from bond distances (l) and from van der Waals' radii (r_w) is given in Chapter 2 (Fig. 2.2).

The van der Waals' volume of the interacting system is estimated[1] by using the equation

$$V_w = \phi V_w(\text{solute}) + (1-\phi)\, V_w(\text{solvent}) \qquad \textbf{(4.3.18)}$$

where ϕ is the solute concentration. The values of $(\Gamma_{aniso}/\ V_w)$ have been determined for each solvent (tables 4.4, 4.5, 4.6, 4.7) and plotted as a function of solvent concentration (Fig.4.9). This graph is an exponential curve in all the solvents. This indicates that the repulsive type of potential $e^{-\alpha R}$ may be playing a significant role. The relative magnitudes of these forces will determine the bandwidths as well as the anisotropy shift of the molecular systems. In short, the present study indicates that different multipolar interactions, which are repulsive in nature, are playing an important role in such complex molecular systems containing aliphatic and aromatic compounds.

Table 4.4

van der Waals' volume and (Γ_{aniso} / V_w) of the OCBD-CCl_4 system

Solvent concentration	Van der Waals' volume of the solution $V_w = \phi\ V_w(solute) + (1-\phi)\ V_w(solvent)$	Γ_{aniso} / V_w
.1	22.00	0.76
.2	32.31	0.52
.3	42.61	0.38
.4	52.91	0.30
.5	63.22	0.24
.6	73.52	0.21
.7	83.82	0.18
.8	94.12	0.16
.9	104.43	0.14

Table 4.5

van der Waals' volume and (Γ_{aniso}/ V_w) of the OCBD-CH_3CN systems

Solvent concentration	van der Waals' volume of the solution $V_w=\phi V_w(solute)+ (1-\phi) V_w(solvent)$	Γ_{aniso}/ V_w
.1	16.47	1.08
.2	21.25	0.86
.3	26.02	0.72
.4	30.8	0.61
.5	35.57	0.53
.6	40.34	0.45
.7	45.12	0.41
.8	49.89	0.35
.9	54.67	0.30

Table 4.6

van der Waals' volume and (Γ_{aniso}/ V_w) of the OCBD-$CH_3C_6H_5$ system

Solvent concentration	Van der Waals' volume of the solution $V_w=\phi V_w(solute)+ (1-\phi) V_w(solvent)$	Γ_{aniso}/ V_w
.1	16.74	0.91
.2	21.77	0.70
.3	26.81	0.60
.4	31.85	0.48
.5	36.89	0.40
.6	41.92	0.35
.7	46.96	0.29
.8	51.99	0.23
.9	57.03	0.21

Table 4.7

van der Waals' volume and (Γ_{aniso}/ V_w) of the OCBD-C_6H_5Cl system

Solvent concentration	Van der Waals' volume of the solution $V_w=\phi V_w(solute)+(1-\phi) V_w(solvent)$	Γ_{aniso}/ V_w
.1	16.84	0.94
.2	21.98	0.74
.3	27.12	0.62
.4	32.26	0.49
.5	37.41	0.41
.6	42.55	0.36
.7	47.69	0.31
.8	52.83	0.28
.9	57.97	0.25

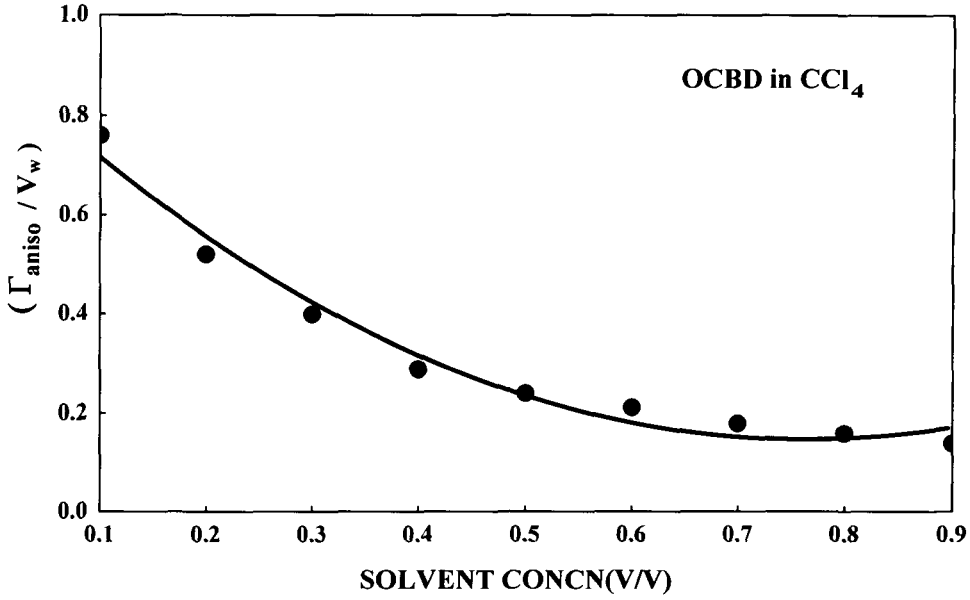

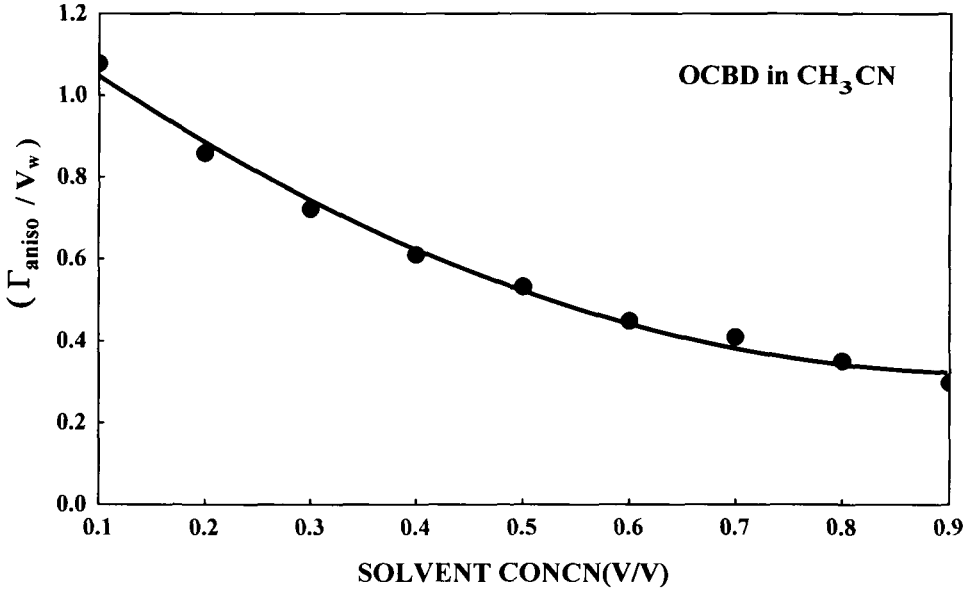

Fig. 4.9 (a) Variation of (Γ_{aniso}/ V_w) with solvent concentration

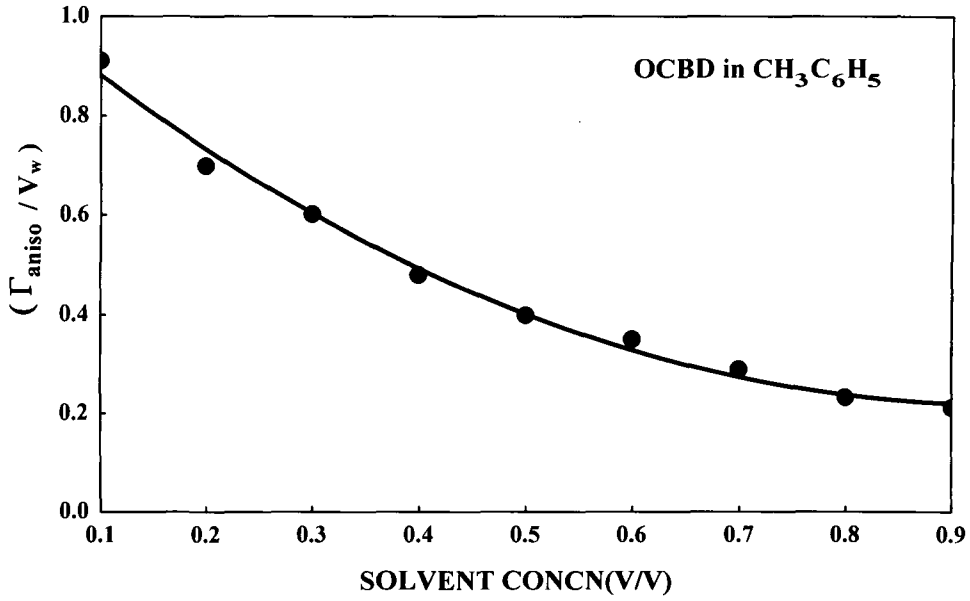

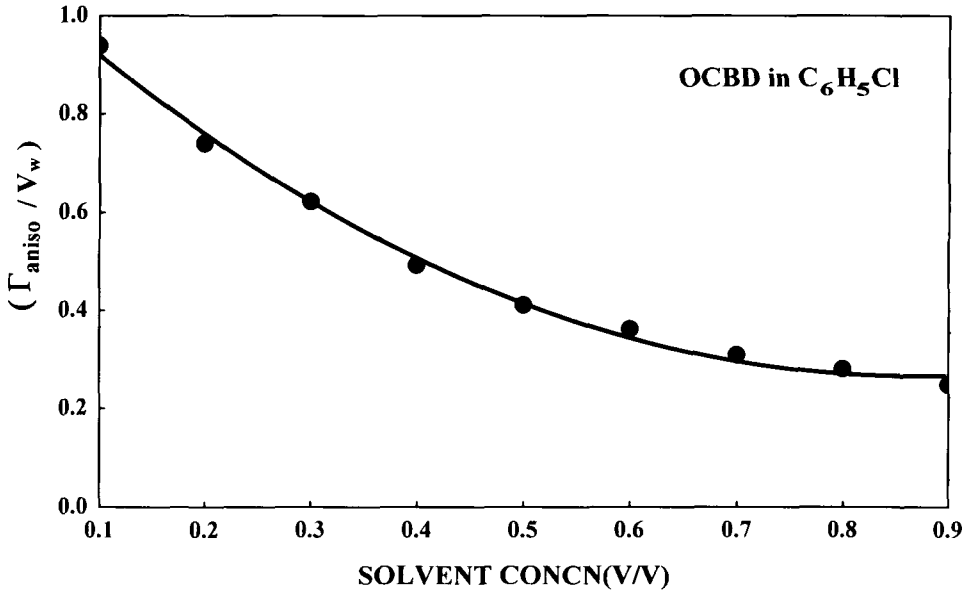

Fig. 4.9 (b) Variation of (Γ_{aniso}/ V_w) with solvent concentration

REFERENCES:

1. A. Das and K. Kumar, J. Raman Spectrosc. **30**, 547 (1999).
2. A. Das, K. Kumar, Spectrochim. Acta, **54A**, 793 (1998).
3. M. Musso, H.Torii, M. G. Giorgini and G. Döge,J. Chem. Phys. **110**, 10076 (1999).
4. G. Fini, P. Mirone and B. Fortunato, J. Chem. Soc. Faraday Trans. **269**, 1243 (1973).
5. G. Fini, P. Mirone, Spectrochim. Acta, **32A**, 625 (1976).
6. *P. Mirone, G. Fini, J. Chem. Phys.* **71**, *2241 (1979).*
7. C. H. Wang, J. McHale, J. Chem. Phys. **72**, 4039 (1980).
8. J. McHale, J. Chem. Phys. **75**, 30 (1981).
9. D. E. Logan, Mol. Phys. **58**, 79 (1986).
10. D. E. Logan, Chem. Phys. **103**, 215 (1986).
11. D. E. Logan, Chem. Phys.**131**, 199 (1989).
12. H. Torii and M. Tasumi, J. Chem. Phys. **99**, 8459 (1993).
13. H. Torii, J. Phys. Chem.**103A**, 2843 (1999).
14. H. Torii in "Novel approaches to the structure and dynamics of liquids: Experiments, Theories and Simulations", J.Samios and V.A.Durov(Eds.), Kluwer, 343 (2004).

15. H. D. Thomas and J. Jonas, J. Chem. Phys. **90**, 4144 (1989).

16. W. Schindler, T. W. Zerda and J. Jonas, J. Chem. Phys. **81**, 4306 (1984).

17. A. Purkayastha and K. Kumar, Spectrochim. Acta, **42A**, 1379 (1986).

18. A. Purkayastha and K. Kumar, Spectrochim. Acta, **43A**, 1269 (1987).

19. A. Purkayastha and K. Kumar, J. Raman Spectrosc. **22**, 721 (1991).

20. A. Das and K. Kumar, J. Raman Spectrosc. **30**, 563 (1999).

21. M. G. Giorgini, Pure Appl. Chem. **76**, 157 (2004).

22. M. Musso, H. Torii, P. Ottaviani, A. Asenbaum and M. G. Giorgini, J. Phys. Chem. **106A**, 10152 (2002).

23. A. Morresi, M. Paolantoni, P. Sassi, R. S. Cataliotti and G. Paliani, J. Phys. Condens. Matter, **12**, 3631 (2000).

24. M. G. Giorgini, M. Musso, A. Asenbaum and G. Döge, Mol. Phys. **98**, 783 (2000).

25. H. Torii, M. Musso, M. G. Giorgini and G. Döge, Mol. Phys. **94**, 821 (1998).

26. M. Musso, M. G. Giorgini, G. Döge and A. Asenbaum, Mol. Phys. **92**, 97 (1997).

27. R. J. Bartholomew and D. E. Irish, J. Raman Spectrosc. **29**, 115 (1998).

28. M. G. Giorgini, M. Musso and P. Ottaviani, Mol. Phys. **99**, 1485 (2001).

29. M. G. Giorgini, G. Fini and P. Mirone, J. Chem. Phys. **79**, 639 (1983).

30. G. Döge, R. Arnt and J. Yarwood, Mol. Phys. **52**, 399 (1984).

31. T. F. Sun, J. B. Chan, S. L. Wallen and J. Jonas, J. Chem. Phys. **94**, 7486 (1991).

32. M. A. Ricci, G. Signorelli and V. Mazzacurati, J. Phys.Condens. Matter, **2**, 183 (1990).

33. C. J. Fecko, J. D. Eaves and A. Tokmakott, J. Chem. Phys. **117**, 1139 (2002).

34. K. Tanabe, Spectrochim. Acta, **40A**, 437 (1984).

35. H. Torii, J. Chem. Phys. **119**, 2192 (2003).

36. G. Moser, A. Asenbaum and G. Döge, J. Chem. Phys. **99**, 9389 (1993).

37. G. Moser, A. Asenbaum, J. Barton and G. Döge, J. Chem. Phys. **102**, 1173 (1995).

38. S. Bratos and G.Tarjus, Phys. Rev. A, **24**, 1591 (1981).

39. S. Bratos and G. Tarjus, Phys. Rev. A, **32**, 2431 (1985).

40. S. Bratos and G. Tarjus, Can. J. Chem. **63**, 2047 (1985).

41. G. Tarjus and S. Bratos, Phys. Rev. A, **34**, 4202(1986).

42. W. Schindler, T. W. Zerda and J. Jonas, J. Chem. Phys. **79**, 639 (1983).

43. G. Fini, P. Mirone, Spectrochim. Acta, **32A**, 625 (1976).

44. P. Mirone, G. Fini, J. Chem. Phys. **71**, 2241 (1979).

45. D. W. Oxtoby, J. Phys. Chem. **87**, 3028 (1983).

46. C. H. Wang, J. McHale, J. Chem. Phys. **72**, 4032 (1980).

47. D. W. Oxtoby, Annu. Rev. Phys. Chem. **32**, 77 (1981).

48. A. Das, R. Das, K. Kumar, Spectrochim. Acta, **58A**, 1583(2002).

49. A. Bondi, J. Phys. Chem. **68**, 441(1964).

50. Lee B., F. M. Richards, J. Mol. Biol. **55**, 379 (1971).

51. Eisenberg. D, A. D. Mclachlan, Nature, **319**, 199(1986).

52. C. P. Smyth, "Molecular Interactions", edited by H. Ratajczak and W. J. Orville-Thomas, **Vol2**, John Wiley and Sons, Chichester (1981).

53. C. G. Gray and K. E. Gubbins, Theory of Molecular Fluids, **Vol.1** Fundamentals, Clarendon Press, Oxford (1984).

54. W. H. de Jeu, Physical properties of liquid crystalline Materials, Liquid Crystal Monographs **Vol.1**, Gordon and Breach Science publishers, New York (1981).

CHAPTER 5

CHAPTER 5

RAMAN BAND SHAPE ANALYSIS OF O-CHLOROBENZALDEHYDE: MICROVISCOSITY DEPENDENT STUDY

1. Introduction

The effect of dilution on the Raman band shape of liquids has always been a subject of considerable interest. The Raman band shape of a reference mode in a molecule is dependent upon the microscopic environment[1,2]. The band shape gives valuable information about the interaction of the reference molecules with its environment and about the structure and dynamics of the bath where the intermolecular forces play an important role. The wavenumber as well as the bandwidth of vibrational bands of the solute system is influenced by the solvent induced perturbations[3-12]. According to Knapp and Fischer[9], the frequency shift and asymmetry of spectral line profile depend on the concentration fluctuation due to the interaction with nearest neighbours and their diffusion dynamics. Schweizer and Chandler[10] have shown the effects of

repulsive and spatially slowly varying attractive forces on the linewidths of the vibrational band in the molecular liquids. This model simultaneously examines both the broadening mechanisms and the frequency shifts. The theory of Schweizer and Chandler is more illustrated by the theory proposed by Ben-Amotz et al[13]. The lineshape contribution from the rapidly changing repulsive forces would be homogeneously broadened leading to Lorentzian lineshape whereas the lineshape contribution due to slowly changing attractive forces would be inhomogeneously broadened with the lineshape becoming Gaussian. The vibrational relaxation in molecular liquids is playing a very important role in analyzing the band shape of such complex molecular systems. This process is responsible for the line broadening of the isotropic Raman spectral component and is generally considered to be due to contributions from vibrational dephasing, population relaxation and resonant energy transfer[11,14] and expected to give detailed information in the study of solution dynamics. To have a better picture of the solute-solvent systems, one may consider the so-called solvent cage effect where the molecules of a solute are confined in a potential well, created by solvent molecules. The molecule is considered to be vibrating against its immediate neighbours, with an occasional escape to its adjacent position. Lee and Richards[15] while explaining the interacting situations of solute and solvents showed that the centres of the atoms of the surrounding molecules

are allowed to be placed near the probe(C=O). According to Eisenberg and Mclachlan [16], the solvent accessible areas and volumes of molecules may be used to quantify their interaction with the solvent. Moser et al[17] proposed a stochastic model which describes the exchange processes of two particles in the nearest neighbour shell of the reference molecule responsible for the line broadening. However, the vibrational relaxation process for complex molecular systems, sometimes cannot explain based on a macroscopic perception of the interacting systems. There may be a marked difference between the interacting situations in the pure solute and when dissolved in solvents, especially at high dilution. A detailed study at the microscopic level is therefore required in order to explain the interacting situations, especially the solvent effects on relaxation rates. Earlier works have done on solvent dependent relaxation rates at the microscopic level[1-2,18-20]. However, the molecules containing the benzene ring have not been fully studied yet. In an attempt to provide further support to the previous findings [1-2,18-20], the *o*-Chlorobenzaldehyde (OCBD) molecule containing C=O stretching mode of vibration has been chosen as the reference mode using different polar and non-polar solvents ($CH_3C_6H_5$, C_6H_6, C_6H_5Cl, CCl_4 and $CHCl_3$ solvents respectively). Moreover, the C=O stretching vibration of OCBD is well isolated from other normal modes of vibration and hence, is a

good candidate for the study of hydrodynamic properties in solute-solvent interactions.

2. Experimental

The measurements were carried out by means of a SPEX Ramalog 1403 double monochromator equipped with a cooled RCA C31034 photomultiplier and photon counting arrangement. The spectrometer control and data processing were achieved with the help of a Datamate using DM-3000 software. The 4880 Å line from the Spectra Physics model 165 Ar^+ laser was used as the excitation source. The spectral slit width was kept at 2 cm^{-1}. The compounds were commercial products and they were used without further purification. The accuracy of measurement is believed to be ± 0.5 cm^{-1}. The effect of finite slit width was corrected by using the equation [21]

$$\Gamma_t = \Gamma_a [\, 1 - (S/\Gamma_a)^2] \qquad \textbf{(5.2.1)}$$

where Γ_t and Γ_a are the true and apparent Raman linewidth (FWHM) respectively, and S is the spectral slit width in cm^{-1}.

We also used the method of Singh et al [22] for the correction of the effect of finite slit width on the observed Raman linewidth. The values are found to be the same as the values calculated using equation (5.2.1).

3. Results and Discussion

The Raman spectra of OCBD dissolved in various polar and non-polar solvents ($CH_3C_6H_5$, C_6H_6, C_6H_5Cl, CCl_4 and $CHCl_3$) have been recorded and the isotropic components were obtained. Vibrational phase relaxation leads to the broadening of the isotropic Raman band, which requires the knowledge of the potential coupling between the molecules and bath. The different mechanisms that contribute to the coupling potential are dispersion interaction, dipole and multipole interactions, repulsive forces etc.

The term $\frac{1}{2}\sum_{ij}\left(\frac{\partial^2 V}{\partial Q_i \partial Q_j}\right)_0 Q_i Q_j$ of the perturbation potential[23] (as explained earlier in chapter 2) is responsible for resonant energy transfer from one oscillator to another and leads to non-coincidence effect. The transition dipole-transition dipole coupling contributes to the resonant energy transfer relevant to the non-coincidence effect and hence

$$\Delta E_{TD\text{ - }TD} = \left(\frac{\delta \mu}{\delta Q}\right)^2 \left\langle \frac{K_{ij}}{R_{ij}^3} \right\rangle \left(< 1|Q|0 > \right)^2 \qquad \textbf{(5.3.1)}$$

where μ is the dipole moment of the molecule, R_{ij} is the distance between the two dipoles and K_{ij} is the geometric factor describing the relative orientation of the two dipole moments.

According to Kubo[24] theory, the resonant energy transfer is due to the modulation of long-range dipolar potentials and to other dephasing mechanisms involving short-range potentials.

Using this theory, the correlation functions, which involve the process of pure dephasing are given by the expression,

$$\Phi_{pp}(t) = \exp[-<\Delta\omega i^2>\{\tau_c^2(e^{-t/\tau_c} - 1) + t\tau_c\}] \qquad \textbf{(5.3.2)}$$

where τ_c is the correlation time describing the fluctuations in the intermolecular potential, $<\Delta\omega_i^2>$ is the root mean square frequency displacement of the instantaneous transition frequency. It measures the range of frequency distribution due to various molecular interactions. τ_C and $<\Delta\omega_i^2>$ contain valuable information about the nature of the intermolecular potential. In the slow modulation limit where $<\Delta\omega_i^2> >> \tau_C^{-1}$, the broadening of the vibrational band is inhomogeneous and the linewidth and lineshape reflect the width and shape of the static probability distribution for the frequency fluctuations which is often assumed to be Gaussian.

In the fast modulation limit, $<\Delta\omega_i^2> << \tau_C^{-1}$, the broadening is homogeneous and the lineshape is narrowed to Lorentzian.

In the slow modulation limit, the phase relaxation functions are described by the vibrational second moment $<\Delta\omega_i^2> = (M_2)_v$ and in the rapid modulation limit, the vibrational relaxation rate is taken to be directly proportional to the product of parameters $(M_2)_v$ and τ_c and thus the relaxation rate[25] is given by

$$\tau_v^{-1} = (M_2)_v\tau_c$$

$$= <\Delta\omega i^2> \tau_c \qquad \textbf{(5.3.3)}$$

Therefore,

$$\tau_v = (<\Delta\omega i^2> \tau_c)^{-1}$$

The vibrational relaxation time can be defined as, $\tau_v = \int_0^\infty \phi_{pp}(t)dt$

This is for the case of long approximation.

For the fast modulation regime,

$$\tau_v = [\pi c(FWHM)]^{-1} \qquad \textbf{(5.3.4)}$$

where FWHM= full width at half maximum of I_{iso} and c is the velocity of light.

Therefore depending upon the rate of modulation process, one may predict the band profile. Thus, the Kubo lineshape theory is appropriate in determining the vibrational dephasing. In case of long-range dipolar interaction, τ_c is directly proportional to dynamic viscosity [25] and hence the vibrational relaxation rate is expected to depend on the viscosity of the medium.

The isotropic band shapes for OCBD in different solvents were checked by curve fitting and found to be more Lorentzian in nature at high dilutions (~90%). Raman spectrum of OCBD at 90% benzene solvent is shown in Fig.5.1. The peak wavenumber position of I_{iso} and I_{aniso} components of OCBD spectrum do not coincide at low solvent concentrations and it is due to the non-coincidence effect[26-38].

For the Lorentzian lineshape, the vibrational relaxation rate is related to the isotropic bandwidth given by

$$\tau_v^{-1} = \pi c \Gamma_{iso} \qquad \textbf{(5.3.5)}$$

where Γ_{iso} is the bandwidth (full width at half maximum intensity, FWHM) of the isotropic component of the Raman band and c is the velocity of light. The bandwidths of the isotropic component of C=O stretching mode of OCBD were measured at 90% solvent concentration. The data were used to determine the vibrational relaxation rate (τ_v^{-1}).

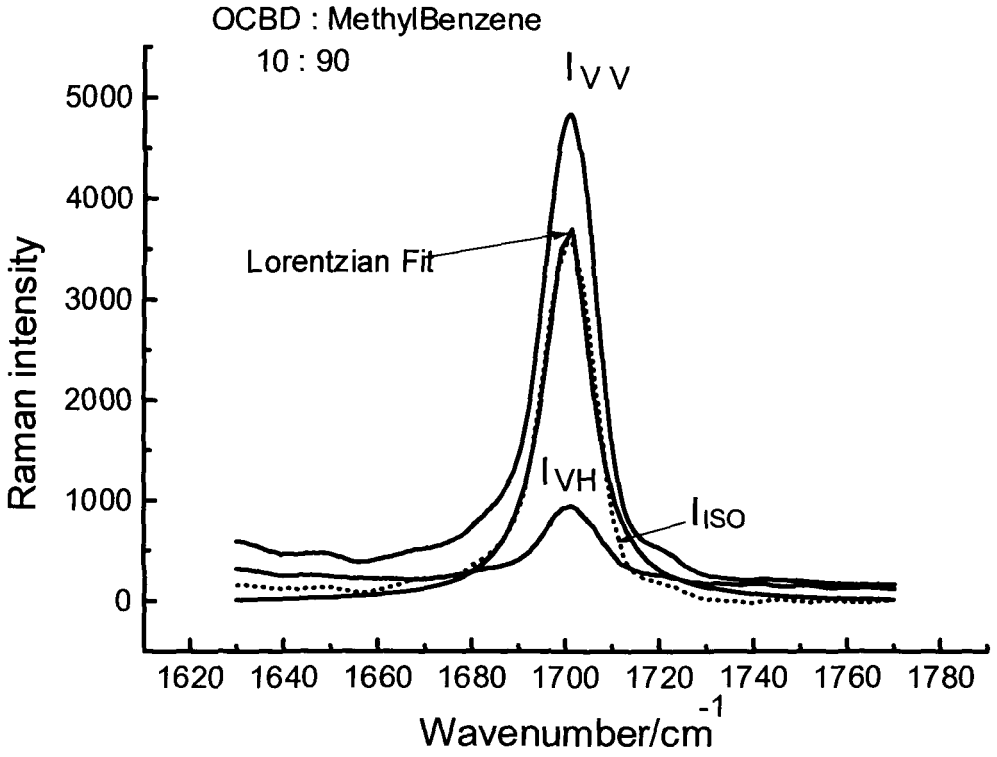

Fig. 5.1 (a) Raman spectrum of OCBD in Methylbenzene solvent

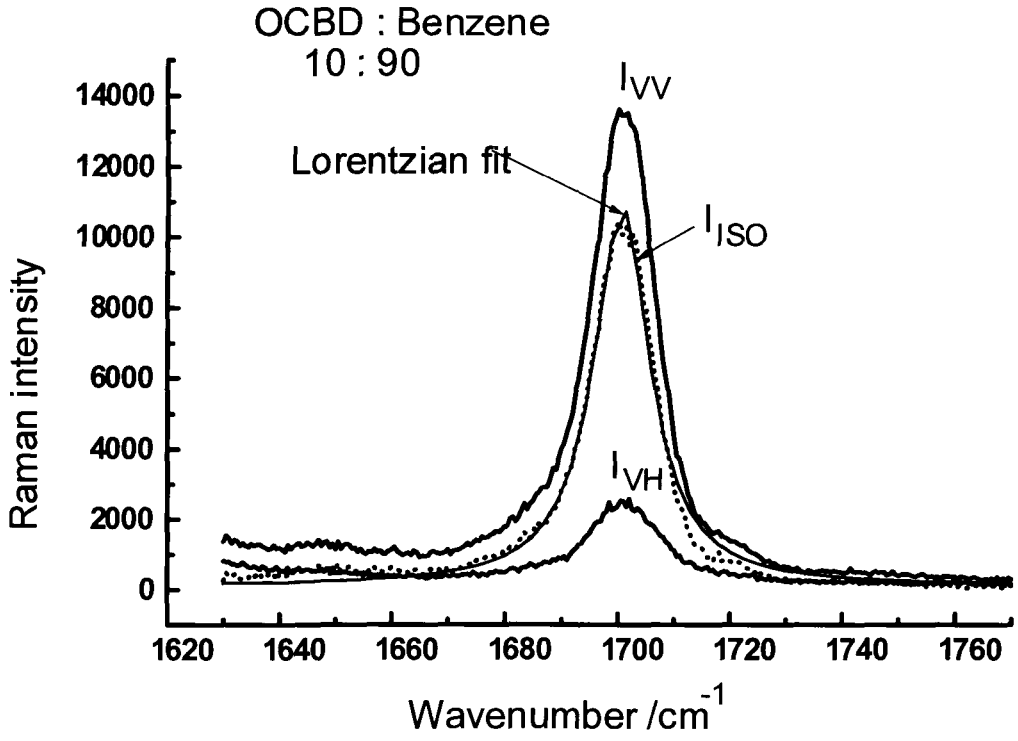

Fig.5.1(b) Raman spectrum of OCBD in Benzene solvent

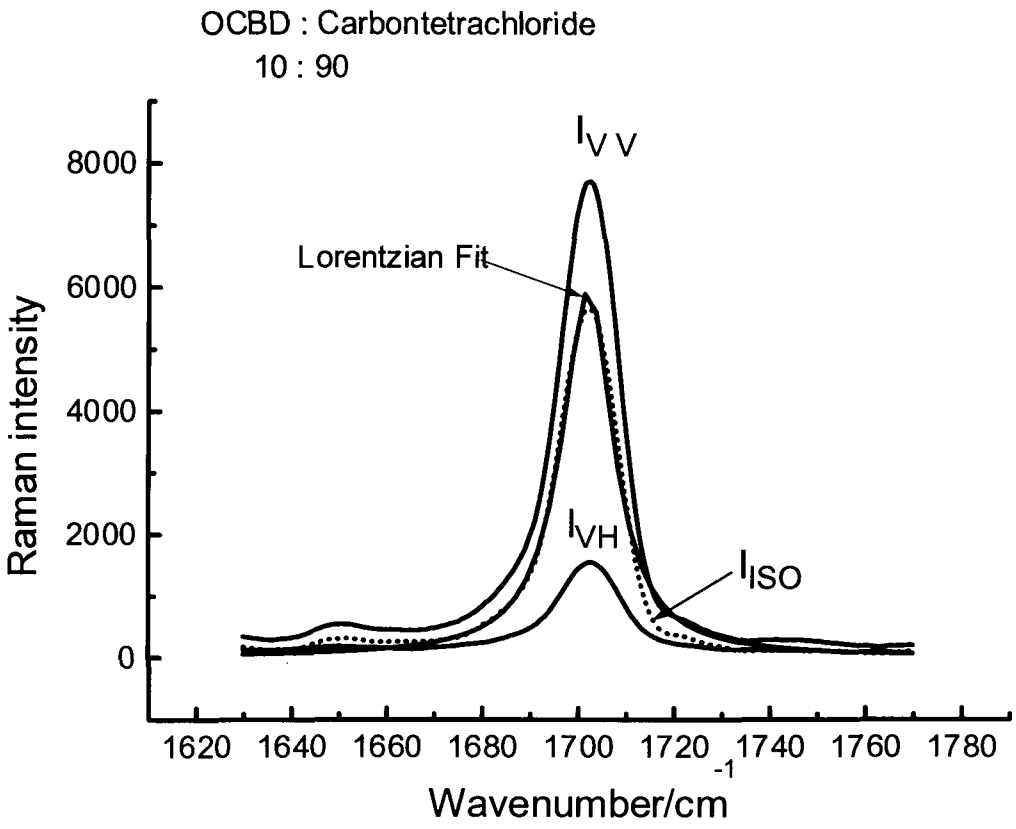

Fig. 5.1 (c) Raman spectrum of OCBD in Carbontetrachloride solvent

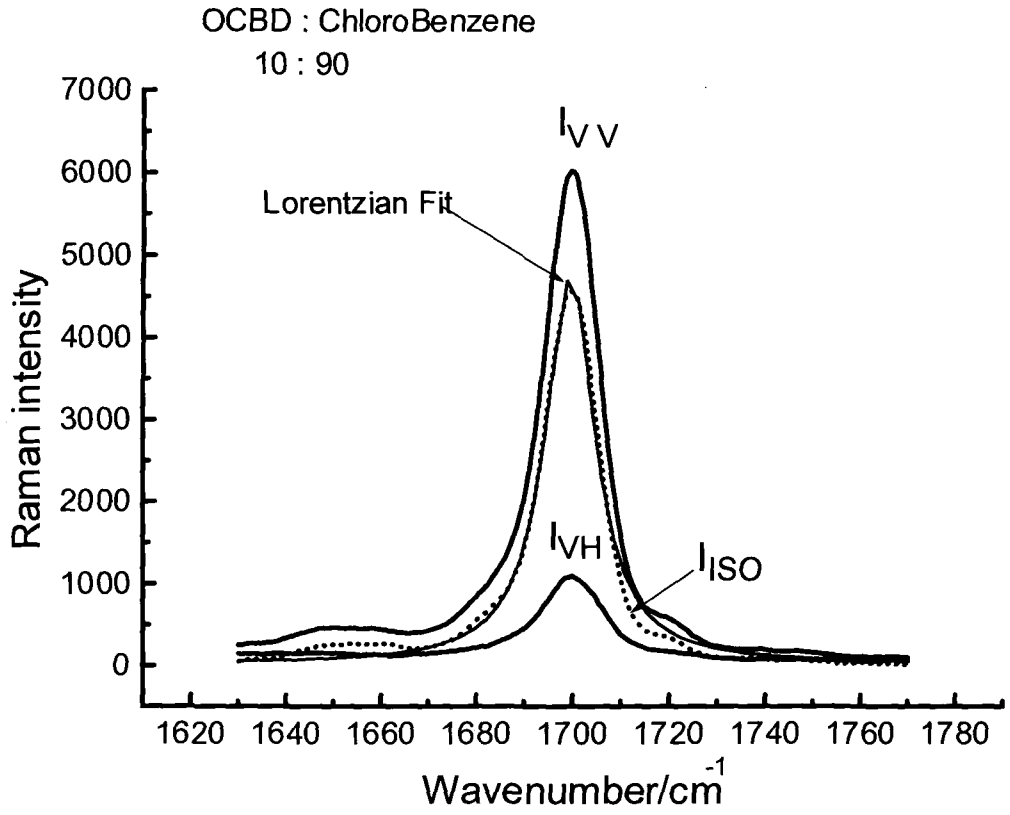

Fig. 5.1 (d) Raman spectrum of OCBD in Chlorobenzene solvent

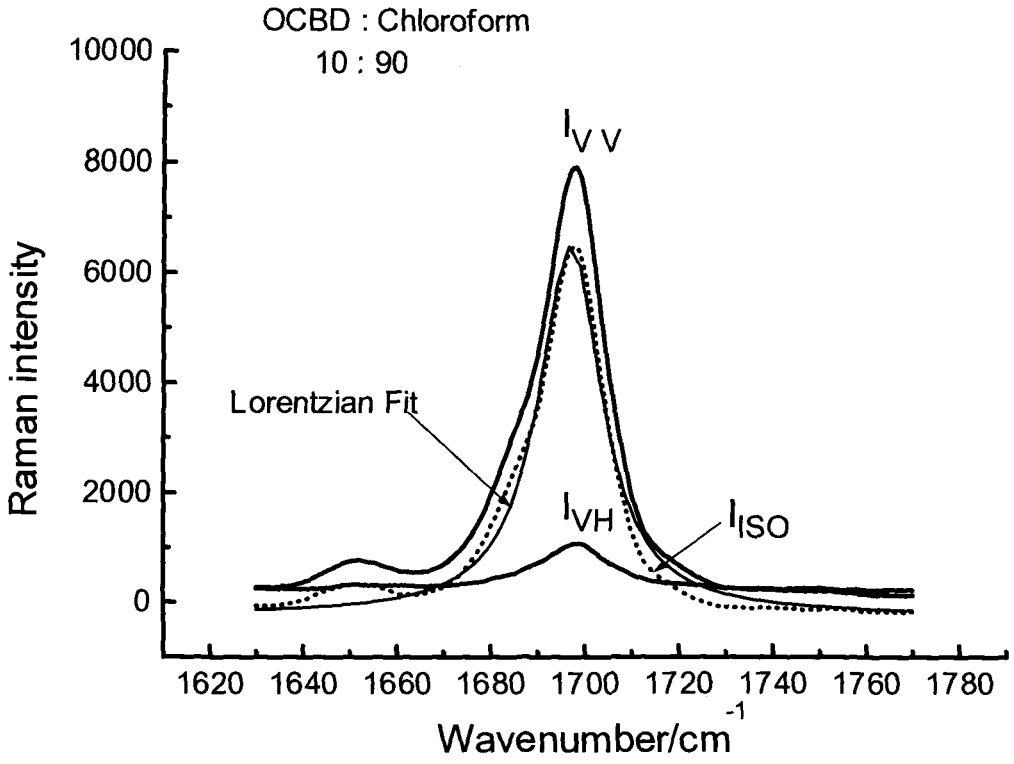

Fig. 5.1 (e) Raman spectrum of OCBD in Chloroform solvent

The electrical and electronic properties of solvent induced environment also play a significant role in determining the vibrational relaxation rate[18]. Considering a simple model[18] for the vibrational relaxation based on the electrical properties of solvent induced disordered systems, the steady state conductivity (σ) for the disordered system is given by

$$\sigma = Nq\mu \qquad (5.3.6)$$

where N is the density of a moving charge q and μ is the mobility. The charge **q** may be taken as a partial charge generated on solute molecules by the solvent molecules.

The average relaxation time τ for a system [18] may be given as

$$\tau = \tau_0 \exp\left(\frac{\Delta W}{KT}\right) \qquad (5.3.7)$$

where the symbols have their usual meanings.

Considering the model of solvent cage effect where the molecules of the solute and solvent are assuming of the same size (Fig.5.2), then the frequency with which the two solute molecules will accidentally become neighbours by the process of diffusion can be estimated. The elementary jump distance λ of the molecules from one position to the next is about 2r where r is the radius of the molecule. Then the diffusion coefficient is given by

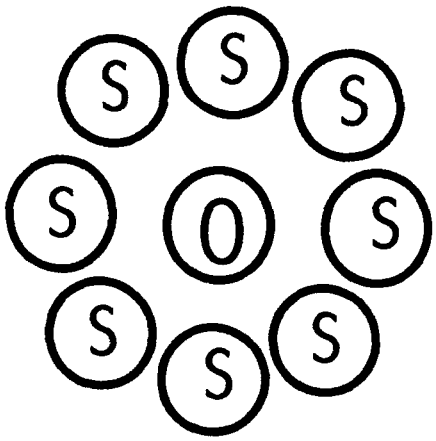

(a)

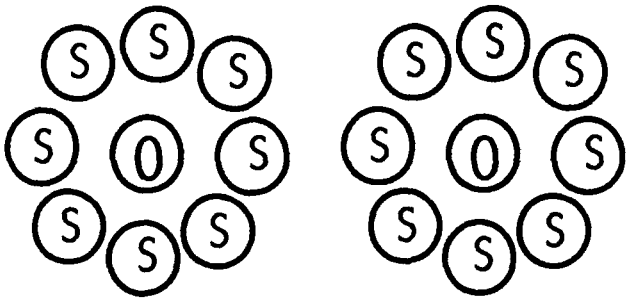

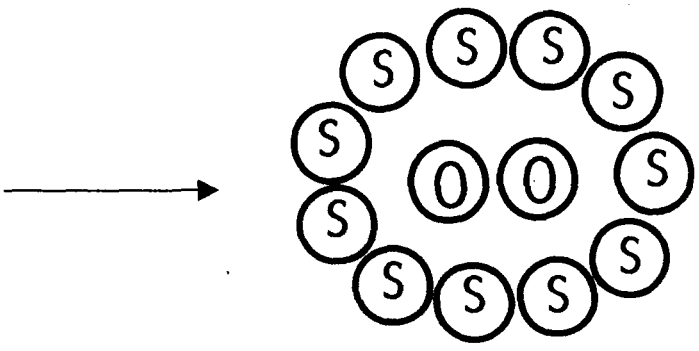

(b)

Fig. 5.2 (a) The solvent cage effect where O - OCBD solute and S – Solvent molecules

(b) Interaction of the solvation layers of the solutes with solvents, where the size of solvent and solute molecules are comparable

$$D = \frac{\lambda^2}{6\tau} \qquad (5.3.8)$$

where τ is the average time between collisions.

The conductivity due to such a process may depend on the hopping probability between two adjacent molecular positions and this probability depends on the distance between two solute molecules. The conductivity may be calculated by taking the average over jumps between molecular positions **i** and **j**.

From Kubo equation, the electrical conductivity tensor [39] is given by

$$\sigma_{\mu\nu} = \frac{1}{KT}\int_0^\infty < j_\mu(t) j_\nu(0) > dt \qquad (5.3.9)$$

which shows that conductivity depends on the time correlation between a component of the current operator $j_\mu(0)$ at time zero and the component $j_\mu(t)$ at time **t**, integrated for all times and evaluated as the average of the expectation value of the product over the equilibrium ensemble.

The conductivity (σ) in equation (5.3.6) can be expressed in terms of λ and τ as

$\frac{\lambda}{\tau} = v = \mu E$, then

$$\sigma = Nq\ \mu = \frac{Nq\ \lambda}{\tau\ E} \qquad (5.3.10)$$

It is also related to the dynamic viscosity (η). Using the stokes' law[40] for the motion of a sphere of radius r moving with velocity **v** in a viscous medium under the action of a constant force, we have

$$\sigma = \frac{Nq^2}{6\pi r\eta} \qquad \textbf{(5.3.11)}$$

Here E is the reaction field of the solvent molecules and may be taken as due to the dispersion forces (ca 10^{14} Hz) at the high frequency given by

$$E = \frac{2\mu}{a^3}\left(\frac{n^2-1}{2n^2+1}\right) \qquad \textbf{(5.3.12)}$$

where μ is the dipole moment of the solute molecule and a is the radius of the spherical cavity in which the solute molecule is sitting. Eliminating the value of σ from equations (5.3.10) and (5.3.11), and then substituting the value of E from (5.3.12), the average relaxation time τ can be written as

$$\tau = \frac{6\pi\eta r^2 a^3}{q\mu}\left(\frac{n^2-1}{2n^2+1}\right)^{-1} \qquad \textbf{(5.3.13)}$$

If the radius of the spherical cavity is small enough, then **a** can be taken approximately equal to the radius of the molecules **r**. Then equation (5.3.13) can be written as

$$\tau = \frac{6\pi\eta r^6}{\mu^2}\left(\frac{n^2-1}{2n^2+1}\right)^{-1} \qquad \textbf{(5.3.14)}$$

The quantity **qr** can be taken as the dipole moment of the solute molecule.

This collision time τ may be considered as the correlation time τ_c. Hence, equation (5.3.3) can be written as

$$\tau_v^{-1} = (<\Delta\omega i^2> \tau_c)$$

$$= <\Delta\omega i^2> \frac{6\pi\eta r^6}{\mu^2}\left(\frac{n^2-1}{2n^2+1}\right)^{-1} \qquad \textbf{(5.3.15)}$$

The vibrational second moment $<\Delta\omega i^2> = (M_2)_v$ is related to the density ρ of the liquid [25] as

$$<\Delta\omega i^2> = A\rho \qquad \textbf{(5.3.16)}$$

where **A** is a constant depending mainly on the solute properties.

Hence, equation (5. 3.15) can be written as

$$\tau_v^{-1} = A\rho \frac{6\pi\eta r^6}{\mu^2}\left(\frac{n^2-1}{2n^2+1}\right)^{-1} \qquad \textbf{(5.3.17)}$$

$$= C_m f(\rho,\eta, n) \qquad \textbf{(5.3.18)}$$

where $C_m = A\frac{6\pi r^6}{\mu^2}$ is a solute dependent constant and

$$f(\rho,\eta, n) = \rho\eta\left(\frac{n^2-1}{2n^2+1}\right)^{-1} \qquad \textbf{(5.3.19)}$$

Hence, the vibrational relaxation rate is dependent on the parameter f (ρ,η,n). The various models were proposed for examining the dephasing process taking into account of the dynamic viscosity (η) which is a macroscopic property[19]. The parameter f (ρ,η,n)[1, 18-20] was calculated for OCBD and correlated with the experimental values of the vibrational relaxation rate. The correlation is shown in Fig.5.3. The correlation is roughly linear for all the solvents, with the exception of chloroform. The point for $CHCl_3$ is too far away from the correlation line. This indicates that the bandwidth cannot be explained by the molecular properties contained in f (ρ,η, n) parameter.

It is probable that the discreteness of the medium[2] due to solvent may be playing a role. Hence, a microscopic model was used [2, 19, 20] in order to explain the microscopic environment. In this model, since the solute-solvent systems may not always be homogeneous and some heterogeneity may exist due to associative nature of the molecules, the concept of microviscosity[41] was introduced. The van der Waals' interactions between solute and solvent are taken into account in this case.

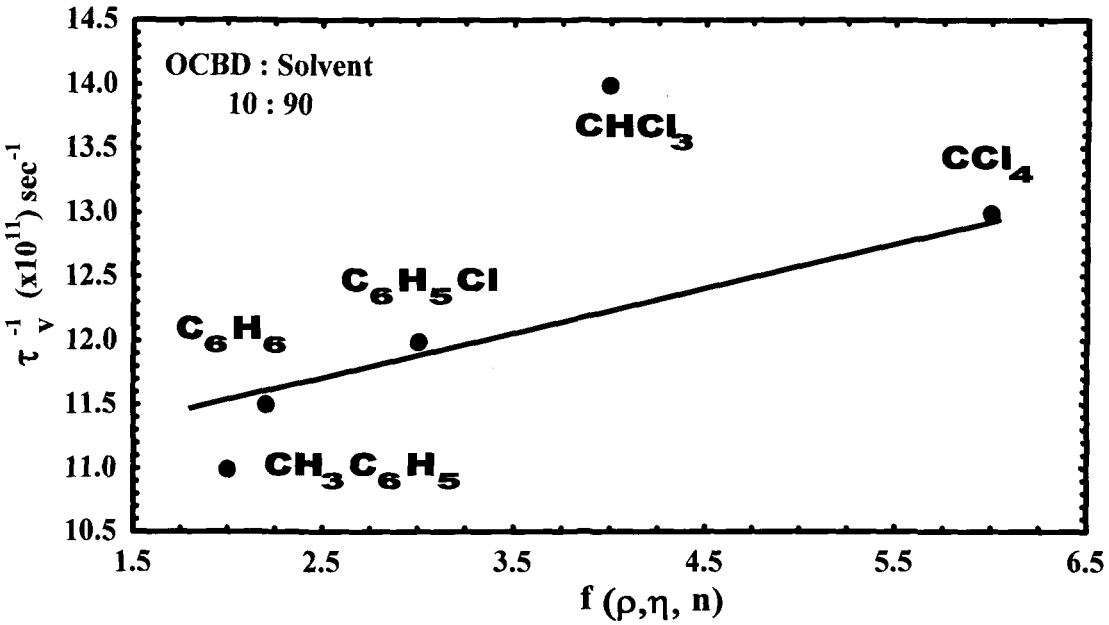

Fig. 5.3 Variation of vibrational relaxation rate as a function of the parameter f(ρ,η,n)

The microviscosity (η_m) may be calculated[41] using the relation

$$\eta_m = \eta\left[0.16 + 0.4\left(\frac{a}{b}\right)\right] \qquad \textbf{(5.3.20)}$$

$$\eta_m = \eta\gamma$$

where $\gamma = \left[0.16 + 0.4\left(\frac{a}{b}\right)\right]$ is the microfriction factor;

a and **b** are the radius of solute and solvent molecules respectively.

The modified parameter [20] has the form

$$f_m = \rho\eta_m\left[\frac{n^2 - 1}{2n^2 + 1}\right]^{-1} \qquad \textbf{(5.3.21)}$$

where ρ is the density and **n** is the refractive index of the solvent molecule.

The OCBD molecule may be assumed to be planar; the dipole-dipole interaction may therefore create stacking of solute molecules. Due to molecular motion and diffusion, the orientation of the benzene molecule will not be fixed with respect to any particular fragment. The benzene ring may occupy any random position and may not be able to influence much through its π electron system. Therefore, the entire molecular volume would not be effective in the interaction process.

For the case of OCBD-$CH_3C_6H_5$, the benzene solvent may interact with the benzenoid portion of the OCBD molecule in its entirety and the interaction

may be governed by the π electron system of the solute and solvent molecules. Therefore, radii of both solute and solvent molecule have been chosen as the benzene van der Waals' radii (1.77Å) in case of above molecular system[42]. The molecular parameter for solute and solvents are given in Table5.1 and Table 5.2. For solute-C_6H_6, the interaction between the benzene rings is more favourable, hence the van der Waals' radii for solute and solvent are taken as that of benzene radius (1.77 Å).

For solute - C_6H_5Cl, the solvent being planar in structure is more likely to sit in its entirety over the benzenoid portion of OCBD. The Cl atom may occupy place near the para-position of the benzene ring of the combine structure and hence the favourable position of these two interacting molecules in this process mimics 2,4-dichlorobenzaldehyde molecule (Fig.5.4). In this kind of structure, the main interaction is likely to be between the benzenoid portions of the two molecules. Hence, the van der Waals' radii for solute and solvent are taken as that of benzene van der Waals' radii (1.77Å) in this molecular system[42] also.

For the case of OCBD and the chlorinated solvent CCl_4, the CCl_4 molecule while approaching near the solute molecule acquires a net electrical charge due to the high polarizability of the molecule. As a result, an electrostatic potential is developed in the vicinity of the molecule whose value

Table 5.1

Molecular Parameters

Solvents	Density (ρ)	Refractive index (n)	Viscosity (η) (cp)
$CH_3C_6H_5$	0.869	1.49	0.526
C_6H_6	0.873	1.498	0.564
C_6H_5Cl	1.1058	1.523	0.631
CCl_4	1.584	1.457	0.843
$CHCl_3$	1.479	1.45	0.542

Table 5.2

The molecular parameters of the solute-solvent system

Molecular system	Solute radius a(Å)	Solvent radius b(Å)	Microfrict-ion factor γ=0.16+ 0.4(a/b)	Microv-iscosity η_m (cp)	f_m	Γ_{iso} (cm^{-1})	τ_v^{-1} ($psec^{-1}$)
OCBD-$CH_3C_6H_5$	1.77	1.77	0.56	0.29	1.11	11.50	1.08
OCBD-C_6H_6	1.77	1.77	0.56	0.32	1.23	12.00	1.13
OCBD-C_6H_5Cl	1.77	1.77	0.56	0.35	1.67	13.00	1.23
OCBD-CCl_4	1.40	3.50	0.32	0.27	2.01	14.00	1.32
OCBD-$CHCl_3$	1.40	1.20	0.63	0.34	2.37	14.50	1.4

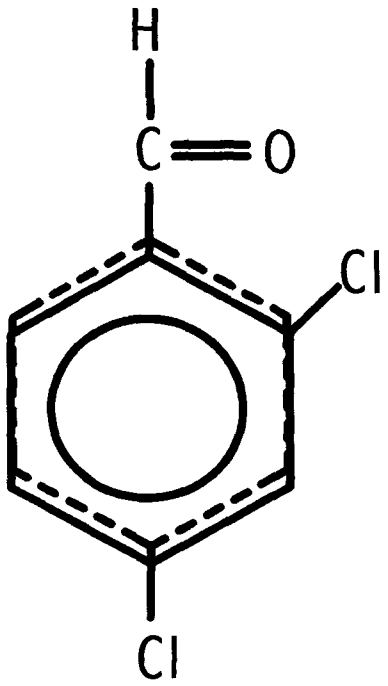

(a)

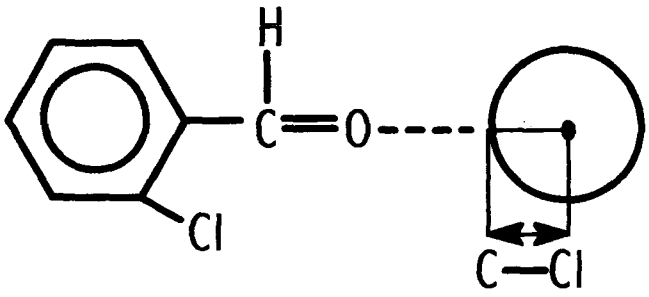

(b)

Fig. 5.4 A representative diagram showing
(a) Possible interaction between OCBD and C_6H_5Cl solvent
(b) Possible interaction between OCBD and CCl_4 solvent

decreases with the increasing distance between the two (solute and solvent) molecules. Moreover in solute molecule, a quadrupole moment from the benzene ring is present in addition to the permanent dipole moment of the C=O bond. The quadrupole moment of the benzenoid fragment of the solute molecule induces dipole moment in the solvent approaching it. Hence, the interaction between the quadrupole moment present in OCBD molecule and the induced dipole moment from the solvent is likely to play an important role. This is in addition to the induced dipole moment induced by the permanent dipole moment of the C=O bond. As the benzenoid portion of OCBD is plate like structure, the spherical CCl_4 molecule can easily roll over the planes of the solute molecule. Hence the main interaction is likely between the C=O bond of OCBD and C-Cl bond of CCl_4 molecule (Fig.5.4). Moreover, the CCl_4 is highly polarizable spherical shaped molecule and therefore, the van der Waals' radius[19] of Cl atom (1.8 Å) and bond distance of C-Cl (1.7 Å) has been taken as the radius of the solvent molecule. Again in this dipole-induced dipole interaction, the C-Cl bond may orient itself towards the C=O bond of OCBD and the oxygen atom limits the closest approach and hence the van der Waals' radius[19] for solute is taken as 1.4 Å, the radius of double bonded oxygen atom.

In the case of solute-$CHCl_3$ also, the van der Waals' radii of the interacting system is calculated by considering the fragments of the molecule

under interaction. The $CHCl_3$ molecule has the tendency to form hydrogen bond due to acidic nature of the hydrogen and hence hydrogen bonding is likely to be present between the OCBD and $CHCl_3$ molecules. It may only be weakly associated with the C=O bond and the oscillations between the oxygen and carbon atoms may not be feasible as in the case of strongly hydrogen bonded systems. Nevertheless, the interaction may be sufficient to weaken the pair interaction at sufficiently high concentration of the solvent where several $CHCl_3$ molecules may surround the solute in a cage effect fashion. In such a hydrogen-bonded system, the C-H bond of $CHCl_3$ orients itself in a head to tail configuration with the C=O bond of OCBD forming C=O....H-C interacting system (Fig. 5.5). Hence the solvent radius is taken as the van der Waals' radius for the hydrogen atom[19], which is the closest approach for the C=O...H-C hydrogen bonded system and the solute radius 1.4 Å, the van der Waals' radius for oxygen atom.

The variation of the vibrational relaxation rate (τ_v^{-1}) as a function of f_m is shown in Fig.5.6, which is clearly a linear plot indicating the better fitting of data points. This shows that the discreteness of the medium due to the solvents has a significant influence in such complex molecular systems. The correlation coefficient (r) for the τ_v^{-1} against f_m and $f(\rho,\eta,n)$ plots have been calculated and their values are found to be 0.993 and 0.824 respectively. We may therefore

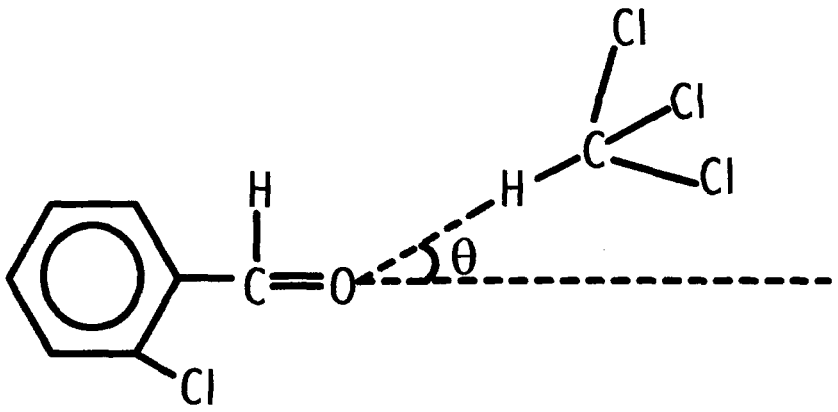

Fig. 5.5 A representative diagram showing the formation of hydrogen bond between C=O and H-C bond

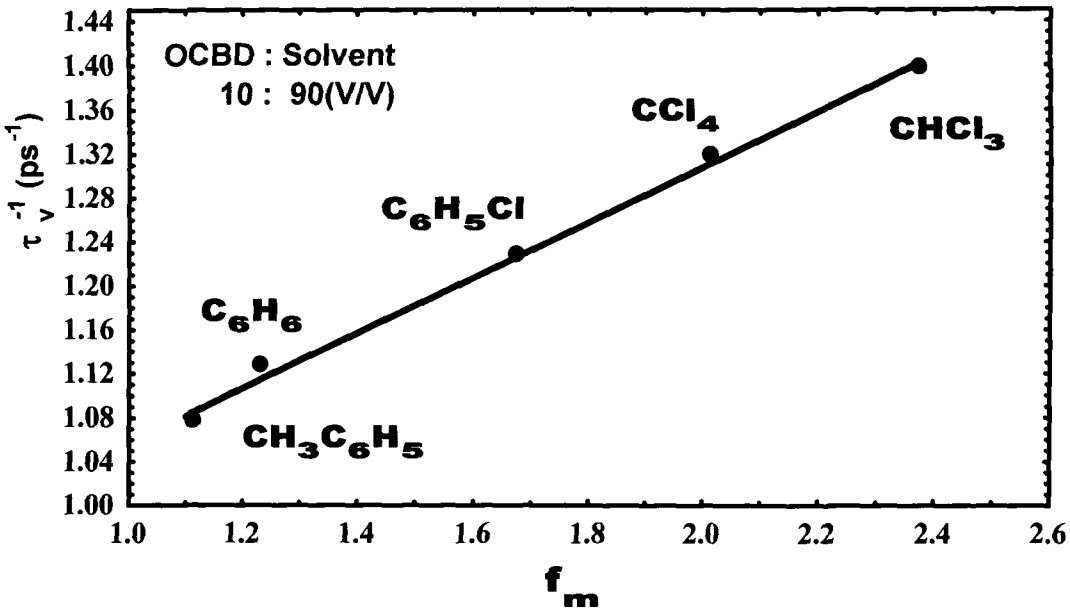

Fig. 5.6 Variation of vibrational relaxation rate as a function of the parameter f_m

conclude that 'f_m' is a better parameter compared to 'f' for explaining the vibrational relaxation rates of OCBD molecule. Thus, the solvent microviscosity rather than dynamic viscosity is playing a major role in analyzing the Raman band shape in these solute-solvent systems.

REFERENCES:

1. A. Purkayastha, R. Das and K. Kumar, J. Raman Spectrosc. **21,** 227 (1990).
2. A. Das and K. Kumar, Spectrochim. Acta, **54A**, 793 (1998).
3. A. Das and K. Kumar, J. Raman Spectrosc. **30**, 547 (1999).
4. A. Das and K. Kumar, J. Raman Spectrosc. **30**, 563 (1999).
5. A. Das, R. Das and K. Kumar, Spectrochim. Acta, **58A**, 1583 (2002).
6. G. J. Remar and R. A. Macphail, J. Chem. Phys. **103**, 4381 (1995).
7. C. H. Wang and J. Mchale, J. Chem. Phys. **72**, 4039 (1980).
8. D. W. Oxtoby, Annu. Rev. Phys. Chem. **32**, 77 (1981).
9. E. W. Knapp and S. F. Fischer, J. Chem. Phys. **76**, 4730 (1982).
10. Schweizer and D. Chandler, J. Chem. Phys. **76**, 2296 (1982).
11. D. W. Oxtoby, J. Phys. Chem. **87**, 3028 (1983).
12. P. Mirone and G. Fini, J. Chem. Phys. **40**, 1 (1979).
13. D. Ben Amotz, M. R. Lee, S. Y. Cho and D. J. List, J. Chem. Phys. **96**, 8781 (1992).
14. J. Jonas, Act. Chem. Res. **17**, 74 (1984).
15. Lee B., F. M. Richards, J. Mol. Biol. **55**, 379 (1971).
16. Eisenberg. D, A. D. Mclachlan, Nature, **319**, 199 (1986).

17. G. Moser, A. Asenbaum, J. Barton and G. Doge, J. Chem. Phys. **102**, 1173 (1995).

18. A. Purkayastha and K. Kumar , J. Raman Spectrosc. **19**, 249 (1988).

19. A. Purkayastha, R. Das and K. Kumar, Spectrochim. Acta, **47A**, 525 (1991).

20. A. Purkayastha, R. Das and K. Kumar, Spectrochim. Acta, **46A**, 1545 (1990).

21. K. Tanabe, Spectrochim. Acta, **40A**, 437 (1984).

22. R. K. Singh, S. N. Singh, B. P. Asthana and C. M. Pathak, J. Raman Spectrosc. **25**, 423 (1994).

23. W. Schindler, T. W. Zerda and J. Jonas, J. Chem. Phys. **81**,4306 (1984).

24. R. Kubo, in fluctuations, relaxation and resonance in magnetic systems, edited by D. ter Haar, pp.23, Oliver and Boyd, Edinburgh (1962).

25. J. Yarwood and R. Arndt, in Molecular Association, edited by R.Foster, **Vol.2**, pp.287, 297-300, Academic Press, London (1979).

26. P. Mirone, G. Fini, J. Chem. Phys. **71**, 2241 (1979).

27. C. H. Wang, J. McHale, J. Chem. Phys. **72**, 4039 (1980).

28. J. McHale, J. Chem. Phys. **75**, 30 (1981).

29. D. E. Logan, Mol. Phys. **58**, 79 (1986).

30. D. E. Logan, Chem. Phys. **103**, 215 (1986).

31. D. E. Logan, Chem. Phys.**131**, 199 (1989).

32. H. Torii and M. Tasumi, J. Chem. Phys. **99**, 8459 (1993).

33. R. J. Bartholomew and D. E. Irish, J. Raman Spectrosc. **29**, 115 (1998).

34. H. Torii, J. Phys. Chem.**103A**, 2843 (1999).

35. A. Morresi, M. Paolantoni, P. Sassi, R. S. Cataliotti and G. Paliani, J. Phys. condense matter. **12**, 3631 (2000).

36. M. G. Giorgini, M. Musso, A. Asenbaum and G. Doge, Mol. Phys. **98**, 783 (2000).

37. M. G. Giorgini, M. Musso and P. Ottaviani, Mol. Phys. **99**,1485 (2001).

38. M. Musso, H. Torii, P. Ottaviani, A. Asenbaum and M. G. Giorgini, J. Phys. Chem. **106A**,10152 (2002).

39. J. M. Ziman, Principles of Theory of Solids, pp.214, Cambridge University Press, Cambridge (1972).

40. B. Tareev, Physics of Dielectric materials, pp.49, MIR publishers, Moscow (1975).

41. V. V. Frolov, in Nuclear Magnetic Resonance(edited by P.M.Borodin), 13-29 (Translated from the Russian), Amerind, New Delhi (1975).

42. A. Bondi, J. Phys. Chem. **68**, 441 (1964).

CHAPTER 6

CHAPTER 6

RAMAN ANISOTROPIC BANDWIDTH STUDY OF C=O STRETCHING VIBRATION OF METHYL ISOBUTYL KETONE: ROLE OF VAN DER WAALS' VOLUME OF THE INTERACTING SYSTEMS

1. Introduction

In recent years, considerable progress has been made towards a deeper understanding of the Raman band shape especially due the intermolecular coupling in liquids. Raman band shape of a reference mode of any molecule is dependent on the microscopic environment. The concentration fluctuations in the environment influence the band shape in the liquid mixture [1-3]. Moreover, the solvent induced perturbations influence the frequency as well as the bandwidth of the vibrational bands of the solute. The dependence of bandwidth and frequency of Raman vibrational bands on environment provides useful information regarding the solute-solvent interactions and intermolecular forces. Different models have been proposed to describe the influence of a solvent on vibrational frequencies and bandwidths. The models developed by Schweizer

et al [4] and Ben-Amotz et al [5,6] are based on a partitioning of intermolecular forces into repulsive and attractive components in a manner consistent with the van der Waals fluids where the short-range repulsive forces determine the fluid structure and the long-range attractive forces can be treated by mean field or perturbation theories. This approach really helps as it allows one to relate the solvent contributions to the vibrational frequencies and bandwidths to fundamental intermolecular interactions involving repulsive and attractive forces.

Bratos and Tarjus[7] have proposed a theory for Raman band shapes of binary mixtures of van der Waals' liquids. Widely different spectral effects are predicted for chemical and isotopic solutions. Knapp and Fischer[8] elaborated the concentration dependence of the vibrational band shape of molecules in liquid binary mixtures with an analytical model applicable to all modulation speeds. Moser et al [9] proposed a stochastic model for vibrational broadening of Raman lines in binary mixtures, which also gives analytic solutions for the band shape. The models proposed by them permitted analysis of Raman band shapes of binary mixtures of van der Waals' liquids.

Further, the spherically symmetric and anti-symmetric intermolecular forces play role in determining the bandshape of isotropic and anisotropic components respectively. The isotropic component of Raman band is governed

by the angular independent inter-and intra-molecular potentials, while the anisotropic vibration is governed by angular dependent inter- and intra-molecular forces. The anisotropic components of the Raman band associated with C=O stretching mode of the p-methylacetophenone (PMA), Benzaldehyde, Cyclohexanone, and N,N-Dimethylacetamide (DMA) have been studied earlier[10] and it was shown that the van der Waals' volume of the interacting systems plays a significant role in the line broadening mechanism.

The effect of van der Waals' volume of the sphere of influence on the Raman anisotropic bandwidth of C=O stretching mode of *o*-Chlorobenzaldehyde has been studied by us and is already reported in chapter 4. In order to get more information about the intermolecular interactions in anisotropic Raman component in different molecules, we have chosen an aliphatic carbonyl-containing molecule Methyl Isobutyl Ketone (MIBK) for the present study. The solvent dependence study of the anisotropic Raman component corresponding to C=O stretching vibration of MIBK in several solvents like benzene, carbon tetrachloride, methylbenzene, chlorobenzene, acetonitrile and chloroform was undertaken in order to see the effect of varying solvents of different nature in this aliphatic molecule also. Purkayastha et al[11] have studied the isotropic component of Raman spectrum of C=O stretching mode of MIBK. However, the anisotropic component of the Raman spectrum of

C=O stretching mode of this molecule has not been studied which may give valuable information about the angular dependent intermolecular forces. The C=O stretching mode in MIBK is well isolated from other modes of vibration and is suitable for such studies. The measurements in liquid mixtures were also carried out to correlate the anisotropic Raman bandwidth with changing environment by the measurement of the capacitance of the liquid mixtures.

2. Experimental

The sample used for spectroscopic measurements were of either spectroscopic or extra-pure analytical reagent grade and were used without further purification. Raman spectral measurements were made for C=O stretching band of MIBK in benzene, carbon tetrachloride, methylbenzene, chlorobenzene, acetonitrile and chloroform solvents. The experiments were performed using Spex Ramalog 1403 double monochromator equipped with a cooled RCA 31034-photomultiplier tube and a photon counting arrangement. The spectrometer control and data processing were achieved with the help of Datamate using DM-3000 software. The 4880 Å line from the Spectra Physics model 165 Ar^+ Laser was used as the excitation source. The slit width was kept at ~1.5 cm^{-1}. All the spectra showed good reproducibility and were recorded at least three times. The accuracy of measurement is believed to be ± 0.5 cm^{-1}. The

HP-4263B multi-frequency LCR-meter was used for the measurement of capacitance. The measurements of capacitance were carried out in the series equivalent circuit mode. The four terminal test fixture HP-16089B was used for all measurements. The effect of finite slit width was corrected by using the equation [12]

$$\Gamma_t = \Gamma_a [\, 1 - (S/\Gamma_a)^2] \qquad \textbf{(6.2.1)}$$

where Γ_t and Γ_a are the true and apparent Raman linewidth (FWHM) respectively, and S is the spectral slit width in cm^{-1}.

3. Results and Discussion

The Raman spectra of MIBK were recorded at different solvent concentrations ranging from 10% to 90 % using polar and non-polar solvents (C_6H_6, CCl_4, $CH_3C_6H_5$, C_6H_5Cl, CH_3CN and $CHCl_3$) of varying dielectric constant. The representative anisotropic Raman band shape is shown in Fig.6.1. The band positions in various solvent concentrations for each solvent are shown in Table 6.1. The peak wavenumber positions of isotropic and anisotropic Raman components of neat MIBK spectrum (Fig.6.1) do not coincide (separation ~4 cm^{-1}). This difference is due to the non-coincidence effect (NCE) [13-19]. The bandwidths of the anisotropic Raman band (Γ_{aniso}) were measured at different solvent concentrations for each solvent. Examination of

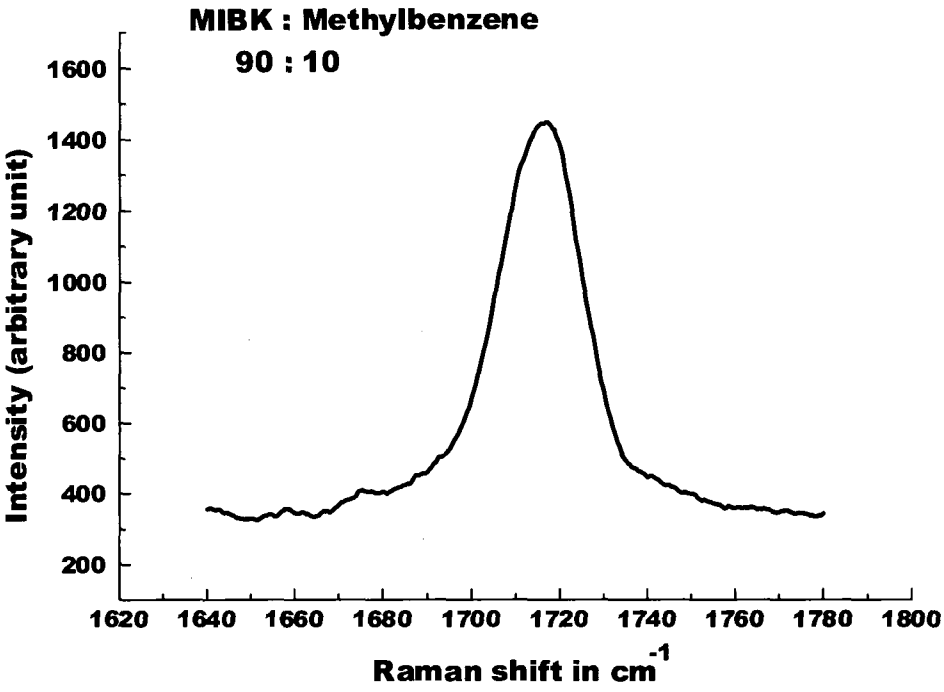

(A)

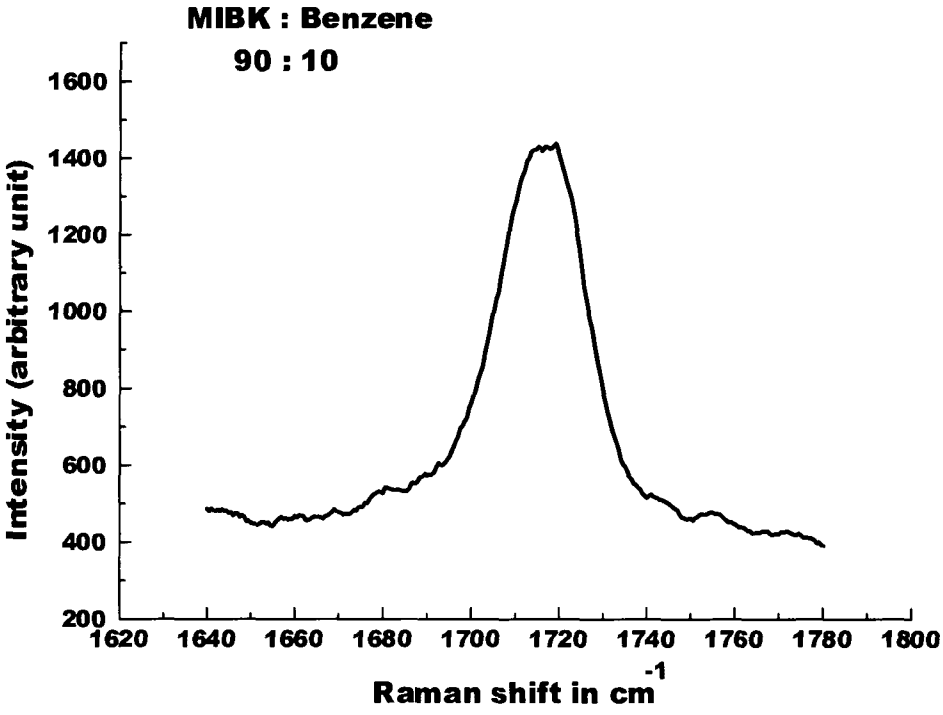

(B)

Fig.6.1(a) Anisotropic Raman spectrum of MIBK in
(A) Methylbenzene and (B) Benzene

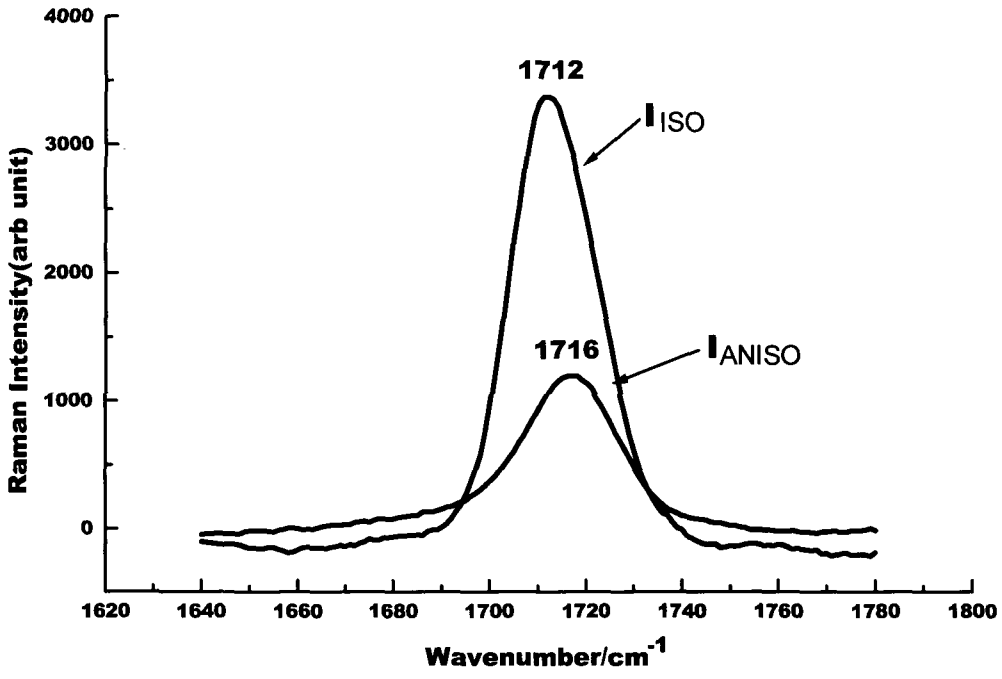

Fig. 6.1(b) Raman spectrum of neat Methyl Isobutyl Ketone

Table-6.1

Band positions of Anisotropic Raman components in various solvent concentrations for different solvents

Concentration Solute-MIBK						
MIBK/ Solvent	Max I_{VH} Solvent C_6H_6	Max I_{VH} Solvent CCl_4	Max I_{VH} Solvent $CH_3C_6H_5$	Max I_{VH} Solvent C_6H_5Cl	Max I_{VH} Solvent CH_3CN	Max I_{VH} Solvent $CHCl_3$
10/90	1718	1719	1718	1715	1714	1712
20/80	1718	1719	1719	1716	1714	1712
30/70	1718	1719	1719	1716	1714	1713
40/60	1718	1719	1719	1716	1714	1714
50/50	1718	1718	1718	1716	1714	1714
60/40	1718	1718	1718	1716	1715	1714
70/30	1718	1718	1718	1716	1715	1715
80/20	1718	1718	1718	1717	1716	1715
90/10	1718	1718	1718	1717	1717	1716

spectral properties reveals that the anisotropic Raman bandwidth strongly depends on the concentration and is sensitive to environmental changes. Fig. (6.2) shows the variation of anisotropic bandwidth with solvent concentration. The data points are scattered and cannot be fitted to a particular curve. In low solvent concentration region, the plot of Γ_{aniso} as a function of solvent concentration shows marked curvatures for all solvents except for CH_3CN. However, the data points in higher solvent concentration region appear to be linear for most of the solvents. In case of C_6H_5Cl solvent, the data points may be fitted in two curvatures in the lower and higher solvent concentration with a discontinuity in the intermediate region. For CH_3CN solvent, not all the data points can be fitted in a single straight line. However, two separate straight lines may be drawn with a discontinuity in the intermediate region.

Bratos and Tarjus [7] have developed a model for isotopic and chemical solutions. They show that for isotopic solutions (consisting of two different isotopes) the variation with concentration of the half width of an isotropic Raman band strongly depends on the speed of vibrational modulation. This difference is due to the fluctuations of the local chemical composition of the solution and to the structure-breaking effect occurring when a liquid is progressively diluted. It has been shown that for chemical solution, the halfwidth of isotropic and anisotropic Raman bands is concentration

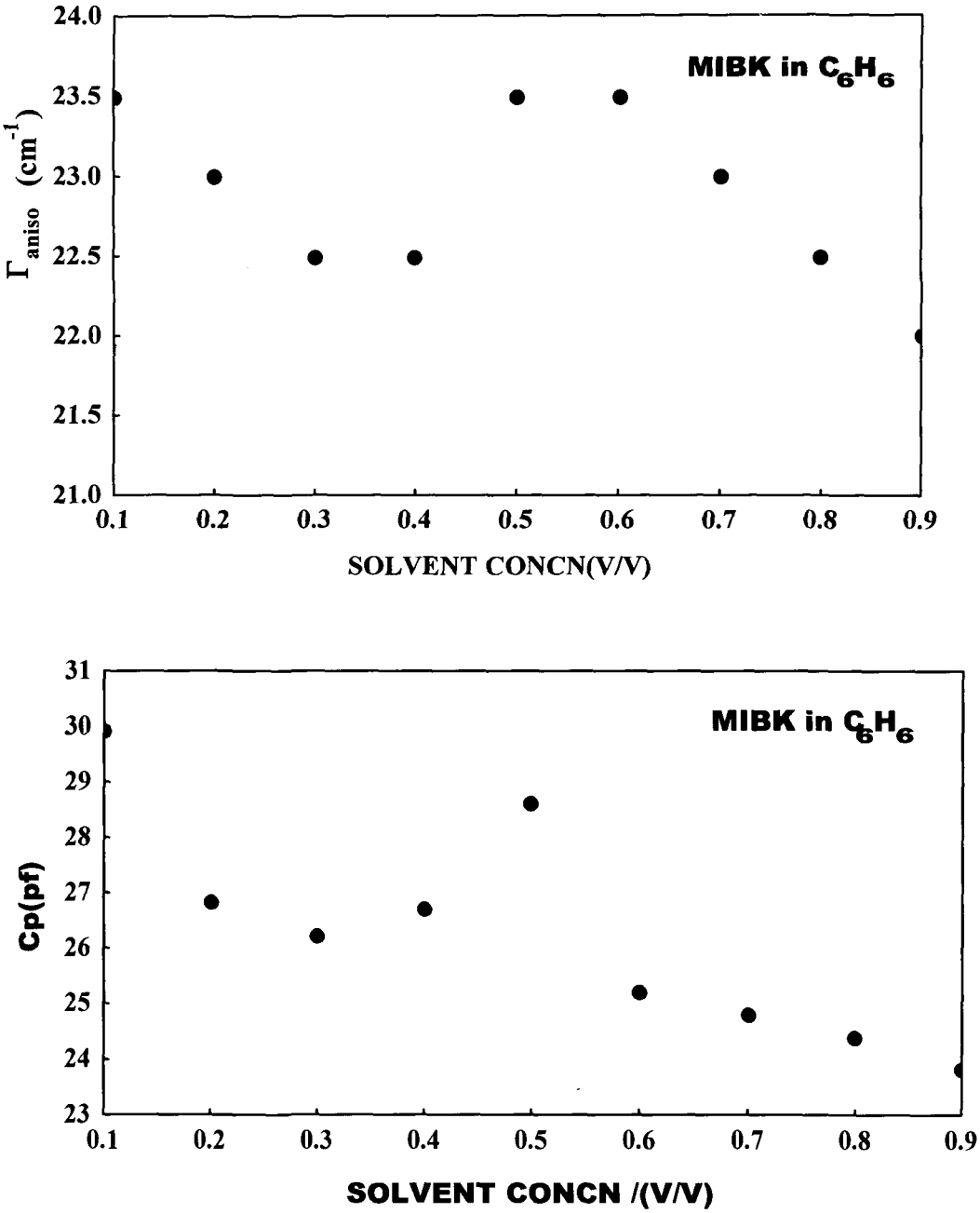

Fig.6.2(a) Variation of anisotropic bandwidth and capacitance as a function of solvent concentration

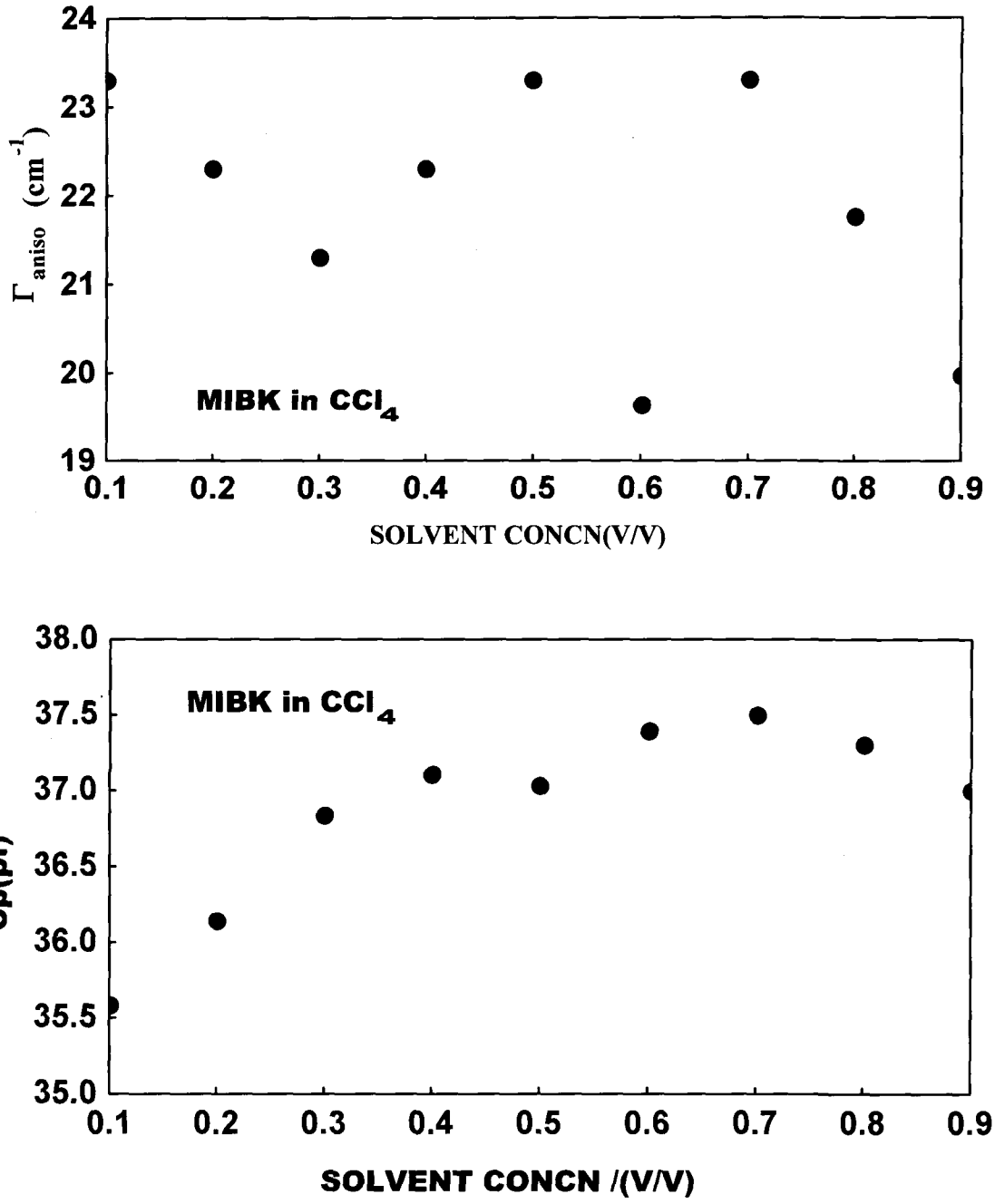

Fig.6.2(b) Variation of anisotropic bandwidth and capacitance as a function of solvent concentration

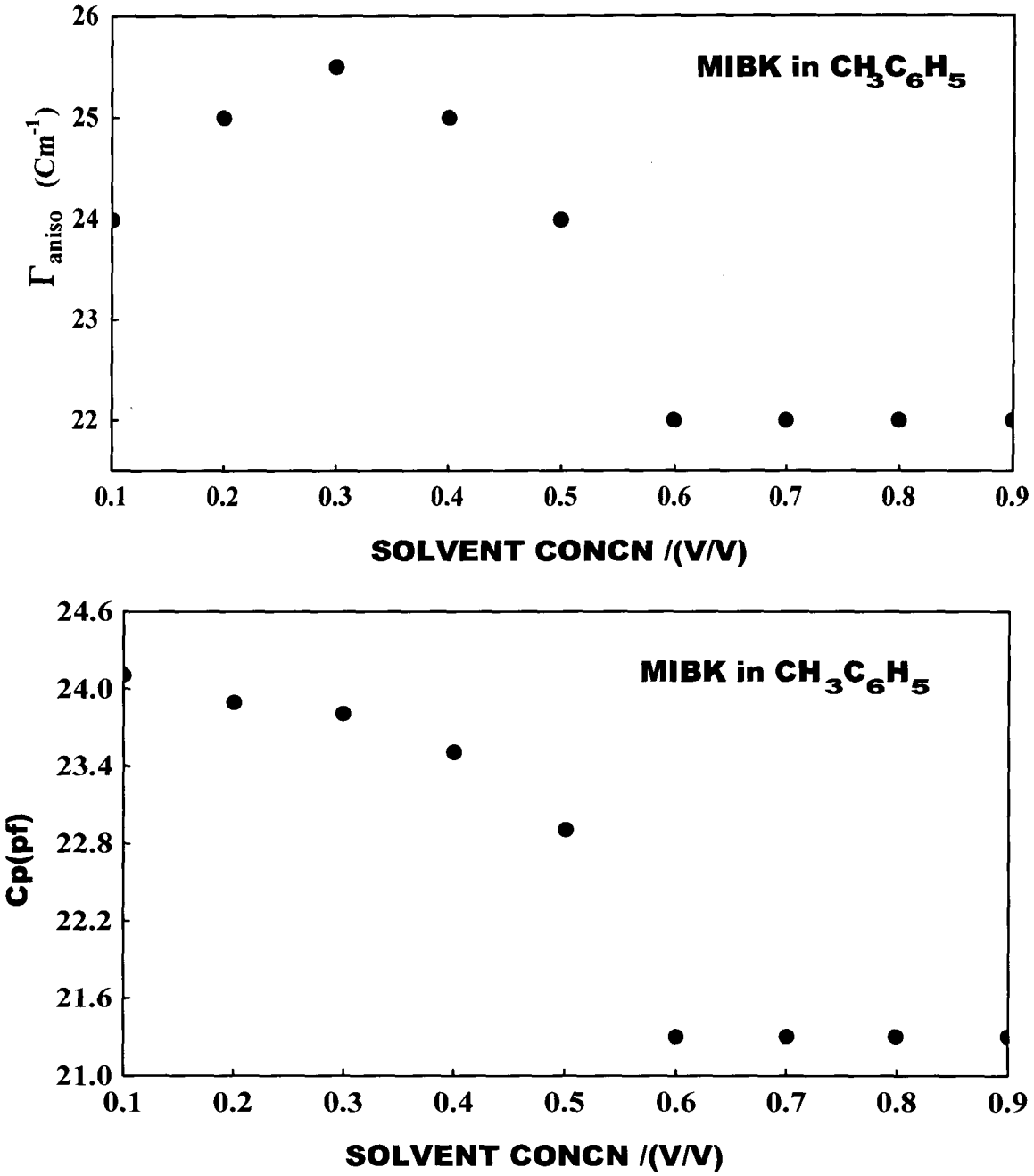

Fig.6.2(c) Variation of anisotropic bandwidth and capacitance as a function of solvent concentration

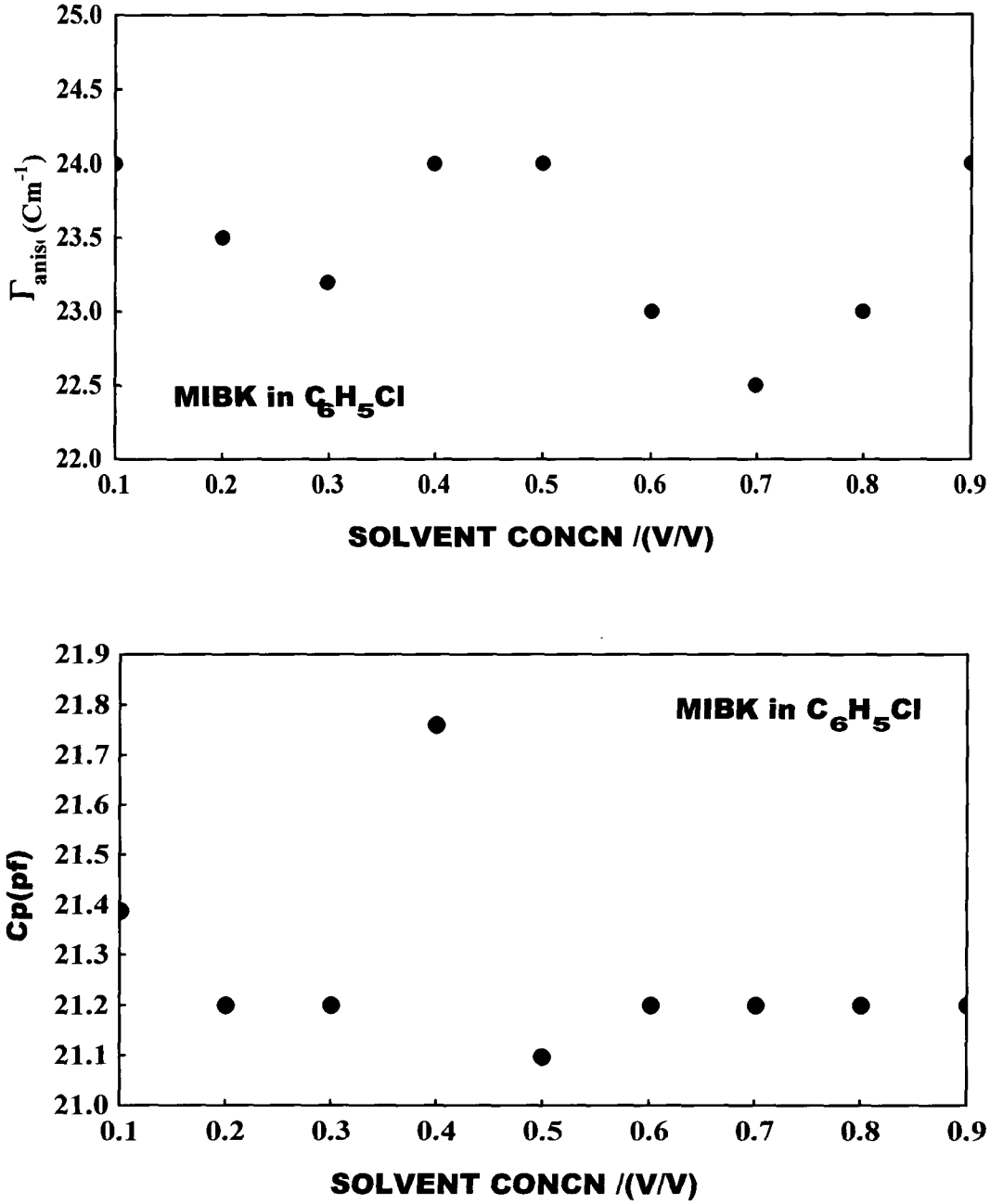

Fig.6.2(d) Variation of anisotropic bandwidth and capacitance as a function of solvent concentration

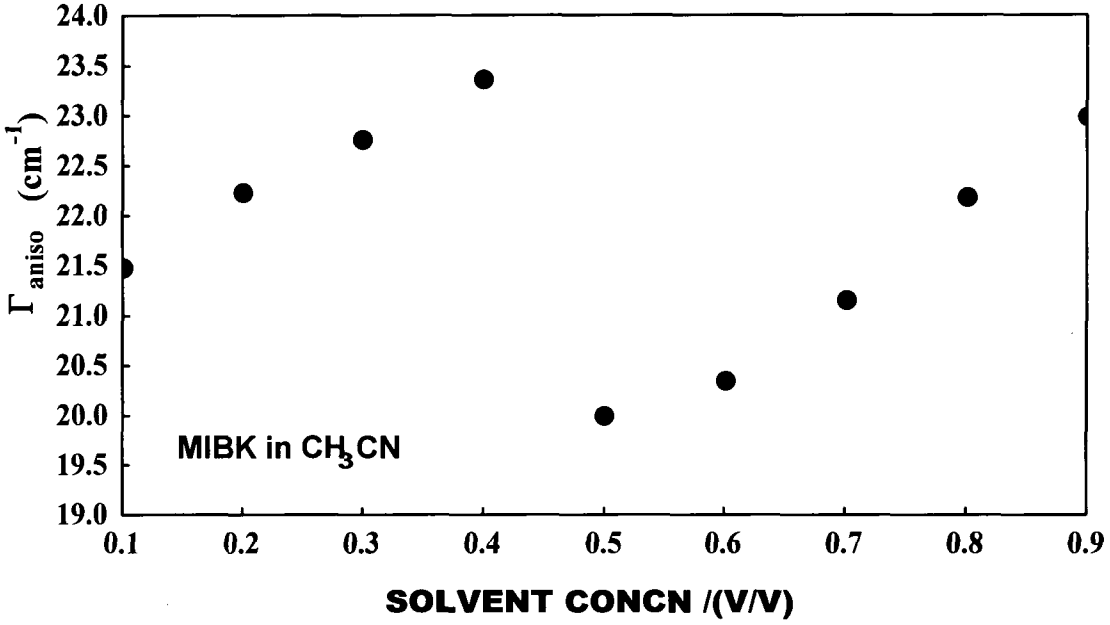

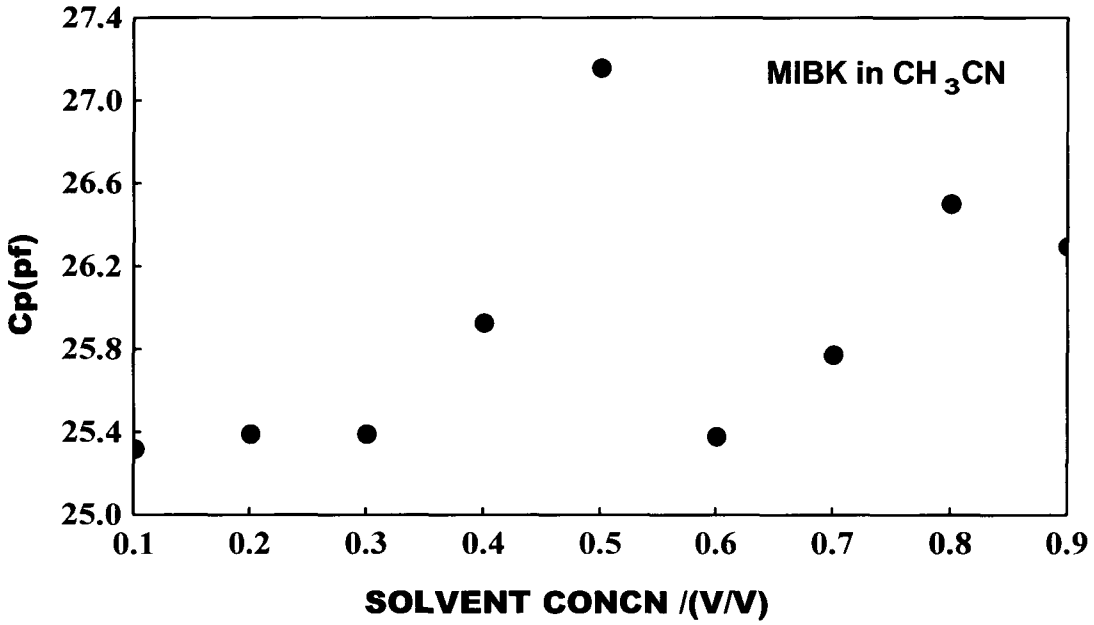

Fig.6.2(e) Variation of anisotropic bandwidth and capacitance as a function of solvent concentration

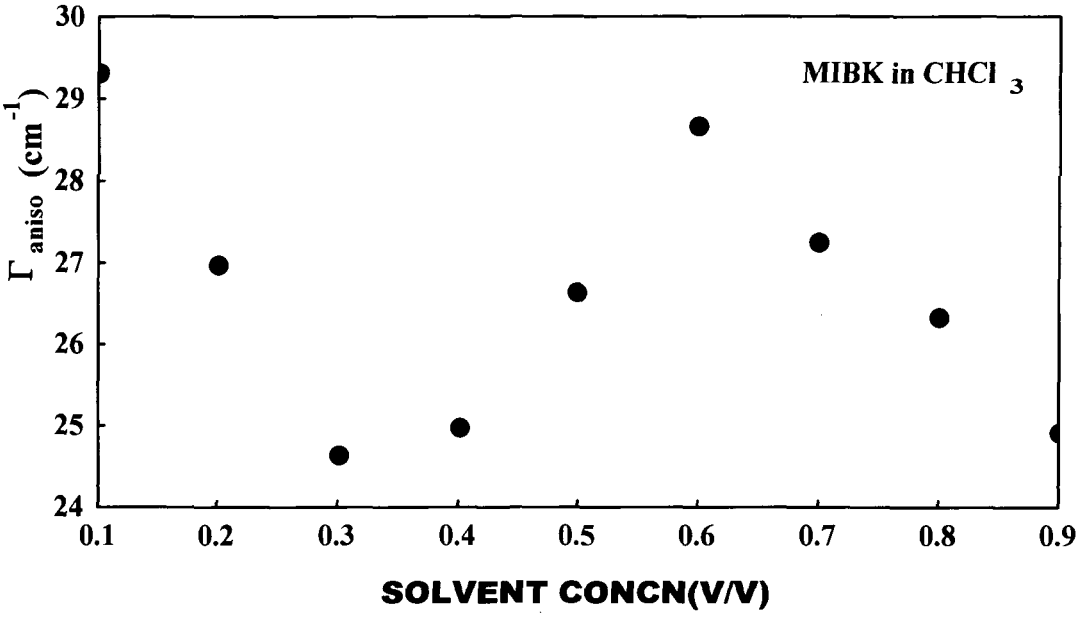

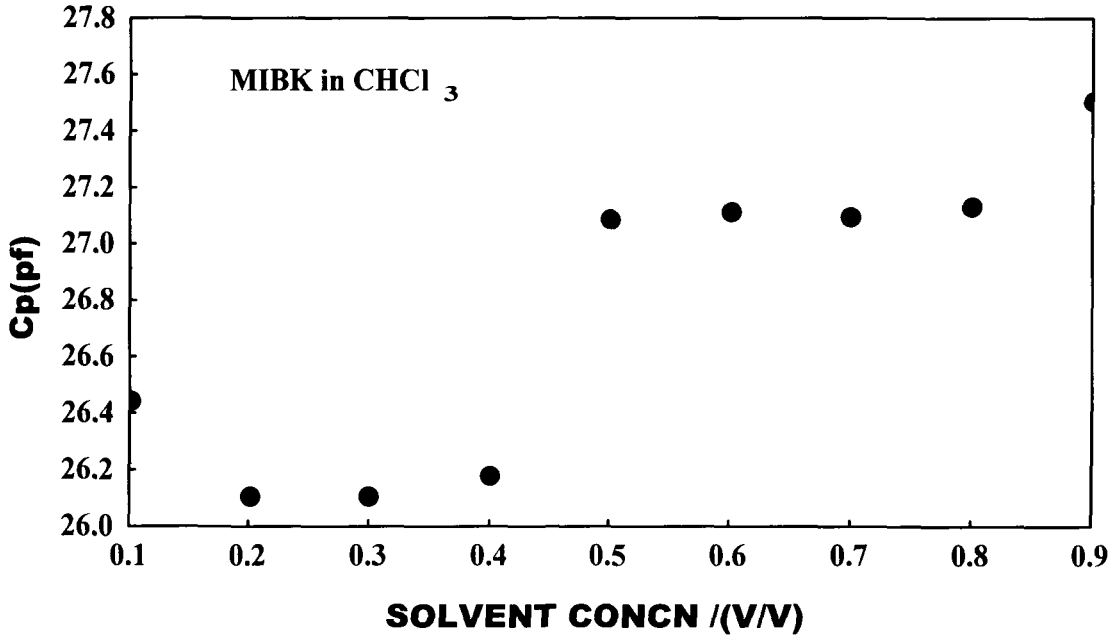

Fig.6.2(f) Variation of anisotropic bandwidth and capacitance as a function of solvent concentration

dependent and the solvent-induced effects on the band shape are of a similar magnitude in isotropic and anisotropic Raman spectra. The theory developed by Bratos and Tarjus [7] to interpret Raman band shapes of binary mixtures of van der Waals' liquids has been explained in detail in chapter 4.

In our present study, the change in Γ_{aniso} from the region of lower to higher solvent concentration reflects that the structural characteristics and the interacting nature of the substituents in the molecules are also responsible in determining the band shape. At low solvent concentration region, the Raman band shape appears to derive its major contribution through the resonant energy transfer (RET) processes where the microscopic local order in liquid phase permits the coupling between the vibrational states of the solute molecule through neighbouring transition dipoles [20-26]. With the increase in solvent concentration, the changes incorporated in terms of spatial distribution of active molecule compounded with the diminution in the degree of microscopic local order by the solvent molecules result in the gradual fall of the contribution through RET mechanism. The interaction energy due to solute-solvent interaction may arise due to the contribution from one or more coupling terms, such as dipole-dipole, dipole-quadrupole and quadrupole-quadrupole, dipole-induced dipole[27-29] etc.

chlorobenzene molecule will form a planar structure with the solute molecule. The presence of Cl atom in C_6H_5Cl may not hinder the smooth flow of the molecules. However, the orientation of the dipole moment of the C=O bond of the solute molecule (hereafter called as the director) will not be fixed in the liquid and therefore, the equation of motion of the director will come into play in addition to the flow of the liquid [33]. The equation of motion of the director has explained in chapter 4. For the case when the solvent is parallel to the director, one may find a torque which leads to change in the orientation of the C=O bond due to strong dipole-quadrupole repulsive type of interaction. Due to the changed orientation of one of the C=O bonds in the attracting pair, the interaction becomes weaker under the influence of the solvent. The orientation of the C=O bond of the solute systems comes in close proximity of the benzenoid portion of the solvent molecules. Hence, the van der Waals' volume of the solute is taken as that of C=O and that for the solvent the entire molecular structure is taken into account. For the case of OCBD-$CH_3C_6H_5$ system, the van der Waals' volume of the solvent molecule is taken as the sum of van der Waals' volume of the benzene ring and the van der Waals' volume of CH_3 group [30]. Similarly, for OCBD-C_6H_5Cl system, the van der Waals' volume of the C_6H_5Cl is taken as the sum of van der Waals' volume of the benzene ring and the van der Waals' volume of Chlorine atom.

For solute-CH_3CN system, the interaction is mainly between the dipole moment of the C=O bond of the solute and the dipole moment of the solvent. In this case, the dipole-dipole interactions between the fragments of molecules in solution are comparable to the interactions in the neat liquid. The dipole of CH_3CN molecule will try to interact with the dipole of the solute and align along the electric field of the solute dipole. The equation of motion that involves the reorientation of the dipolar molecule by cooperative movement with the immediately surrounding molecules was explained in chapter 4. The distance of closest approach in this case will be determined by the orientation of C-C≡N fragment of the solvent molecule. The dipole of CH_3CN will try to align along the field of the dipole of the solute molecule and thus an average component will be there along the director[34]. However, the liquid nature of the system will mainly maintain the smooth flow because the hydrodynamic forces may be dominant over electrical forces. For this molecular system, the van der Waals' volume for the solvent has been taken to be equal to the sum of van der Waals' volume of CH_3 group[30] and the van der Waals' volume of C-C≡N fragment.

The CCl_4 molecule has spherical shape and is highly polarizable. The solvent CCl_4 molecule due to polarization acquires electric charge and as a result of which electrostatic potential is developed in the vicinity of the

molecule whose value decreases with the increasing distance between the two molecules (solute and solvent). It has been pointed out that the C-Cl bond of each CCl_4 molecule points to the carbonyl oxygen and a strong electric field is operating on the C=O bond in the direction that the chlorine atom looks as if they had large positive charges in contrast to the expectations from the values of electronegativity[35]. The solvent's van der Waals' volume is to be calculated by taking into account the fact that the distance of closest approach will be determined by the van der Waals' radii of the chlorine atom. Therefore, the effective radius for the purpose of van der Waals' volume is the sum of the C-Cl bond distance and the van der Waals' radii of the chlorine atom.

In case of MIBK- $CHCl_3$ molecular system, the acidic nature of the proton in $CHCl_3$ molecule may lead to an interaction where the hydrogen bonding may have to be taken into account. The $CHCl_3$ molecule while coming into the proximity with the solute molecule has a possibility to orient itself with respect to the dipole of the C=O group thus leading to hydrogen bonding. The van der Waals' volume of the solvent is the combination of C-H and $C-Cl_3$ structures. Therefore, the cylinder like structure and the cone like structure will determine the van der Waals' volume of the chloroform molecule for this interaction. This interaction may be sufficient to weaken the pair interaction at sufficiently

higher concentration of the solvent. Table 6.2 shows the van der Waals' volume of the molecular system.

The van der Waals' volumes of the interacting systems described above were calculated using the equation:

$$V_w = \Phi\, V_w(\text{solute}) + (1- \Phi)V_w(\text{solvent}) \qquad \textbf{(6.3.1)}$$

where Φ is the concentration of the solute.

The values of $(\Gamma_{aniso}/\ V_w)$ have been determined for each solvent and plotted as a function of solvent concentration (Fig.6.3). This graph is an exponential curve in all the solvents, which shows that the repulsive potential of the type $e^{-\alpha R}$ is playing a significant role. Tables (6.3-6.8) show the van der Waals' volume and molecular parameter of the interacting systems. While explaining the non-coincidence effect, the pair interaction between the solute molecules is considered to lead to the local ordering in liquids. This leads to in-phase and out-of-phase type of vibrations. However, due to the increasing concentration of the solvent the weakening of the pair correlation may occur. This is possible if the interactions between the fragments of the molecules are of comparable nature to the interactions in the neat liquid.

To have detailed information about the various interactions involved, the dielectric properties of the liquid have to be taken into account. The capacitance of the liquid mixture was measured for each solvent at varying solvent

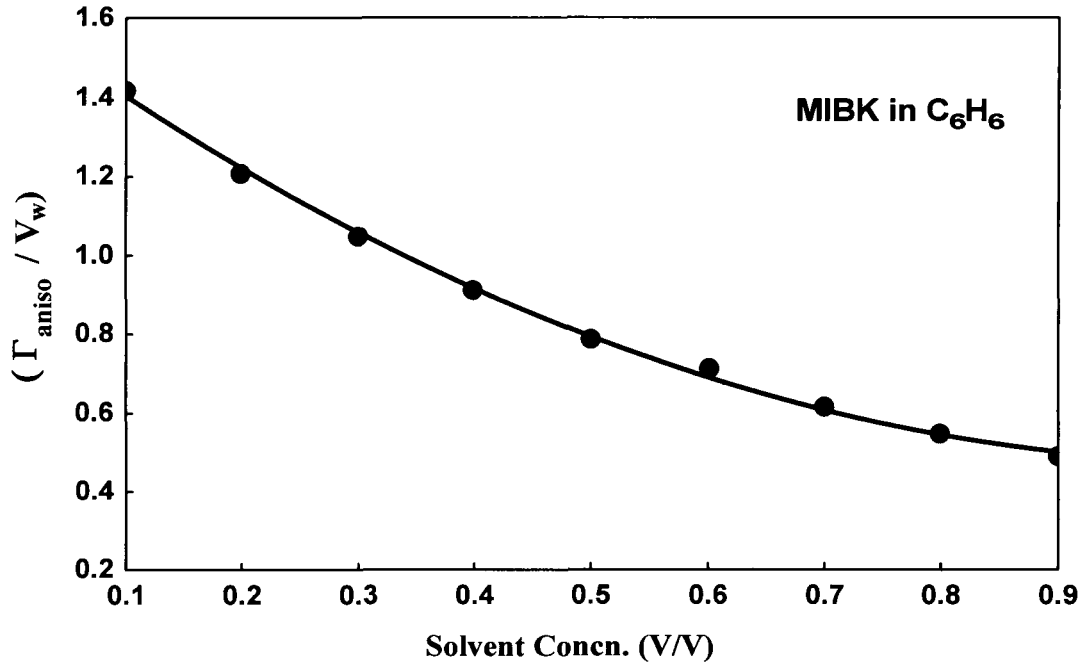

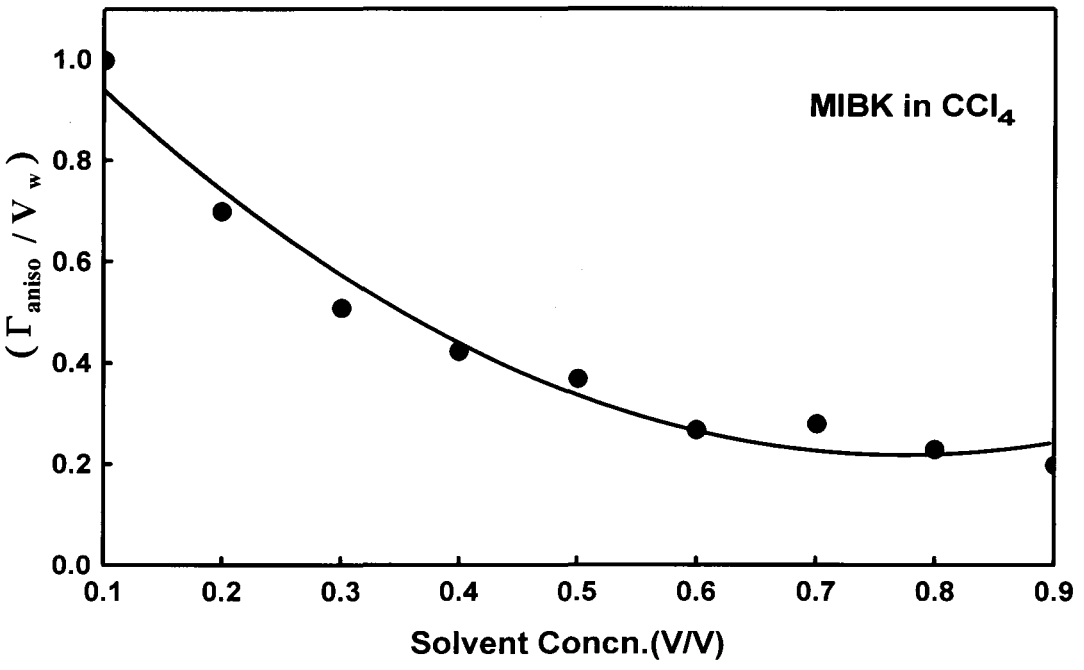

Fig. 6.3 (a) Variation of (Γ_{aniso}/V_w) with solvent concentration

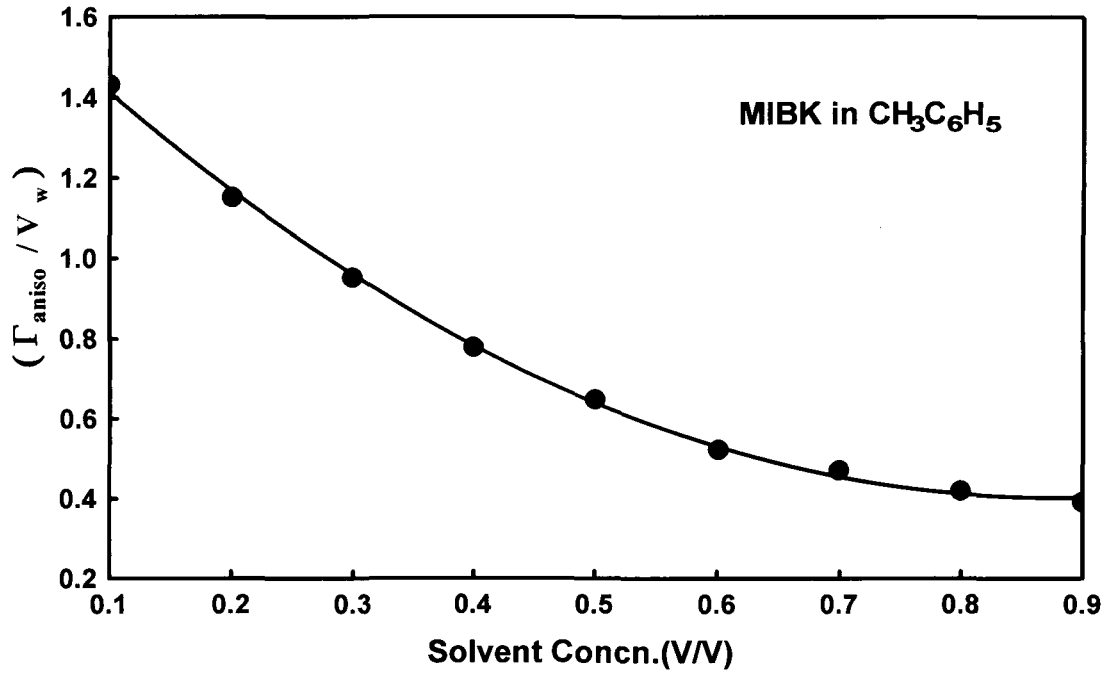

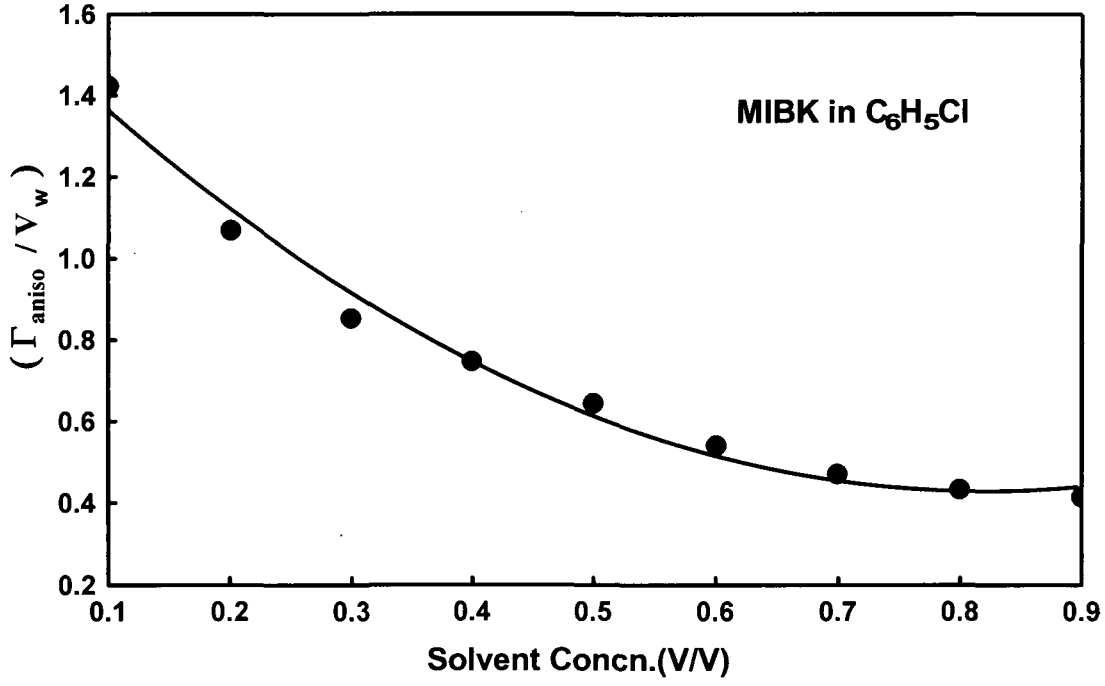

Fig.6.3 (b) Variation of (Γ_{aniso}/V_w) with solvent concentration

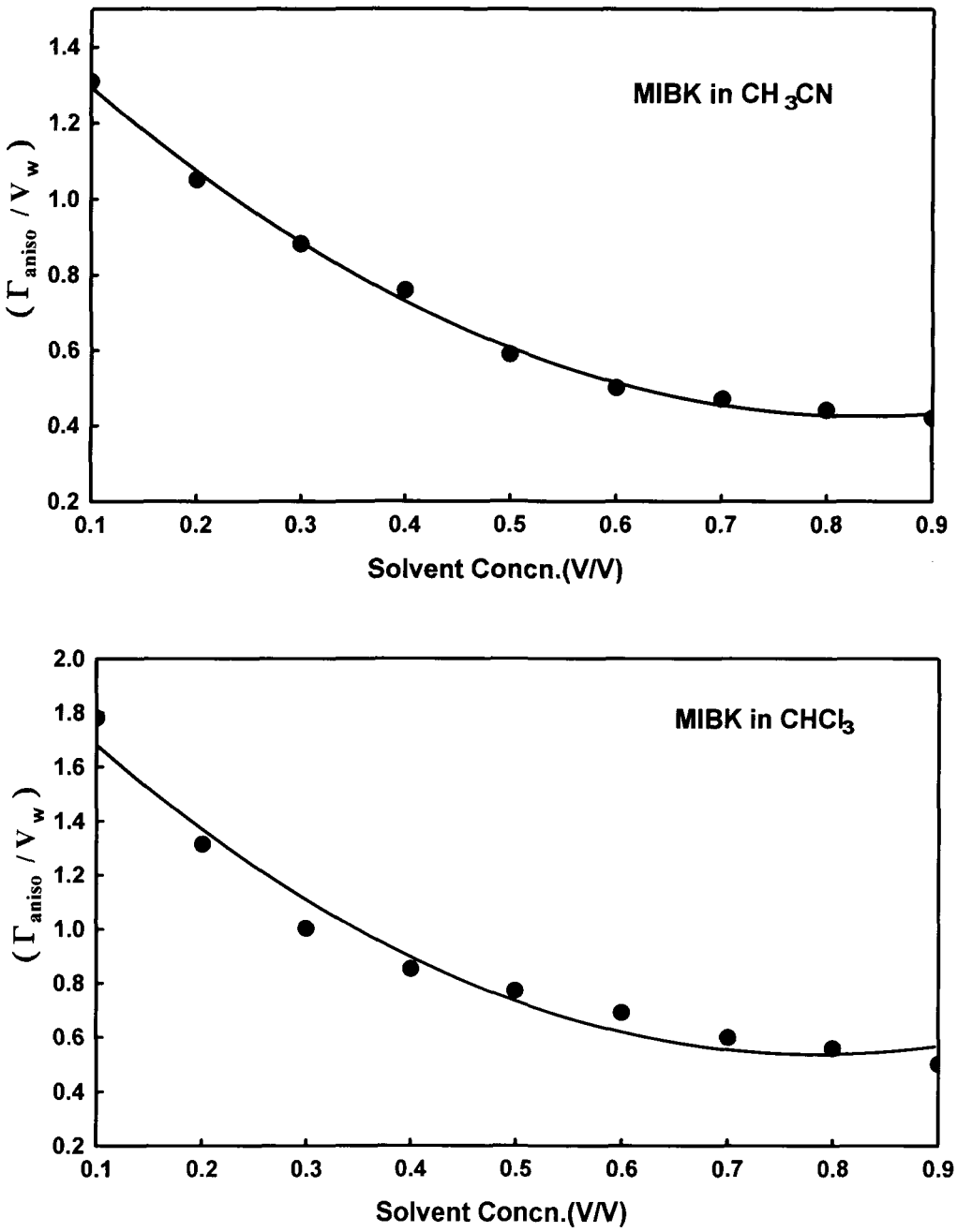

Fig. 6.3 (c) Variation of (Γ_{aniso}/V_w) with solvent concentration

Table 6.2

Van der Waals' volume of the molecular parameters

C=O (cm^3/mole)	C_6H_6 (cm^3/mole)	CCl_4 (cm^3/mole)	$CH_3C_6H_5$ (cm^3/mole)	C_6H_5Cl (cm^3/mole)	CH_3CN (cm^3/mole)	$CHCl_3$ (cm^3/mole)
11.7	48.4	114.73	62.07	63.11	59.44	55.93

Table 6. 3

van der Waals' volume and molecular parameters of MIBK-C_6H_6 systems

Solvent concentration	Van der Waals' volume of the solution $V_w = \phi V_w(\text{solute}) + (1-\phi) V_w(\text{solvent})$	Γ_{aniso} / V_w
.1	15.37	1.42
.2	19.04	1.21
.3	22.71	1.05
.4	26.38	0.91
.5	30.08	0.78
.6	33.72	0.71
.7	37.39	0.62
.8	41.06	0.55
.9	44.73	0.49

Table 6.4

van der Waals' volume and molecular parameters of MIBK-CCl_4 systems

Solvent concn.	Van der Waals' volume of the solution $V_w = \phi V_w(\text{solute}) + (1-\phi) V_w(\text{solvent})$	Γ_{aniso} / V_w
.1	22.00	1.00
.2	32.31	0.70
.3	42.61	0.51
.4	52.91	0.42
.5	63.22	0.37
.6	73.52	0.27
.7	83.82	0.28
.8	94.12	0.23
.9	104.43	0.20

Table 6.5

van der Waals' volume and molecular parameters of MIBK-$CH_3C_6H_5$ systems

Solvent concn.	Van der Waals' volume of the solution $V_w = \phi V_w(\text{solute}) + (1-\phi) V_w(\text{solvent})$	Γ_{aniso} / V_w
.1	16.74	1.43
.2	21.77	1.15
.3	26.81	1.12
.4	31.85	0.95
.5	36.89	0.78
.6	41.92	0.65
.7	46.96	0.52
.8	51.99	0.47
.9	57.03	0.39

Table 6.6

van der Waals' volume and molecular parameters of MIBK-C_6H_5Cl systems

Solvent concn.	Van der Waals' volume of the solution $V_w = \phi V_w(\text{solute}) + (1-\phi) V_w(\text{solvent})$	Γ_{aniso} / V_w
.1	16.84	1.42
.2	21.98	1.07
.3	27.12	0.86
.4	32.26	0.74
.5	37.41	0.64
.6	42.55	0.54
.7	47.69	0.47
.8	52.83	0.44
.9	57.97	0.41

Table 6.7

van der Waals' volume and molecular parameters of MIBK-CH_3CN systems

Solvent concn.	Van der Waals' volume of the solution $V_w = \phi V_w(\text{solute}) + (1-\phi) V_w(\text{solvent})$	Γ_{aniso} / V_w
.1	16.47	1.31
.2	21.25	1.05
.3	26.02	0.88
.4	30.79	0.76
.5	35.57	0.59
.6	40.34	0.50
.7	45.12	0.47
.8	49.89	0.44
.9	54.67	0.42

Table 6.8
van der Waals' volume and molecular parameters of MIBK-$CHCl_3$ systems

Solvent concn.	Van der Waals' volume of the solution $V_w = \phi V_w(\text{solute}) + (1-\phi) V_w(\text{solvent})$	Γ_{aniso} / V_w
.1	16.12	1.78
.2	20.55	1.31
.3	24.96	1.00
.4	29.39	0.85
.5	33.82	0.79
.6	38.24	0.69
.7	42.66	0.60
.8	47.08	0.56
.9	51.51	0.50

concentrations. The capacitance of empty cell being constant gives the variation of dielectric constant as a function of solvent concentration. The plot of capacitance as a function of solvent concentration is shown in Figs.6.2. It is evident from the graph that the capacitance of the liquid does depend on the solvent concentration and there is a prominent discontinuity in the intermediate range of solvent concentration. Among all the solvents chosen CCl_4 has the least value of dielectric constant (ε = 2.24). The values of dielectric constant for C_6H_6 and $C_6H_5CH_3$ are 2.28 and 2.4 respectively. The variation of bandwidth with solvent concentration shows somewhat similar nature for these solvents. In the slow modulation limit, the graph shows a curvature while in the fast modulation limit the bandwidth decreases with solvent concentration. The slow and fast modulation limits have been checked by finding the extent of Gaussian and Lorentzian lineshape (measurement of correlation coefficient with Lorentzian lineshape). For solvents of comparatively higher dielectric constants such as $CHCl_3$ (ε = 4.8) and C_6H_5Cl (ε = 5.7), the variation of bandwidth with solvent concentration shows two curvatures in the two modulation regimes. When a solvent of much higher dielectric constant CH_3CN (ε = 37.5) was used, the graph separates into two linear curves whereby the bandwidth increases with increase in solvent concentration in the two modulation regimes.

The homogeneous field of the permanent dipole μ of the solute molecule polarizes its environment and moments proportional to the polarizability are induced in the surrounding molecules. If these molecules have a permanent dipole moment, their orientation is influenced. The orientation function φ describing the distribution of molecular orientation as a function of the electric field strength F is also influenced the complex environment. For the case of molecules having permanent dipole the orientation function [36] is given as

$$\varphi_P = 1 - \frac{3\left(\coth\beta - \frac{1}{\beta}\right)}{\beta} \qquad \text{with } \beta = \frac{\mu_P F}{kT} \tag{6.3.2}$$

where kT is the thermal energy and μ_P is the permanent dipole.

For the other limiting case of an induced dipole, the orientation function is given by

$$\varphi_i = \frac{3}{4}\left\{\left(\frac{e^{\gamma}}{\sqrt{\gamma}}\int_0^{\sqrt{\gamma}} e^{x^2}dx\right) - \frac{1}{\gamma}\right\} - \frac{1}{2} \qquad \text{with } \gamma = \frac{\alpha F^2}{2kT} \tag{6.3.3}$$

where α is the polarizability.

The resulting inhomogeneous polarization of the environment will give rise to a reaction field R. R will have the same direction as μ. In the case of a polarizable point dipole having an average polarizability, the reaction field R induces a dipole [37] and satisfies the equation

$$R = \frac{4\pi}{3} N \frac{2(\varepsilon - 1)}{2\varepsilon + n_D^2} \frac{n_D^2 + 2}{3} \mu \qquad \textbf{(6.3.4)}$$

where n_D is the index of refraction, N is the number of particles per cm^3 and ε is the dielectric constant of the medium. Under the influence of the reaction field the dipole moment increases considerably. If μ* is the increased moment, then the ratio of increased moment to permanent moment is given by

$$\frac{\mu^*}{\mu} = \frac{2\varepsilon + 1}{2\varepsilon + n_D^2} \frac{n_D^2 + 2}{3} \qquad \textbf{(6.3.5)}$$

When the dipole is not surrounded by the molecules of the same kind, the reaction field and the ratio $\frac{\mu^*}{\mu}$ are changed. The changes in R and in $\frac{\mu^*}{\mu}$, when environment of the dipole is changed result in a change in the factors $\frac{2\varepsilon + 1}{2\varepsilon + n_D^2}$ and $\frac{2(\varepsilon - 1)}{2\varepsilon + n_D^2}$ in the above equations.

In dilute solution of a dipolar solute in a non-polar solvent, the polar molecules are far apart and the interaction between them is weak. There will be an interaction between the polar molecules and the molecules of the solvent and the dipole-induced dipole interaction energy may be sufficient for weakening the pair interaction.

REFERENCES:

1. A. Purkayastha and K. Kumar , J. Raman Spectrosc. **19**, 249 (1988).
2. A. Purkayastha, R. Das and K. Kumar, J. Raman Spectrosc. **21**, 227 (1990).
3. A. Purkayastha, R. Das and K. Kumar, Spectrochim. Acta, **46A**, 1545 (1990).
4. K. Schweizer and D. Chandler, J. Chem. Phys. **76**, 2296 (1982).
5. D. Ben-Amotz and D. R. Herschbach, J. Phys. Chem. **97**, 2295 (1993).
6. D. Ben-Amotz , M. R. Lee, S. Y. Cho and D. J. List, J. Chem. Phys. **96**, 8781 (1992).
7. S. Bratos and G. Tarjus, Phys. RevA, **32**, 2431 (1985) and references cited therein
8. E. W. Knapp and S. F. Fischer, J. Chem. Phys. **76**, 4730 (1982).
9. G. Moser, A. Asenbaum, J. Barton and G. Döge, J. Chem. Phys. **102**, 1173 (1995).
10. A. Das and K. Kumar, J. Raman Spectrosc. **30**, 547 (1999).
11. A. Purkayastha, R. Das and K. Kumar, Spectrochim. Acta, **47A**, 525 (1991).
12. K. Tanabe, Spectrochim. Acta, **40A**, 437 (1984).
13. A. Das and K. Kumar, J. Raman Spectrosc. **30**, 563 (1999).
14. M. G. Giorgini, Pure Appl. Chem. **76**, 157 (2004).

15. M. Musso, H.Torii, P. Ottaviani, A. Asenbaum and M. G. Giorgini, J. Phys. Chem., **106A**, 10152 (2002).

16. A. Morresi, M. Paolantoni, P. Sassi, R. S. Cataliotti and G. Paliani, J. Phys. Condens. Matter, **12**, 3631 (2000).

17. M. G. Giorgini, M. Musso, A. Asenbaum and G. Döge, Mol. Phys. **98**, 783 (2000).

18. H. Torii, M. Musso, M. G. Giorgini and G. Döge, Mol. Phys. **94**, 821 (1998).

19. M. Musso, M. G. Giorgini, G. Döge and A. Asenbaum, Mol. Phys. **92**, 97 (1997).

20. W. Schindler, T. W. Zerda, J. Jonas, J. Chem. Phys. **79**, 639 (1983).

21. G. Fini, P. Mirone, Spectrochim. Acta, **32A**, 625 (1976).

22. P. Mirone, G. Fini, J. Chem. Phys. **71**, 2241 (1979).

23. D. W. Oxtoby, J. Phys. Chem. **87**, 3028 (1983).

24. G. Döge, R. Arndt, J. Yarwood, Mol. Phys. **52**, 399 (1984).

25. C. H. Wang, J. McHale, J. Chem. Phys. **72**, 4039 (1980).

26. D. W. Oxtoby, Annu. Rev. Phys. Chem. **32**, 77 (1981).

27. A. Das, K.Kumar, Spectrochim. Acta, **54A**, 793 (1998).

28. A. Das, K.Kumar, J. Raman Spectrosc. **30**, 547 (1999).

29. A. Das, R. Das, K.Kumar, Spectrochim. Acta, **58A**, 1583 (2002).

30. A. Bondi, J. Phys. Chem. **68**, 441 (1964).

31. Lee B., F. M. Richards, J. Mol. Biol. **55**, 379 (1971).

32. Eisenberg. D, A. D. Mclachlan, Nature, **319**, 199 (1986).

33. W. H. de Jeu, Physical properties of liquid crystalline Materials, Liquid Crystal Monographs **Vol.1**, Gordon and Breach Science publishers, New York (1981).

34. C. P. Smyth, "Molecular Interactions", edited by H. Ratajczak and W.J. Orville-Thomas, **Vol. 2**, John Wiley and Sons, Chichester(1981).

35. H. Torii, J. Chem. Phys. **119**, 2192 (2003).

36. D. Porschke, Ann. Rev. Phys. Chem. **36,** 159 (1985).

37. C. J. F. Bottcher, Theory of electric polarization, **Vol.1**, p-134, Elsevier, Amsterdam, (1973).

CHAPTER 7

CHAPTER 7

CONCLUSION

Vibration relaxation process is emerging as a useful tool in probing the nature of the solute-solvent interactions. Such dynamic and structure processes in liquid phase are studied using Laser Raman scattering techniques. The Raman scattering experiments have been carried out on C=O stretching mode of o-Chlorobenzaldehyde (OCBD) and Methyl Isobutyl Ketone (MIBK) using benzene, carbon tetrachloride, methylbenzene, chlorobenzene, acetonitrile and chloroform as solvents. The solvent induced perturbations lead to fluctuations in the solute vibrational frequency, which contribute to the bandwidth of the corresponding vibrational band. The conclusions drawn are based upon the study of non-coincidence effect, isotropic bandwidth and anisotropic bandwidth respectively. They are given in point wise below:

(a) The dependence of the bandwidth and frequency of Raman vibrational bands on the environment provides useful information regarding the solute-solvent interactions and intermolecular forces. Therefore, a solvent dependent study of the non-coincidence effect (NCE) and anisotropic components of the

Raman band on the interacting systems is carried out to contribute information regarding the solute-solvent interactions.

The Raman Spectra of C=O stretching mode of OCBD were measured using CCl_4, CH_3CN, $CH_3C_6H_5$ and C_6H_5Cl solvents at different solvent concentrations ranging from 10% to 90% solvent concentration. The isotropic and anisotropic Raman components were found out and anisotropy shift ($\delta\nu = \nu_{aniso} - \nu_{iso}$) were measured at different solvent concentrations ranging from 10% to 90% solvent concentrations using the above four solvents. In order to have a detailed information about the various interactions involved, the NCE (Anisotropy shift) was studied by taking into account the screening factor related to the permanent and transition dipoles. The anisotropy shift ($\delta\nu$) of the liquid mixture was measured for each solvent at varying solvent concentrations. It has been found that the anisotropy shift decreases as the concentration of the solvent is increased which may be due to the transition dipole-transition dipole (TD-TD) interactions of the vibrations of two adjacent molecules. For the molecules having aromatic rings, the coupling mechanism responsible for the NCE may be associated with quadrupolar resonant coupling. The Onsager- Fröhlich dielectric model, which treats the dielectric as a continuum has been tested.

The dielectric constant of the solution was calculated by using the relation

$$\varepsilon_{solution} = \phi\, \varepsilon_{solute} + (1- \phi)\, \varepsilon_{solvent}$$

The value of the parameter $F= \delta\nu(2\varepsilon +n^2)^2\varepsilon^{-1}$ was found out and plotted as a function of the solute volume fraction ϕ for different solvents. The graph clearly shows that the data points fit well in exponential curves for all the solvents except CH_3CN. In case of OCBD- CH_3CN system, the data points are lying in a straight line, which indicates that the dielectric continuum theory holds better in this system. The high dielectric constant of CH_3CN solvent may be playing a significant role for such behaviour. The exponential curves for the three solvents (CCl_4, $CH_3C_6H_5$ and C_6H_5Cl solvents) show that the Onsager-Fröhlich dielectric continuum model does not hold good in these systems. Therefore, in these solute-solvents, the discreteness of the medium exists. It is also clear that the screening effect may not be as effective as envisaged by the Onsager-Fröhlich model in such systems. The fitting of the data in exponential curves clearly indicates that the repulsive forces are active in most of the interacting solute-solvent systems.

The bandwidths of anisotropic component (Γ_{aniso}) were also found out to see the effect of bandwidths in the interacting systems and plotted as a function of solvent concentration. The data points are scattered and cannot be fitted into a particular curve. For CCl_4 solvent, the data points show a decrease

in the bandwidth while going from lower to higher solvent concentration, whereas for CH_3CN and C_6H_5Cl solvents, the data points show an initial increase and then a decrease in the bandwidth as the concentration increases. In case of $CH_3C_6H_5$ solvent, the data points show somewhat different pattern as compared to others. However, the bandwidth is found to decrease at high solvent concentration for all the solvents. The bandwidths of isotropic Raman component (Γ_{iso}) were also found out in order to see the changing pattern according to different solvent concentrations and plotted with respect to the solvent concentration. Interestingly, the isotropic bandwidths are also found to decrease at higher solvent concentration. The dramatic change in shape on going from lower to higher solvent concentration region reflects the changes in liquid dynamics brought about by solvent collisions where the structural characteristics and the interacting nature of the substituents in the molecules are also responsible. The theory proposed by Bratos and Tarjus predicts different spectral behaviour of Raman bands for isotopic and chemical solutions. This difference is due to the fluctuations of the local chemical composition of the solution and to the structure-breaking effect occurring when a liquid is progressively diluted. At low solvent concentration region, the Raman band shape appears to derive its major contribution through the resonant energy transfer (RET) processes where the microscopic local order in

liquid phase permits the coupling between the vibrational states of the solute molecule through neighbouring transition dipoles. With the increase in solvent concentration, the changes incorporated in terms of spatial distribution of active molecule compounded with the diminution in the degree of microscopic local order by the solvent molecules result in the gradual fall of the contribution through RET mechanism. In order to interpret the complicated nature, the van der Waals' volume of the sphere of influence in a solute dissolved in four solvents CCl_4, CH_3CN, $CH_3C_6H_5$ and C_6H_5Cl solvents is taken into account. The interaction energy due to solute-solvent interaction may arise due to the contribution from one or more coupling terms, such as dipole-dipole, dipole-induced dipole, dipole-quadrupole and quadrupole-quadrupole, etc.

The van der Waals' volumes of the interacting systems were estimated and the values of (Γ_{aniso}/ V_w) were calculated for each solvent and plotted as a function of solvent concentration. This graph is an exponential curve in all the solvents stating that the repulsive potential $e^{-\alpha R}$ is playing a significant role.

(b) The vibrational relaxation in molecular liquids is very important in analyzing the band shape of complex molecular systems. This process is responsible for the line broadening of the isotropic Raman spectral component. The solute-solvent interacting systems contemplate the so-called solvent cage

effect where the molecules of a solute are confined in a potential well, created by solvent molecules. The molecule is considered to be vibrating against its immediate neighbours, with an occasional escape to its adjacent position. However, the vibrational relaxation process for complex molecular systems sometimes cannot be explained on the basis of a macroscopic perception of the interacting systems. There may be a marked difference between the interacting situations in the pure solute and as dissolved in solvents especially at high dilution. A detailed study of dephasing processes at microscopic level is therefore required in order to explain the interacting situations, especially the solvent effects on relaxation rates.

The Raman spectra of OCBD dissolved in various polar and non-polar solvents ($CH_3C_6H_5$, C_6H_6, C_6H_5Cl, CCl_4 and $CHCl_3$) have been recorded and the isotropic components were obtained. The isotropic band shapes for OCBD in different solvents were checked by curve fitting and found to be more Lorentzian in nature at high dilutions (~90%). For the Lorentzian lineshape, the vibrational relaxation rate is related to the isotropic bandwidth by the expression,

$$\tau_v^{-1} = \pi c \Gamma_{iso}$$

where Γ_{iso} is the bandwidth (full width at half maximum intensity, FWHM) of the isotropic component of the Raman band and c is the velocity of light.

The bandwidths of the isotropic component of C=O stretching mode of OCBD were measured at 90% solvent concentration. The data were used to determine the vibrational relaxation rate (τ_v^{-1}). The various models proposed for examining the dephasing process took into account of the dynamic viscosity (η) which is a macroscopic property. The P-K parameter f (ρ,η,n) was calculated for OCBD and correlated with the experimental values of the vibrational relaxation rate. The correlation is roughly linear for all the solvents, with the exception of chloroform. The point for $CHCl_3$ is too far away from the correlation line.

It is probable that the discreteness of the medium due to solvent may be playing a role. Hence, a microscopic model was used in order to explain the microscopic environment. In this model, since the solute-solvent systems may not always be homogeneous and some heterogeneity may exist due to associative nature of the molecules, the concept of microviscosity was introduced. The van der Waals' interactions between solute and solvent are taken into account in this case.

The microviscosity (η_m) may be calculated using the relation

$$\eta_m = \eta[0.16+0.4(a/b)]$$

or, $\eta_m = \eta\gamma$

where $\gamma = [0.16+0.4(a/b)]$ is the microfriction factor.

a and **b** are the radius of solute and solvent molecules respectively.

The modified parameter has the form

$$f_m = \rho\eta_m\left[(n^2-1)/(2n^2+1)\right]^{-1}$$

where ρ is the density and n is the refractive index of the solvent molecule.

The variation of the vibrational relaxation rate (τ_v^{-1}) as a function of f_m has been plotted, which is clearly a linear plot indicating the better fitting of data points. This shows that the discreteness of the medium due to the solvents has a significant influence in such complex molecular systems. The correlation coefficient (r) for the τ_v^{-1} against f_m and f (ρ,η,n) plots have been calculated and their values are found to be 0.993 and 0.824 respectively. We may therefore conclude that 'f_m' is a better parameter compared to 'f' for explaining the vibrational relaxation rates of OCBD molecule. Thus, the solvent microviscosity rather than dynamic viscosity is playing a major role in analyzing the Raman band shape in this solute-solvent system.

(c) In order to have more information about the angular dependent intermolecular forces, which contribute to the anisotropic bandwidths, the solvent dependence of the Raman band corresponding to C=O stretching vibration of methyl isobutyl ketone (MIBK) in several solvents like benzene,

carbon tetrachloride, methylbenzene, chlorobenzene, acetonitrile and chloroform was undertaken. The dielectric measurements (capacitance) in liquid mixtures were also carried out to correlate the anisotropic bandwidth with changing environment. The bandwidths of the anisotropic component (Γ_{aniso}) of MIBK were measured in different solvent concentrations ranging from 10% to 90% using polar and non-polar solvents (C_6H_6, CCl_4, $CH_3C_6H_5$, C_6H_5Cl, CH_3CN and $CHCl_3$) of varying dielectric constant. Examination of spectral properties reveals that the anisotropic bandwidth strongly depends on solvent concentration and is sensitive to environmental changes. The data points are scattered and cannot be fitted to a particular shape. There is no uniformity or continuity in the intermediate region for all the solvents. In low solvent concentration region, the plot of Γ_{aniso} as a function of solvent concentration shows marked curvatures for all solvents except for CH_3CN. However, the data points in higher solvent concentration region appear to be linear for most of the solvents. In case of C_6H_5Cl solvent, the data points show two curvatures and in the intermediate region, there is no uniformity or continuous pattern of the plot. For CH_3CN solvent, the data points may be fitted in two straight lines rather than one implying a discontinuity in the uniform linear pattern in the intermediate region. This is a complicated nature of interaction, which may be

due to the fluctuation of the chemical composition in a given site of the liquid and to the structure breaking effects.

In order to interpret the complicated behaviour we have taken into accounts the van der Waals' volume (V_w) of the sphere of influence in solute dissolved in all solvents. The van der Waals' volume of the interacting system was calculated by using the equation

$$V_w = \Phi\ V_w(\text{solute}) + (1- \Phi)\ V_w(\text{solvent})$$

where Φ is the concentration of the solute. The values of ($\Gamma_{aniso}/\ V_w$) were calculated and plotted at different solvent concentrations. The graph shows an exponential curve for the entire region, which is indicative of the repulsive potential $e^{-\alpha R}$ playing an important role in such complex interacting systems.

In order to study the influence of screening effect on the bandwidth, the capacitances of the liquid mixture at different solvent concentrations varying from 10% to 90% were measured for all the solvents. The plot of capacitance at different solvent concentrations for each solvent shows a discontinuity around 50% of solvent concentration. This shows somewhat similar nature, as compare with the variation of anisotropic bandwidth with solvent concentrations, which supports the idea that repulsive type of intermolecular forces are responsible in the line broadening mechanism.

Particulars of the Candidate

Name of the Candidate	**: Ms. Thongam Gomti Devi**
Degree	**: Ph. D.**
Department	**: Physics**
Title of the Dissertation	**: Vibrational Band Shape analysis in Complex Molecular Systems**
Date of payment of admission fee	**: 14. 8. 2000**
Approval of Research proposal	**:**
School Board	**: 26. 4. 2001**
Registration No. and Date	**: 543 of 26. 4. 2001**
Extension (if any)	**: No**

17.5.05

(Prof.M.K.Parida)
Head
Department of Physics
NEHU, Shillong

Head,
Ph[illegible]rtment,
N.E.[illegible]-793022.

LIST OF PUBLICATIONS

1. Raman anisotropic bandwidth study of C=O stretching vibration of Methyl Isobutyl Ketone: Role of van der Waals' volume of the interacting systems,
   Th. Gomti Devi, A. Das and K. Kumar, *Spectrochimica Acta*, **60A**, 211(2004)

2. Raman bandshape analysis of Ortho-Chlorobenzaldehyde: Microviscosity dependent study,
   Th. Gomti Devi and K. Kumar, *J. Raman Spectrosc.* **35**, 835 (2004)

3. Anisotropy shift And Raman bandwidth studies in Carbonyl containing molecule o-Chlorobenzaldehyde : Role of repulsive forces
   Th. Gomti Devi and Kamal Kumar, Accepted for publication in Spectrochimica Acta

4. Dependence of Raman anisotropic bandwidth on van der Waals' volume of the complex interacting systems
   Th. Gomti Devi, S. Datta and K. Kumar, in *Proceedings of IVth DAE-BRNS National Laser Symposium,* edited by B. M. Suri, V. K. Mago and Alok. K. Ray, p. 454, Allied Publishers Pvt. Ltd., New Delhi (2005)

5. Solvent dependent Raman bandshape analysis of C=O stretching mode of Methyl Ethyl Ketone
   S. Datta, Th. Gomti Devi and K. Kumar, in *Proceedings of DAE-BRNS National Laser Symposium*, edited by B. M. Suri, V. K. Mago and Alok. K. Ray, p. 718, Allied Publishers Pvt. Ltd., New Delhi (2005)

6. Solvent dependent electrical property studies on Raman bandshape analysis of complex interacting systems
   Th. Gomti Devi and K. Kumar, in *Proceedings of the XVth national conference on Atomic and Molecular Physics*, p-24, PRL, Ahmedabad (2004)

7. Role of van der Waals' volume and influence of electrical properties on Raman bandshape analysis of N,N-Dimethylformamide,
   Th. Gomti Devi and K. Kumar, in *Proceedings of VIth Asian international seminar on Atomic and Molecular Physics*, P. 94, Beijing, China (2004)

8. Vibrational relaxation studies in C=O stretching mode of Ethyl Acetate
   Th. Gomti Devi and K. Kumar, in *Proceedings of the Golden Jubilee DAE-BRNS National Laser Symposium*, edited by A. K. Nath and K. S. Bartwal, P. 522, Allied Publishers Pvt. Ltd., New Delhi (2003)

9. Role of van der Waals' volume on Raman bandshape analysis of o-Chlorobenzaldehyde
   Th. Gomti Devi and K. Kumar, in *Proceedings of the Golden Jubilee DAE-BRNS National Laser Symposium,* edited by A. K. Nath and K. S. Bartwal , p. 512, Allied Publishers Pvt. Ltd., New Delhi (2003)

10. Raman bandshape analysis of Methyl Isobutyl Ketone:Effect of van der Waals' volume
    Th. Gomti Devi and K. Kumar, in *Proceedings of DAE-BRNS National Laser Symposium,* edited by L. M. Kukreja and S. K. Dixit, p. 359, Allied Publishers Pvt. Ltd., New Delhi (2002)

11. Solvent dependent Raman band shape analysis of C=O stretching mode of Acetophenone
    Th. Gomti Devi and K. Kumar, in *Proceedings of international conference on CDAMCP*, P.57, New Delhi (2002)